January 2020

Algorithms Enabling Communications in the Presence of Adjacent Channel Interference

Berker Peköz
University of South Florida

Algorithms Enabling Communications in the Presence of Adjacent Channel Interference

by

Berker Peköz

A dissertation submitted in partial fulfillment
of the requirements for the degree of
Doctor of Philosophy
Department of Electrical Engineering
College of Engineering
University of South Florida

Co-Major Professor: Hüseyin Arslan, Ph.D.
Co-Major Professor: Selçuk Köse, Ph.D.
Kwang-Cheng Chen, Ph.D.
Dmitry B. Goldgof, Ph.D.
Gangaram S. Ladde, Ph.D.

Date of Approval:
March 26, 2020

Keywords: Interference Elimination, Interference Suppression, Multiple Access Interference,
Orthogonal Frequency Division Multiplexing, Pulse Shaping Methods

Dedication

To my renunciant father & enduring mother, for everything.

To my family, for supporting me through all of life hardships.

To my friends and teachers, for inspiring and encouraging my pursuit of knowledge.

To my most lovely beloved, for giving a meaning, and future to it all.

Acknowledgments

Respect and thanks to my grandparents Sultan and İsmail Peköz, and Keziban and Ziya Tatar for their bravery in leaving their homes and crossing steep mountains to provide better opportunities and education to my parents. None of this would have been possible had they chose the easy way. Respect and thanks, to my mother Nurten and my late father Ali Peköz, for keeping up with this legacy by devoting their lives to surrounding me with top-notch environments. Your unconditional love is unexampled, and your sacrifices cannot be repaid. Thanks to all my family for dropping everything they had and being there for me with their whole network whenever I needed support or guidance, and always loving me plenty. My family is my highest luck and wealth.

Praises to my love Merve Kaçar for keeping me on track whenever I thought of quitting as my health and finances deteriorated over the course of my pursuit and patiently calming me down for years as tension bore unbearable. I would have given up had not that meant not building a future together. I can never pay back the support of Gül and Erdinç Kaçar, who enfolded me as their son, during the tough times of my course and providing facilities and beauties to my life.

A greetings to all my friends who pulled me through life's hardships and promoted the better in me at all times. The influence of you all on who I am today cannot be underestimated. Hadn't I met with Mustafa Kemal Altınok, Mehmet Yener Çalışkaner, Onur Memioğlu, Deniz Sargun, Kaan Sel, Metin Dündar Özkan, Çağrı Şakiroğulları and Utku Norman I could certainly not develop myself to this extent. Parisa Sharif, Nasim Esmailzadeh; and Drs. Serdar Görümlü, Mohammad Maadi, Serra Altınoluk, Sedat Doğru, Onur Yılmaz, Yağız Kaymak, and Yanjia Sun have demonstrated to me early that the resilient thrive at the end of graduate studies. No space could accommodate the names of all the wonderful companions I had on my way here, thus I hope this shout out would suffice. I thank my friends İsmail Ulutürk, Selahattin Burak Sarsılmaz,

Kadriye Merve Doğan, Mehmet Aktukmak and Anıl İmren; and Drs. Orhun Aras Uzun, Mohamed Elkourdi, Adrian Jaesim, and Asim Mazin for all the emotional support and friendship over my graduate school years. I can never thank Dr. Emre Seyyal enough for his help when I first arrived in Tampa, and now on my way to Bridgewater. Nor can I forget similar logistic and academic support of Dr. Harun Yılmaz. I will remain grateful to Dr. Ertuğrul Güvenkaya for getting me started in this field, Dr. Alphan Şahin for enhancing my creativity, and Dr. Zekeriyya Esat Ankaralı for pushing me to the finish. I will always hold the brotherhood of my officemate Dr. Mohammed Hafez dear. I will remain indebted to my colleagues, Ali Fatih Demir and Murat Karabacak, for looking after me as their brother. Their compassion inspired me to look after and support Emre Arslan, Şinasi Çetinkaya, and Mehmet Mert Şahin to keep up this legacy.

A reverence to all my teachers, professors, and athletic coaches who taught me how to push my mind and body to their limits. I wouldn't be able to withstand to the end hadn't they disciplined me not to quit and suffer throughout this *training* I hated to live the rest of my life as a champion. A salute to Frank McGrath for sharing his journey with me that set me on a still-burning fire 15 years ago. A remembrance to late Dr. Ralph Fehr for teaching me to teach and keep my sane in chaos. A regards to Dr. Christos Ferekides for showing me how to become an outstanding leader.

A remembrance to Yaşar Kemal, for penning novels that inspired me not to give up when things looked desperate and teaching me that *I had to die a thousand deaths to be born to this realm once*, and Galileo Galilei, for inspiring me to fight relentlessly to deliver this truth. This dissertation is inspired by the intellect of İsmail El Cezeri, and is a tribute to Hypatia, Giordano Bruno, Nicolaus Copernicus, Johannes Kepler, Sir Isaac Newton, Nikola Tesla, Alan Turing, Katherine Goble, Mary Jackson, Dorothy Vaughan, and countless other bedeviled geniuses and peoples of the world.

Special thanks to Dr. Kwang-Cheng Chen, Dr. Dmitry Goldgof and Dr. Gangaram Ladde for their commitment to my growth. Special thanks to Dr. Selçuk Köse for academic and financial support, and philosophical guidance. Special thanks to Dr. Hüseyin Arslan for believing in me, providing me the opportunity and the means to achieve this level, and having the patience to allow me to develop my skills.

Table of Contents

List of Tables

List of Figures

Abstract

Newer cellular communication generations are planned to allow asynchronous transmission of multiple numerologies (waveforms with different parameters) in adjacent bands, creating unavoidable adjacent channel interference (ACI). Contemporary windowed-orthogonal frequency division multiplexing (W-OFDM) algorithms have limited ACI rejection capability under high delay spread and small fast Fourier transformation (FFT) sizes. CP is designed to be longer than the maximum excess delay (MED) of the channel to accommodate such algorithms in current standards. Most prior work on windowing assume additional extensions reserved for windowing, which does not comply with standards. The robustness of these algorithms can only be improved against these conditions by adopting additional extensions in a new backward incompatible standard. Whether windowing should be applied at the transmitter or the receiver was not questioned. Such extensions would deteriorate the performance of high mobility vehicular communication systems in particular. In this dissertation, algorithms that enable minimum, even insufficient guards are discussed to achieve the spectral efficiency and latency requirements of cellular communication systems beyond 5G. This leads to interference in both time and frequency domains.

First, a partial-non-orthogonal multiple accessing (NOMA) scenario in which the desired user is experiencing both intersymbol interference (ISI) due to insufficient CP and ACI caused by asynchronous transmitters using non-orthogonal numerologies in adjacent bands is investigated. ISI and ACI depend on the power offset between desired and interfering users, the instantaneous channel impulse responses (CIRs) of interfering users and transmitter and receiver window functions. Therefore, joint and adaptive utilization of CP requires real-time calculation of ISI and ACI. Analytical expressions for expected ISI and ACI at each subcarrier of the desired user are derived to minimize their combination. Accordingly, an adaptive algorithm consisting of windowing each

subcarrier at the receiver with window length that minimizes the combined interference at that subcarrier by optimally exchanging ISI and ACI is proposed. Interference reduction performances of current, outdated and average optimal window length raised cosine receiver windows are assessed and compared to fixed and no receiver windowing. Windowing reduces interference even when CP is shorter than the channel if window length is determined using the proposed design guidelines.

Second, two independent algorithms are proposed that are implemented at the transmitter and receiver, respectively. These algorithms estimate the transmitter and receiver windowing duration of each RE with an aim to improve fair proportional network throughput. While doing so, solely the available extension that was defined in the standard is utilized. Presented standard-compliant algorithms also do not require any modifications on the counterparts or control signaling. Furthermore, computationally efficient techniques to apply per-RE transmitter and receiver windowing to signals synthesized and analyzed using conventional CP-OFDM are derived and their computational complexities are analyzed. The spectrotemporal relations between optimum window durations at either side, as well as functions of the excess SNRs, the subcarrier spacings and the throughput gains provided over previous similar techniques are numerically verified.

Third, a low-complexity Hann receiver windowed-orthogonal frequency division multiplexing (RW-OFDM) scheme that provides resistance against ACI without requiring any ISI-free redundancies is presented. While this scheme is backward compatible with current and legacy standards and requires no changes to the conventionally transmitted signals, it also paves the way towards future spectrotemporally localized and efficient schemes suitable for higher mobility vehicular communications. A Hann window effectively rejects unstructured ACI at the expense of structured and limited inter-carrier interference (ICI) across data carriers. A simple maximum ratio combining (MRC)-successive interference cancellation (SIC) receiver is therefore proposed to resolve this induced ICI and receive symbols transmitted by standard transmitters currently in use. The computational complexity of the proposed scheme is comparable to that of contemporary RW-OFDM algorithms, while ACI rejection and BER performance is superior in both long and short delay spreads. Channel estimation using Hann RW-OFDM symbols is also discussed.

Finally, the extension of this flexible signaling approach to other radio access technologies (radio access technologies), such as characteristics that could be exploited in the cellular structure and application of these approaches to NOMAs schemes are discussed, and such an extension is exemplified using practical multiple-input-multiple-output (MIMO) systems. Practical MIMO systems depend on a predefined set of precoders to provide spatial multiplexing gain. This limitation on the flexibility of the precoders affects the overall performance. Here, we propose a transmission scheme that can reduce the effect of mismatch between users' channels and precoders. The scheme uses the channel knowledge to generate an artificial signal, which realigns the predefined precoder to the actual channel. Moreover, the scheme can provide an additional level of secrecy for the communication link. The performance of the proposed scheme is evaluated using BER, EVM, and secrecy capacity. The results show a significant improvement for the legitimate user, along with a degradation for the eavesdropper.

Chapter 1: Introduction

Third Generation Partnership Project (3GPP) designed 4G-Long Term Evolution (LTE) to deliver broadband services to masses [1]. The design was successful in doing what it promised, but the one-size-fits-all approach resulted in certain engineering trade-offs. This broadband experience was possible at a certain reliability not allowing ultra reliable and low latency communications (uRLLC) operations, is not the most power-efficient design and is only possible below 120 $\mathrm{km/h}$ mobility [2]. Cellular communication standards beyond LTE are envisioned to provide diverse services with various requirements simultaneously to a myriad of devices. 5G new radio (NR) physical layer was designed to utilize the OFDM waveform [3] with different parameters, called numerologies, allowing prioritization of certain aspects in different applications and made the enhanced-mobile broadband (eMBB) experience possible in a wider range of scenarios [4]. Next generation cellular communication standards beyond 5G mobile communication are planned to schedule non-orthogonal numerology sub-frames in adjacent bands [5]. Numerologies, in their current definition, refer to CP-OFDM waveforms using different subcarrier spacings, and in some cases, various CP rates [6]. For example, while low power Internet of Things (IoT) devices are assigned smaller subcarrier spacings to conserve battery, vehicular communications are operating with higher subcarrier spacings and shorter symbol durations to keep the communication reliable in high Doppler spreads caused by higher speeds.

This shift in paradigm brought with it a problem deliberately avoided by the uniform design. Regardless of the domain MA was performed, the use of a unified orthogonal waveform in the point-to-multipoint downlink (DL) avoided the inter-user equipment (UE) interference problem controlled and avoided in the multipoint-to-point uplink (UL) in all preceding generations of cellular communications. That is, users in adjacent bands are assumed to cause negligible ACI. However,

Figure 1.1: Visual demonstration of temporal standard symbol structure.

by allowing coexistence of different OFDM numerologies in adjacent bands, ACI between UEs sharing these bands arises in the DL [5]. Different numerologies interfere with one-another [7] and ACI becomes the factor limiting data rates if the interfering block outpowers the desired block at the intended receiver [8]. In the UL, although orthogonal waveforms were used in principle, power differences and timing and frequency offsets across UEs caused interference. Although they came at certain costs, strict timing and frequency synchronization across UEs [9] and power control [8] have been historically used to mitigate the interference in the UL. Unfortunately, with the use of different numerologies, these remedies are not a solution to the problem and inter-numerology interference (INI) is inevitable [7] even in the DL. 3GPP acknowledges this problem and gives manufacturers the freedom to implement any solution they choose as long as they respect the standard frame structure [10] seen in Figure 1.1.

While many researchers focused on designing numerologies without changing its conventional structure and tailoring this structure to users needs, at the inception of the studies concluding in this dissertation, alternative OFDM based approaches, e.g., unique word-orthogonal frequency division multiplexing (UW-OFDM), discrete Fourier transformation-spread-orthogonal frequency division multiplexing (DFT-s-OFDM), etc., also had traction as potential candidates. Before we delve into the details of the algorithms featured in this dissertation, we will also discuss the advantages and disadvantages of these technologies in the next section[1].

1.1 Notable CP-OFDM Alternatives

We have earlier denoted that CP is a smart way of utilizing the GI. There are other methods which have recently been gaining attention that utilize the GI as good as CP, and the most prominent one among these methods is UW-OFDM [12]. In UW-OFDM, the GI is filled with a deterministic

[1]Part of that section was published in [11]. Permission is included in Appendix A.

sequence called the UW. To obtain the UW, data subcarriers are multiplied by a precoding matrix, which depends on the desired UW, before the IFFT operation. This multiplication generates data dependent redundant subcarriers. Then, these redundant subcarriers are given as input to the IFFT along with the data symbols. At the output of the IFFT, UW is obtained in the time symbol, without needing any other operations such as copying and pasting as performed for CP. The advantages of UW-OFDM comes from the fact that the UW is a natural part of the IFFT interval. Due to this property, symbols with different unique words can be multiplexed in time and frequency without destroying the orthogonality among various users and applications as long as the inverse DFT (IDFT) length is kept the same. Therefore, UW length can be adjusted by selecting the number of redundant subcarriers and UW-OFDM symbols can be flexibly designed based on the delay spreads experienced by different receivers [13]. Furthermore, the corresponding correlation introduced between the redundant and data subcarriers can be exploited to improve the BER performance [12]. On the other hand, due to the increased complexity stemmed from the precoding and decoding processes, UW-OFDM suffers from complicated receiver and the transmitter structures [14].

In addition to the multicarrier derivatives, there are also quasi-single carrier (SC) structures stemming from OFDM. For example, DFT-s-OFDM can be obtained by adding an M-DFT block before the conventional N-IFFT operation where $M < N$. It is a midway between multicarrier and SC, and is usually categorized as a quasi-SC structure due to this generation process. There are two main reasons this well-known modification of OFDM has been used in the UL of LTE [15]. Firstly, although higher from pure SC, it exhibits lower peak-to-average power ratio (PAPR) compared to the CP-OFDM and requires much lower power amplifier back-off resulting in a higher power efficiency. Secondly, since it is an OFDM-based structure, the scheduling flexibility provided by orthogonal frequency division multiple accessing (OFDMA) can still be used [16].

The circularity of DFT-s-OFDM symbols is also satisfied with the help of CP just like the conventional OFDM implemented in LTE. Recently, methods that fill the GI with different sequences have also been proposed for DFT-s-OFDM. Despite the similarity to the UW-OFDM

approach discussed earlier, filling the GI with specific sequences does not require any precoding operation in DFT-s-OFDM because of its inherent structure [17]. When the sequence, desired to fill the GI, is appended to the data symbols at the input of the M-DFT, the interpolated form of this sequence is obtained at the output of the N-IFFT at no expense of complexity. Furthermore, these schemes can be used by existing DFT-s-OFDM receivers without any modifications as the guard sequences do not impact the data symbols [18]. Considering these facts, a popular alternative to the CP-based DFT-s-OFDM is zero tail (ZT) DFT-s-OFDM [19]. The main motivation behind using a ZT is the ability of adaptation to different channel conditions and data rates just by modifying the number of zeroes [20]. Compared to conventional CP-DFT-s-OFDM, this scheme offers a better block error rate (BLER) performance and reduced OOB leakage as the interference power leaking to the consecutive symbols are reduced and the zeroes are a natural part of the IFFT output, respectively [20]. Having a ZT, however, decreases the average power of the transmitted signal, resulting in a PAPR penalty [18]. This penalty recently forced this approach to evolve into what is called Generalized DFT-s-OFDM, and ZT DFT-s-OFDM remained as a special case where the head and tail are set to zeroes [21]. The UW concept can also be combined with ZT DFT-s-OFDM and gives rise to UW DFT-s-OFDM. It replaces the ZTs with nonzero low energy redundant symbols that further reduce the OOB leakage, PAPR and energy in the tail compared to both UW-OFDM and ZT-DFT-s-OFDM [18]. An enhanced version of UW DFT-s-OFDM concept is given in [22], where an additional perturbation signal is introduced to suppress the ISI energy between the consecutive symbols, which remains even less than the ISI between ZT-DFT-s-OFDM symbols. However, this scheme suffers from the increased receiver complexity and transmitter complexity due to the linear precoding [18]. The techniques described in this section are illustrated in Figure 1.2, along with a comparison with the classical CP-OFDM.

After these potential candidates were evaluated, 3GPP decided to stick with the CP-OFDM waveform used in LTE as the mother waveform for 5G. Furthermore, increasing spectral efficiency is crucial to support the projected number of devices, especially, in lower carrier frequencies,

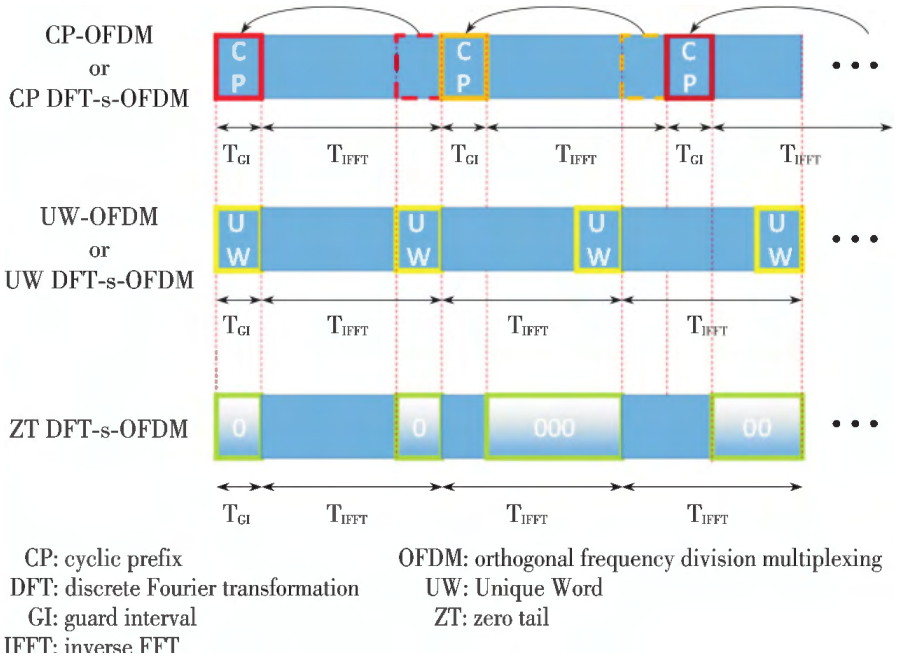

Figure 1.2: Temporal comparison of modified structures' symbols below CP-OFDM, to scale according to LTE extended CP specifications.

favoring reduced guards [5]. Next section discusses contemporary attempts to increase spectral efficiency by reducing the redundancies of modern OFDM systems.

1.2 An Overview of Redundancy Reduction Techniques for OFDM

Classical CP-OFDM is known as one of the most spectrally efficient transmission schemes and sufficiently satisfying the requirements of LTE-Advanced Pro and currently used IEEE 802.11 systems. However, it still suffers from redundancies, in both time and frequency domains. The redundancy in time comes from the use of CP while the redundancy in frequency domain comes from the use of pilot subcarriers and guard bands. In order to adopt OFDM for future radio access technologies and to achieve the aforementioned goals in data rate, these redundancies should be reduced, significantly. The methods that aim to minimize the guard band requirements will be presented throughout this dissertation. Therefore, selected methods that are proposed to reduce the remaining redundancies, i.e., pilots and CP, are drafted in this section[2].

[2]Part of this section was published in [11]. Permission is included in Appendix A.

1.2.1 Pilot Decontamination

A redundancy that has been with OFDM since it became practical is the use of pilots within the subcarriers. In time domain duplexing (TDD) systems, inside a cell, the mobile stations transmit mutually orthogonal pilot sequences to the base station (BS) so that the BS can estimate the channel in the UL, and assuming channel reciprocity, precode accordingly for the DL. In the case of frequency domain duplexing (FDD) systems, because the channel state for the UL and DL is different, a two-stage procedure is required. The BS first transmits pilot symbols and then, the users feedback their channel state information to the BS. For the massive MIMO concept with the TDD case, many beams are established for a vast number of users compared to the past. Each beam requires a different mutually orthogonal sequence, which increases the length of the sequences immensely and decreases the resources available to transmit data symbols. For the FDD case, the same situation happens as the number of transmit antennas at the BS goes to infinity. A proposed method to reduce this overhead is reusing pilot sequences of nearby cells, which introduces inter-cell-interference and gives rise to the "pilot contamination" effect [23]. The high number of lengthy pilots also increases the latency and makes IoT-type sporadic and short messages inefficient.

Some researchers allow the use of the pilots but try to reduce the overhead, which can be referred to as soft pilot mitigation. In [24], the authors propose using only the amplitudes of the subcarriers as the pilots, and the phase of the same subcarriers can be used to transmit information in an effort to increase the data rate. In [25], the author proposes many techniques to mitigate pilot contamination for the TDD case. The terminals are suggested to match the DL reference signal powers in the UL, in order to both reduce overall pilot interference in the neighboring cells and to reduce the pilot overhead required for closed loop power control. Another suggestion is reusing pilots softly to avoid inter-cell-interference. Some pilot sequences are proposed to be assigned for use only at the cell edge whereas the same groups of pilot sequences can be transmitted with less power near the BSs. Even further, the author suggests that the angular resolution provided by the massive number of antennas can be used to coordinate pilot allocation between cells and safely reuse the pilot sequences for spatially separated terminals. In [26], the authors have aligned the

power delay profiles (PDPs) of the users served by the same BS to orthogonalize the pilots sent within the common OFDM symbol. By aligning the PDPs for the same number of users that can be sounded within the same symbol, it has been shown that the average SNR can increase by half.

Another group of researchers has proposed blind channel estimation or signal detection techniques to remove pilots completely, which would be appropriately called hard pilot mitigation. In [27], the authors have shown that pilots can completely be removed as the singular-value decomposition (SVD) of the received signal matrix projects the received signal onto an interference-free subspace governed by an easily predictable non-linear compound. The authors have demonstrated that the proposed subspace projection method outperforms linear channel estimation if a power margin between the users of interest and interfering users are provided, especially when the base station antennas outnumber the coherence time (in number of symbol durations). In [28], the authors have treated the detected UL data as pilot symbols to obtain the least squares estimate of the channel. Also, by estimating the channels of all users sequentially, they obtained extracting vectors which extract the desired data from the mixture signal, accurately.

1.2.2 CP Reduction

In communication channels with multipath delay spread, a guard interval (GI) is required to prevent leakage in time between the successive symbols. CP is a smart way to utilize the guard interval by copying the samples from the end of a symbol and pasting them to its beginning. Thus, the linear convolution of the channel becomes a circular convolution, which makes the channel matrix diagonalizable only by taking its Fourier transform and enables a simple equalization in the frequency domain. The length of the CP is chosen to be larger than the expected delay spread to avoid any ISI and ICI. Also, in order to maintain orthogonal coexistence of neighboring transmission blocks, predefined values have been used for the length of the CP and applied to all the blocks. For example, two CP rates are defined in LTE where the normal CP duration in terms of symbol duration T_{SYM} is given as $T_{SYM} \times 9/128$ while the extended CP duration is $T_{SYM} \times 32/128$.

Recent works have shown that extending the CP duration might not be the best approach to combat against long delay spreads [29–31]. The newly proposed 5G scenarios have introduced their own methods for ISI mitigation. An example is mmWave MIMO systems that employ highly directional transmission using beamforming. For such systems, beam switching reference signals are broadcasted so that the receivers can determine which predefined beam is directed to their way, resulting in higher signal to interference plus noise ratio for all receivers. Inventors have shown in [29] that such signals not only provide support for beam switching but can also be used to estimate delay spread exceeding CP duration. Then, ISI could be canceled from received symbols which reduces the required CP. In [30], authors claim that MIMO receivers can identify the presence of any residual interference after equalization by evaluating the channel matrix. It was shown that decreasing the modulation and coding index instead of extending the CP length, would increase the throughput. In addition to these methods, advanced signal processing techniques can be employed to mitigate the interference. A good example of that is the bi-directional M-algorithm based equalizer proposed in [31]. It has shown that a system which experiences a delay spread six times longer than the CP duration exhibits the same performance of a conventional system with sufficient CP. It is achieved at only the expense of performing two iterations of the proposed algorithm referred to as trellis-based interference detection and mitigation.

In some scenarios, the maximum excess delay might be much less than the duration of normal CP which makes the minimum CP overhead of 7% a pointless guard for LTE systems. To reduce this overhead, the authors of [32] present the idea of a flexible frame design. A wider range of options in terms of subcarrier spacing and CP length are used for the OFDM symbols inside the proposed frame structure. Then, the users experiencing similar channel dispersions are grouped and the proper symbol parameters are determined for each group within the frame. Thus, overall efficiency is enhanced by avoiding inconvenient parameter selection. An extension of this approach to mmWave single user MIMO systems can also be found in [29], where the use of additional subframe configurations is presented independently for each user. Increasing the number of options for the CP duration is also recommended in the 3GPP standard contributions.

CP overhead also constitutes a disadvantage for the low latency required applications as it introduces delays in the transmission which might cause drawbacks for 5G services such as uRLLC. For instance, using CP durations shorter than users' MEDs are proposed [33] to satisfy the lower latency required by new services in systems beyond 5G while increasing spectral efficiency. In the algorithm proposed in [33], the author removed the CPs entirely from all symbols except the first one for reducing total transmission delay. This technique uses the CP of the first symbol to obtain a detailed estimation of the channel time and frequency characteristics. Afterwards, the subcarrier spacing is reduced to $\frac{\Delta_f}{N_{SYM}-1}$ where Δ_f denotes the subcarrier spacing used in the first symbol and N_{SYM} denotes the total number of symbols including the first one. All symbols sent later are combined to fit in the same bandwidth used by the first symbol sampled with N_{OFDM} points using an inverse FFT (IFFT) size of $(N_{SYM}-1) \times N_{OFDM}$, and sent as a single symbol without CP. Thus, the total transmission time is reduced by $(N_{SYM}-1) \times T_{CP}$, where T_{CP} is the CP duration.

Up to this point, we have covered two issues that shadow the success of future cellular communication systems. The first issue regards the INI, or by the more common name, ACI problem that will be limiting the future systems. The second problem is a need to reduce the redundancies in the system. Remedies to the second problem have been covered, thus let us cover the potential remedies to the first problem, and reveal the connection between the two problems.

Historically, possible ACI due to interferers in adjacent bands are either mitigated using interference cancellation [34], avoided by increasing guard bandwidth until ACI power becomes negligible [35], or suppressed [36]. Nodes can reject ACI by filtering [37]. Filtering requires matched filtering operation at the both ends of the communication system for optimal performance [38]. If not already implemented at both nodes, this requires modifying the device lacking this function, which is unfeasible for UEs that are produced and in-use. The additional complex multiplication and addition operations required to filter the signal increase the design complexity of the modem, which in turn increase the chip area, production cost, power consumption, and operational chip temperature and reduces the lifetime of the device and battery [39]. Introducing these operations at the next generation NodeB (gNB) can be justified to improve system performance,

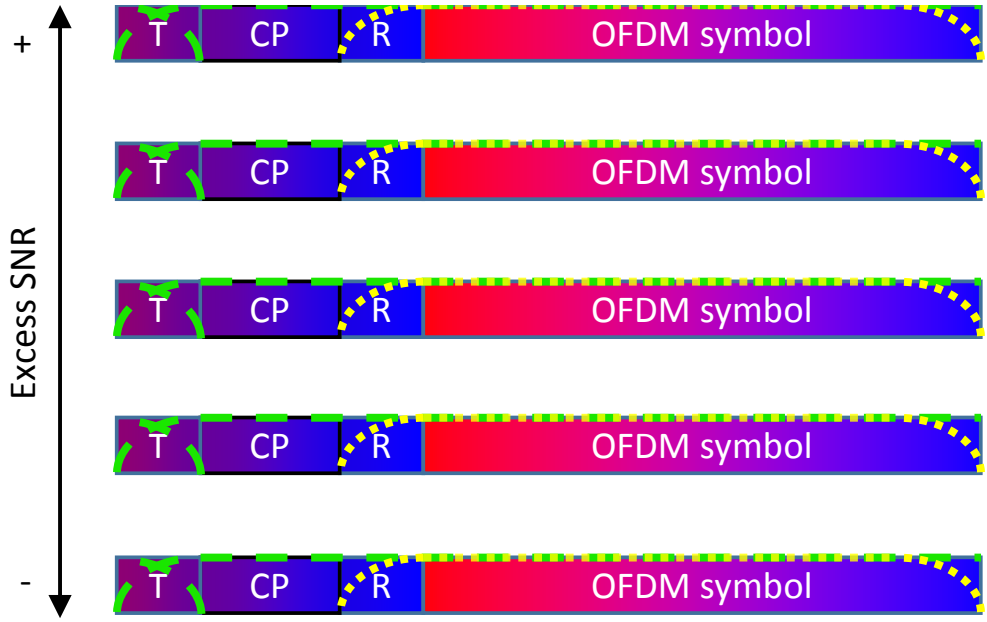

Figure 1.3: Visual demonstration of structure used in previous windowing literature. The rectangles are alotted times for the actual OFDM symbol, CP, and further cyclic extensions for "T"ransmitter and "R"eceiver windowing, while the green dash and yellow round dot overlays demonstrate transmitter and receiver windowing of the underlying area, respectively.

however the takeaways may cause IoT devices to fall short of their key performance indicators (KPIs) and is undesirable [40].

The most prominent alternative approach to suppress ACI is windowing due to its low computational complexity and high efficacy [41]. Windowing can be applied at the transmitter to reduce OOB emission and corresponding ACI before it eventuates [42], or at the receiver [43] to reject present ACI and is extensively studied in the literature [44]. However, all references utilize the same window function at all subcarriers, while it is known that edge subcarriers are more critical in OOB emissions and are more prone to present ACI. Motivated by this property, [45] introduces subcarrier specific window (SSW) concept at the transmitter side whereas [46] introduces optimal SSW function design for both transmitter and receiver.

In [46] and most of the preceding literature focusing on windowing, windowing was performed by extending the symbols by an amount which was arbitrarily chosen without explanation, in addition to standard CP duration seen in Figure 1.3, and the focus was on deriving window func-

tions optimized according to maximize standard performance metrics. These extensions reduce the symbol rate and change the frame structure defined in the standard, thus creating nonstandard signals that are not orthogonal to the symbols that aims to share the same numerology [5]. Thus, the symbol structure defined in both 4G and 5G mobile communication standards [6], shown in Figure 1.1, is modified. Even if any gain for the desired user itself can be made possible by incorporating such extension for receiver windowing, introducing such elevated interference to others is not allowed by the current standards [47]. Furthermore, additional extensions for windowing is the increase in the effective symbol duration which reduces the effective symbol rate. Conventional CP-OFDM receivers are designed assuming the CP is longer than the MED of the desired users channel to not experience ISI. This is achieved by avoiding channels with MEDs longer than CPs by elongating the CP durations, such as the extended-CP option in LTE. Extending the symbol duration relentlessly causes the symbol duration to exceed the coherence time of the channel, which is a critical problem for high-speed vehicular communications [5]. Due to the time variation of the channel in high mobility systems, the additional extensions not only cause a direct reduction in data rate but also either further cuts the data rate back when relative pilot overhead is increased to mitigate the reduction in absolute pilot periodicity or reduces capacity due to the channel estimation errors when no modification is done [48]. In order to achieve reliable high mobility vehicular communications, there is an apparent need to shorten the cyclic extensions instead of further elongating them. In [45], the authors attempted to improve spectral efficiency of windowed OFDM systems by not applying windowing to the REs of inner subcarriers assigned to UEs experiencing long delay spreads and applying windowing on the edge subcarriers using the excess CP assigned to UEs experiencing short delay spreads. While effective, this scheme is only applicable if all UEs utilize the same numerology. Addressing conventional systems, [45] assumes CP is longer than the MED of the channel to accommodate windowing and limit the window length to the guard interval that is not disturbed by multipath reception while [46] even allocates additional samples for windowing, reducing spectral efficiency. Thus, the augmented guards promoted by [46] aside, even the more than sufficient CP required by [45] becomes a luxury in current trend. These conventional

approaches do not address the requirements of communication systems beyond 5G and therefore need to be extended. Furthermore, both ends of the communication must be aware of and agree to make such a change. This causes backward compatibility issues with devices in use. Whether it is more beneficial to window a duration at the transmitter or receiver was not discussed in the literature.

In Chapter 2, we propose the first standard compliant windowing scheme, in which we derive the receiver windowing durations that optimize reception of each subcarrier in the case which ISI and ACI occur simultaneously and pulse shapes of transmitters operating in adjacent bands cannot be controlled, in the absence of any extension designated for windowing. We utilize insufficient CP optimally to jointly minimize ISI and ACI, addressing spectral efficiency requirements of systems beyond 5G and the corresponding real-time conditions adaptively. To the best of authors' knowledge, this is the first work proposing windowing in a system with insufficient CP. We first determine incident ISI caused by insufficient CP, ACI caused by different numerologies in adjacent bands, and the combined interference power for each subcarrier as it is the optimization metric to be minimized. These analyses lay out the framework for optimal SSW functions at the receiver, but we limit the discussion to raised cosine receiver window lengths. We also analyze the interference reduction performances of resulting optimal SSW and fixed length windowing compared to no receiver windowing; with window lengths determined for current and outdated CIRs and PDPs to demonstrate the possible gains and robustness of the design example.

Chapter 3 aims to extend Chapter 2 by evaluating how network capacity can be further improved if the pulse shapes of the transmitted waveforms can also be designed while conserving the standard frame structure, that is, not adding any additional extensions other than CP and using only the present CP for windowing. In Chapter 3, we propose two independent algorithms that aim to determine the amount of windowing that should be applied at either side to maximize fair proportional network capacity. Unlike Chapter 2 in which receiver windowing duration calculations required CIRs knowledge, the proposed receiver windowing duration calculation algorithm in this work solely uses statistics derived from the received signals. This significantly reduces

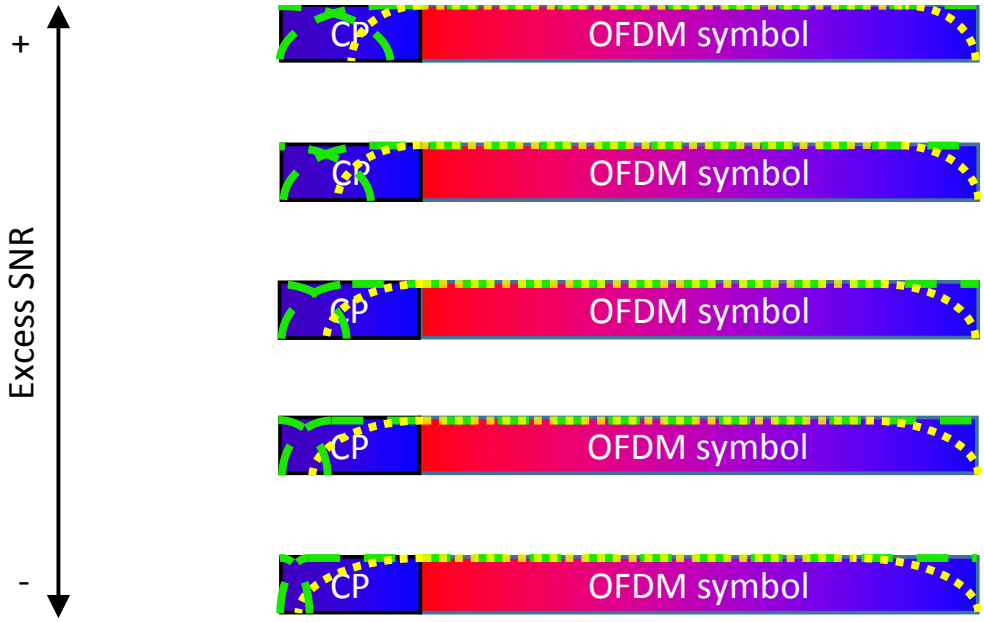

Figure 1.4: Visual demonstration of the adaptive CP concept presented in the Chapter 3 of this dissertation. The rectangles are alotted times for the actual OFDM symbol, CP, and further cyclic extensions for "T"ransmitter and "R"eceiver windowing, while the green dash and yellow round dot overlays demonstrate transmitter and receiver windowing of the underlying area, respectively.

the complexity and eases implementation, and makes the algorithm completely practical as no information is needed. The proposed transmitter windowing duration calculation algorithm aims to maximize the network spectral efficiency by assigning high transmit window durations only to REs with excess signal to interference plus noise ratio (SINR) that can withstand the ISI caused by windowing. This reduces the ACI in the system with minimum impact to the REs applying windowing. Neither algorithm requires any control data transfer to other parties of the communication or changes to the other nodes at any point. The proposed utilization of the standard symbol structure as a function of excess SNR is shown in Figure 1.4. Numerical results confirm that fair proportional network spectral efficiency can be increased greatly without disrupting the standard frame structure by utilizing CP adaptively, and determining transmitter windowing durations using excess SINR of REs and data-aided receiver windowing duration determination are an effective metrics.

Our contributions in Chapter 3 are as follows:

- Computationally efficient per-RE transmitter and receiver windowing of signals synthesized and analyzed using conventional CP-OFDM are derived.
- A computationally efficient per-RE transmitter window duration estimation algorithm for gNBs that maximizes the fair proportional network throughput based on UEs channel conditions and does not require any information transfer to or modification at UEs is presented.
- A computationally efficient per-RE receiver window duration estimation algorithm for gNBs and UEs that maximizes the capacity of each RE and does not require any information transfer from or modification at the transmitter is presented.
- The computational complexities of the aforementioned algorithms are derived.
- The algorithms are numerically analyzed in terms of OOB-emission reduction, throughput improvements, relation of window duration estimates with excess SNR, spectrotemporal correlation and accuracy of window duration estimates.

However, all algorithms proposed in Chapters 2 and 3 still require an abundant periodic extension of the transmitted signal and reducing ACI with these approach comes at the cost of introducing ISI, which consists of the sum of the low powered contributions from all subcarriers of the previous symbol. The computational complexity of canceling the ISI is high due to the large number of interfering components. Furthermore, this approach is not effective with shorter CP durations that are associated with vehicular communication numerologies. Consider Figures 1.5 and 1.6, which shows the PSDs of the the sixth subcarrier from the band-edge of different OFDM variations and window functions. The PSD labeled as "Slepian [49] Win." in Figure 1.5 is obtained by performing receiver windowing operation presented in [46] on an extended CP numerology [6] using the entire CP duration of a small subcarrier spacing, long duration OFDM symbol. In this case, the window works as expected and is able to confine the spectrum within the resource block (RB) as intended, and consistently fades throughout the spectrum. However, if the

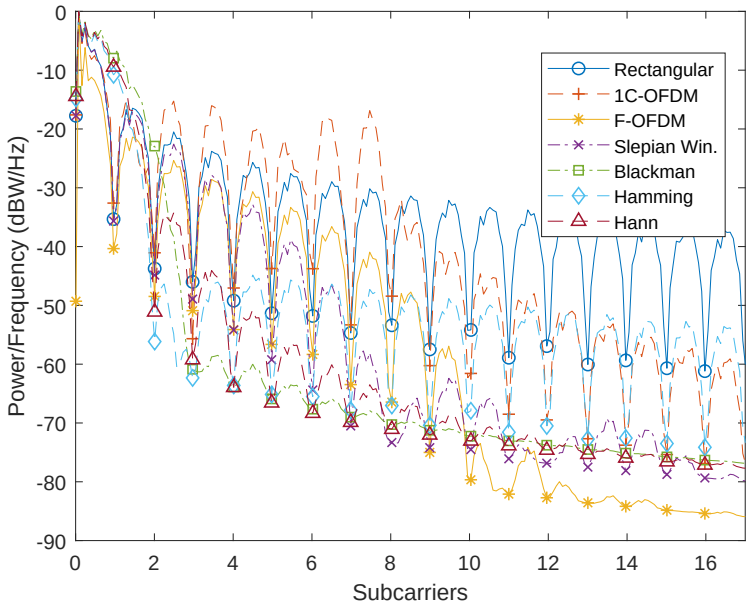

Figure 1.5: The PSDs of OFDM schemes and window functions applied to a long duration OFDM symbol with extended CP rate. The markers indicate FFT sampling points.

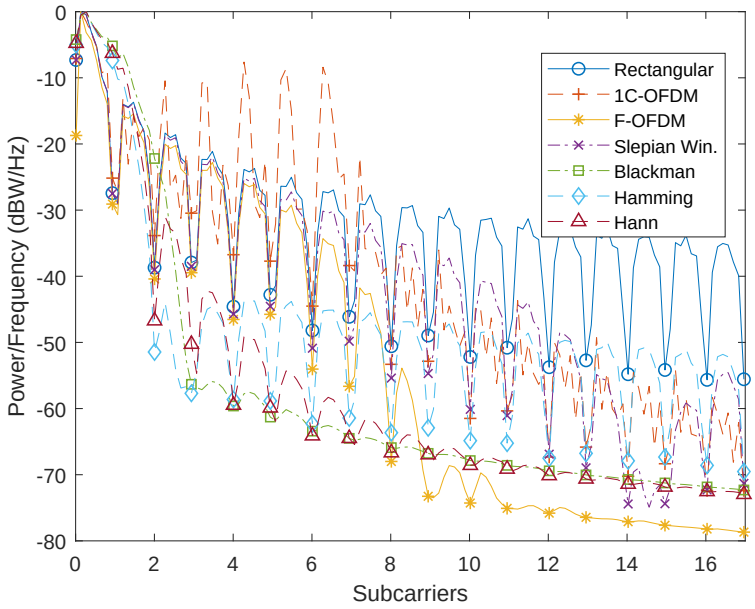

Figure 1.6: The PSDs of OFDM schemes and window functions applied to short duration OFDM symbol with normal CP rate. The markers indicate FFT sampling points.

same algorithm is applied to a short duration vehicular numerology with normal CP overhead, as shown in Figure 1.6, the window underperforms and provides a limited benefit over the standard rectangular window even if the whole CP duration is still used. Furthermore, the PSD behaves inconsistently throughout the spectrum due to the limited resolution especially for the subcarriers of the edgemost RB as presented, oscillating to high powers away from the subcarrier of interest. Also note that this is the performance upper bound for a normal CP overhead. If a shorter window duration is used to utilize part of the CP for its actual purpose to mitigate multipath channel and limit ISI, the performance reduces further. Filtered-Orthogonal frequency division multiplexing (F-OFDM) [37] does not suffer from the same problem, but requires changes at the transmitting device and is computationally complex. N-Continuous orthogonal frequency division multiplexing (NC-OFDM) [50] can be utilized by all devices in the band to consistently reduce the ACI levels regardless of symbol duration, but this scheme also requires changes at both transmitting and receiving devices, and also introduces in-band interference as seen in Figures 1.5 and 1.6. There is an apparent need for a reception algorithm that does not modify the standard transmitter, has low computational complexity, and is robust against delay spread without requiring extensions, and is not affected by the FFT size.

In a regular OFDM based system, if no redundancy is used for windowing, and a receiver window function other than rectangular is used, the zero crossings of the window's frequency response differs from that of the transmitted subcarriers [44]. This causes heavy ICI between the received subcarriers, resulting in problems greater than the avoided ACI [43]. Attempting to cancel the resulting ICI yields little return if the ICI consists of weak contributions from numerous subcarriers, and the computational complexity and success of the cancellation renders such implementation impractical in general. Some window functions commonly used in signal processing reveal special cases [51] if the windowing operation depicted in Figure 1.7 is performed, limiting the number of interfering subcarriers which may be exploited to possibly enable gains. A strong candidate is the Blackman window function, which provides promising ACI rejection seen in Figures 1.5 and 1.6. However, the main lobe of the Blackman window function spans

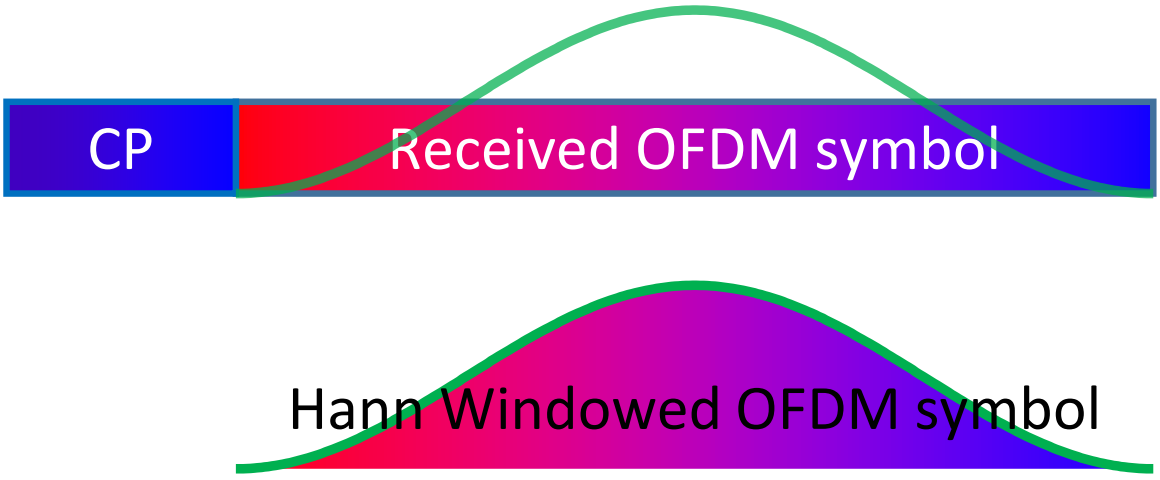

Figure 1.7: Hann receiver windowing process explained in Chapter 4 using standard symbol structures.

2 adjacent subcarriers on the shown right hand side spectrum and 2 more on the not-visible left hand side, thereby including high-power ICI from a total of 4 subcarriers. This results in computationally intensive reception and limits capacity gains. Another strong candidate is the Hamming window function, which only interferes with the closest 2 adjacent subcarriers, hence enabling lower-complexity reception. The ACI rejection performance of Hamming window function in the subcarriers that immediately follow the main lobe is also unmatched. However, considering the ACI rejection performance throughout the rest of the spectrum and the power of the inflicted ICI due to windowing, the Hann window function is distinguished from other candidates and is chosen in this study to satisfy this apparent need. A similar investigation during the design of the Global System for Mobile Communications (GSM) system led in favor of the gaussian minimum shift keying (GMSK) pulse shapes that are inherently non-orthogonal only with a finite number of symbols around them and SIR degradation is manageable in severe multiple access multipath channel conditions, instead of other candidates that are ideally orthogonal but suffer severe SIR degradation once this orthogonality is lost due to multiple access multipath channel [52]. Because of the aforementioned spectral features, Hann windowing similarly converts a complex ACI problem, with its out-of-band rejection performance comparable to optimum windowing as

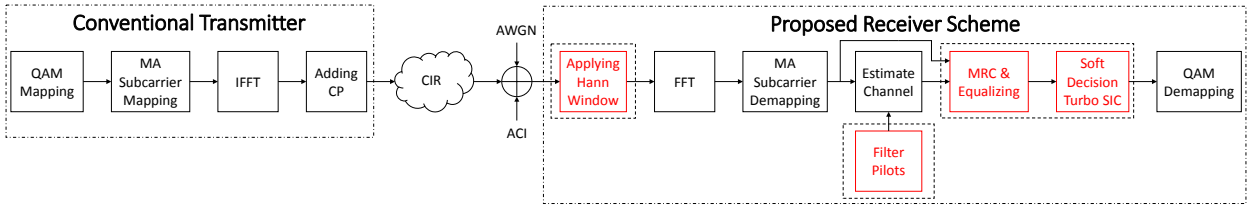

Figure 1.8: The block diagram of the scheme proposed in chapter 4, highlighting the modifications to the standard receiver structure with dashed blocks (standard transmitter is not modified).

shown in Figure 1.5, to a manageable ICI problem requiring little computational complexity at the receiver [53, 54].

In chapter 4, we present a novel transceiver algorithm that mitigates the ICI resulting from Hann windowing. This algorithm performs well regardless of OFDM symbol duration, CP duration or delay spread. The algorithm is solely a receiver algorithm that can be used to receive the signals transmitted from a conventional legacy transmitter using any modulation. Therefore the systems using either of the proposed algorithms are interoperable with future and legacy standards. This algorithm consists of maximizing SINR first using MRC, afterwards mitigating the ICI using a soft decision turbo SIC equalizer. Furthermore, the computational complexity of the algorithm is less than or comparable to [46], while a higher performance is achieved in most conditions. A block diagram of the proposed method is presented in Figure 1.8.

Our contributions in Chapter 4 are as follows:

- A redundancy free RW-OFDM scheme that outperforms prior art without requiring changes to the standard frame structure regardless of channel conditions is proposed. The proposed scheme has high ACI rejection performance at the expense of a structured ICI that can be resolved without computationally intensive computations.

- A channel estimation technique of Hann RW-OFDM symbols and 5G mobile communication system pilots is proposed.

- The ICI contribution from and to each subcarrier resulting from application of a Hann window to a received OFDM signal is derived.

- MRC coefficients maximizing the SINR of a Hann RW-OFDM receiver as a function of the ACI, noise power and ICI is derived.
- The ICI contribution from and to each subcarrier resulting from application of MRC is derived.
- The computational complexity of the proposed scheme is derived.

Up to this point, all discussion takes place on signaling design for single cell, single antenna systems. There are other things that can be taken into consideration such as cellular structure, thing that can be done on a multiple accessing level and extensions to multiple antennae. In Chapter 5, these aspects are discussed and an extension to multiple antenna systems is exemplified.

Multiple antenna systems have been essential part of almost all current wireless systems, and will be part of any upcoming wireless standard. MIMO systems introduce additional degrees of freedom that can be utilized to provide diversity, facilitate multiplexing, or enhance secrecy. The capacity and available degrees of freedom of MIMO systems were thoroughly investigated, and the studies shows the significant gain that can be achieved [55].

With the expected migration towards higher frequency ranges (i.e., mmWave) in the next generation networks, another form of MIMO systems is expected to be adopted, namely, hybrid MIMO. In mmWave a larger number of antennas can be packed into smaller sizes. As promising as that sounds, that large number imposes a huge load on the system in terms of both software and hardware. Hybrid MIMO introduces a cost reduction to the system by reducing the number of used RF chains, where each subset of antennas is derived using a single RF chain [56]. Then, using only a set of phase-shifters, an analog beamformer is applied for that subset of antennas.

On another hand, in a fully digital or hybrid MIMO, signal precoding raises a computational complexity issue. The optimization of the precoders usually involve a heavily computational processes. Moreover, the overhead to transfer the precoding information between the transmitter and receiver deems this approach unfeasible. In order to avoid both issues, the current wireless standards rely on codebooks [57]. The predefined codebook reduces complexity by avoiding the

computational processes. Also, it reduces the overhead as the index of the used precoder is only information required to be transferred.

A downside of having a predefined codebook is the availability of such information to the public. This availability can help any malicious node in the system to receiver the data correctly. This lack of information security goes against the philosophy of next generation networks. The future networks include some application with highly sensitive information (e.g., remote surgery). These applications require additional measures for information security, which brings physical-layer security to the picture. In physical layer security, the unique characteristics of the communications medium (i.e., channel) is used to protect the data from different malicious attacks (e.g., eavesdropping) [58].

To this day, the wireless community has been focusing on the design of precoders in general [59], or codebooks design specifically [60]. Moreover the designed codebooks usually have a single aim either enhanced achievable rate, better energy efficiency, or lower complexity [61]. Beside the precoding design, artificial noise (AN) insertion approaches are used to provide some security measures [62]. AN approaches try to balance the trade-off between performance and security using different noise power allocation algorithms [63].

In Chapter 5, we propose two different approaches to construct an artificial signal. That artificial signal is designed to realign the codebook-based precoders to the actual MIMO communication channel. Such a design has the following benefits:

- Easy direct implementation that avoids the power allocation optimization required by the AN insertion algorithms.
- Enhanced performance for the legitimate user by mitigating the mismatch between codebook precoders and the actual channel.
- Additional layer of secrecy as the transmitted signal is constructed using the channel information of the legitimate user.
- Using the same simple feedback structure, which will keep the adopted reduced overhead.

To summarize, in this dissertation, we will mostly discuss backward compatible windowing algorithms that are transparent to the communication counterpart and can be utilized noncooperatively, and demonstrate an example extension of such algorithm carrying similar characteristics to MIMO systems.

The rest of this dissertation is organized as follows:

- in Chapter 2: we derive the ACI, ISI and ICI affecting a RW-OFDM system under a time-invariant MA multipath channel. Accordingly, we propose a SSW duration calculation algorithm for UL reception that minimizes the combined interference jointly and evaluate the gains of this algorithm.

- in Chapter 3: we extend the derivations of Chapter 2 to time varying channels and accordingly propose two more algorithms. First algorithm comprises calculating the optimum window duration of each RE in a transparent transmitter windowed-orthogonal frequency division multiplexing (TW-OFDM) system computationally efficiently for DL transmission. The second algorithm comprises calculating the optimum window duration of each RE solely using received signal statistics in a transparent RW-OFDM system computationally efficiently at any receiver.

- in Chapter 4: we propose a novel non-redundant transparent non-orthogonal RW-OFDM technique that does not require any redundancy (CP) and outperforms the previously presented RW-OFDM algorithms in the case of narrowband time-varying MA multipath low-SNR telecommunication channels.

- in Chapter 5: we provide our perspective on the possible future research topics in this area, exemplify this with an extension of this work to codebook- and mechanical beamformer based MIMO communication systems.

- in Chapter 6: we conclude the presented work.

Chapter 2: Adaptive Windowing of Insufficient CP for Joint Minimization of ISI and ACI for Beyond 5G Receivers

A 1-indexed algebra is used in this Chapter[3] where $\mathbf{I}_N$ is the $N \times N$ identity matrix, $\mathbf{0}_{N\times M}$ is the $N \times M$ zero and $\mathbf{1}_{N\times M}$ is the $N \times M$ ones matrix. Conjugate, transpose and Hermitian operations are denoted by $(\cdot)^*$, $(\cdot)^T$ and $(\cdot)^{\mathcal{H}}$, respectively. $\mathbf{A} \odot \mathbf{B}$ is the Hadamard product of matrices $\mathbf{A}$ and $\mathbf{B}$ and $\mathbf{A} \oslash \mathbf{B}$ denotes the Hadamard division of $\mathbf{A}$ to $\mathbf{B}$. $\mathbf{X}^{\odot 2}$ is the Hadamard product of matrix $\mathbf{X}$ with itself. $\mathbb{E}_a\{\cdot\}$ is the expectation operator over variable a. $\mathrm{diag}(c_1, c_2, \ldots, c_N)$ represents the $N \times N$ diagonal matrix with diagonal elements $c_1, c_2, \ldots, c_N$, $\mathrm{toep}(A, B)$ denotes the Toeplitz matrix of which first column is A and first row is B, $\delta(\cdot)$ is the Dirac delta function, $\mathcal{N}(\mu; \sigma^2)$ is the normal distribution with mean μ and variance σ^2, and $\bowtie(\cdot)$ is the function that flips a matrix from left to right, i.e., $\mathbf{X}_{M,n} = \bowtie(\mathbf{X}_{M,N-n+1})$. All properties existing with subscripts $\cdot_u$ denote that the given matrix or vector is associated with the uth user.

2.1 System Model

Let $\mathbf{s}_u \in \mathbb{C}^{M_u \times I_u}$ denote the modulated data symbols, where M_u is number of uth user's data subcarriers and I_u is the number of uth user's OFDM symbols in a frame. $\mathbf{Q}_u \in \mathbb{R}^{N_u \times M_u}$ is uth user's subcarrier mapping matrix. $\mathbf{A}_u \in \mathbb{R}^{N_u+K_u \times N_u}$ is uth user's CP insertion matrix , consisting of

$$\mathbf{A}_u = \begin{bmatrix} \mathbf{0}_{K_u \times (N_u - K_u)} & \mathbf{I}_{K_u} \\ & \mathbf{I}_{N_u} \end{bmatrix} \tag{2.1}$$

[3]Part of this chapter was published in [64] and patented [65, 66]. Permission is included in Appendix A.

in case of no transmitter windowing where K_u is the number of CP samples. The CP removal and windowing matrix $\mathbf{B}_{L^{\mathrm{w}}_{n,i,u}} \in \mathbb{R}^{N_u \times N_u + K_u}$ is shown as

$$\mathbf{B}_{L^{\mathrm{w}}_{n,i,u}} = \begin{bmatrix} \mathbf{0}_{N_u - L^{\mathrm{w}}_{n,i,u} \times K_u - L^{\mathrm{w}}_{n,i,u}} & \mathbf{0}_{N_u - L^{\mathrm{w}}_{n,i,u} \times L^{\mathrm{w}}_{n,i,u}} & \mathbf{I}_{N_u - L^{\mathrm{w}}_{n,i,u}} & \mathbf{0}_{N_u - L^{\mathrm{w}}_{n,i,u} \times L^{\mathrm{w}}_{n,i,u}} \\ \mathbf{0}_{L^{\mathrm{w}}_{n,i,u} \times K_u - L^{\mathrm{w}}_{n,i,u}} & \mathrm{diag}\left(\bowtie\left(W_{n,i,u}\right)\right) & \mathbf{0}_{L^{\mathrm{w}}_{n,i,u} \times N_u - L^{\mathrm{w}}_{n,i,u}} & \mathrm{diag}\left(W_{n,i,u}\right) \end{bmatrix}, \quad (2.2)$$

where $L^{\mathrm{w}}_{n,i,u} \in \{0, 1, \ldots, K_u\}$ is the taper length of either side of the window in number of samples, used for the reception of the nth subcarrier of ith OFDM symbol of uth user and $W_{n,i,u} \in \mathbb{R}^{1 \times L^{\mathrm{w}}_{n,i,u}}$, the receiver window coefficients, are calculated using $\mathrm{W}\left(k; L^{\mathrm{w}}_{n,i,u}\right) = 0.5\left(1 + \cos\left(\frac{\pi k}{L^{\mathrm{w}}_{n,i,u}+1}\right)\right)$, $k = 1, 2, \ldots, L^{\mathrm{w}}_{n,i,u}$, which generates raised cosine window coefficients using taper length instead of roll-off. Note that for $L^{\mathrm{w}}_{n,i,u} = 0$, eq. (2.2) simplifies to $\mathbf{B}_0 = \begin{bmatrix} \mathbf{0}_{N_u \times K_u} & \mathbf{I}_{N_u} \end{bmatrix}$, which is the CP removal matrix without windowing.

$h_{i,u} \in \mathbb{C}^{1 \times L_u}$ denotes the CIR invariant during reception of the corresponding OFDM symbol where L_u is the MED uth user experiences in number of samples, which is obtained by $h_{i,u}(k) = \sqrt{P_u \frac{1-\alpha_u}{1-\alpha_u^{L_u}} \alpha_u^k} v(k)$ where P_u is the received power of uth user's signal, α_u is the exponential decay rate of uth user's channel and $v(k) \in \mathbb{C}^{1 \times L_u} \sim \mathcal{CN}(0, 1)\ \forall k \in \{0, 1, \ldots, L_u - 1\}$ [67]. Then, $\mathbf{h}^{\mathrm{conv}}_{i,u} \in \mathbb{C}^{N_u + K_u \times N_u + K_u}$ is the linear channel convolution matrix bounded to one symbol duration, where $\mathbf{h}^{\mathrm{conv}}_{i,u} = \mathrm{toep}\left(\begin{bmatrix} h_{i,u} & 0_{1 \times N_u + K_u - L_u} \end{bmatrix}^T, \begin{bmatrix} h_{i,u}(0) & 0_{1 \times N_u + K_u - 1} \end{bmatrix}\right)$. $H_{i,u} \in \mathbb{C}^{N_u \times 1}$ is the channel frequency response (CFR) of uth user's ith OFDM symbol, which can be calculated as $H_{i,u} = \sqrt{N_u}\mathbf{F_u} \begin{bmatrix} h_{i,u} & \mathbf{0}_{1 \times N_u - L_u} \end{bmatrix}^T$. Let us define the ISI free condition as

$$K_u - L^{\mathrm{w}}_{n,i,u} \geq L_u \quad , \forall n \in \{1, 2, \ldots, N_u\}\ . \quad (2.3)$$

Assume desired OFDM symbol is the dth OFDM symbol of 0th user. Let us first assume the absence of the interfering users and eq. (2.3) is satisfied. In this case the product $\mathbf{B}_{L^{\mathrm{w}}_{:,d,0}} \mathbf{h}^{\mathrm{conv}}_{d,0} \mathbf{A}_0$

results in the perfect circular channel convolution matrix $\mathbf{h}_{d,0}^{\text{circ}} \in \mathbb{C}^{N_0 \times N_0}$ shown as

$$\mathbf{h}_{i,u}^{\text{circ}} = \text{toep}\left(\begin{bmatrix} h_{i,u} & 0_{1\times N_u - L_u} \end{bmatrix}^T, \begin{bmatrix} h_{i,u}(0) & \bowtie \left(\begin{bmatrix} h_{i,u}(1:L_u-1) & 0_{1\times N_u - L_u} \end{bmatrix}\right) \end{bmatrix}\right). \quad (2.4)$$

Furthermore, $\mathbf{F}_0 \mathbf{B}_{L_{:,d,0}^{\text{w}}} \mathbf{h}_{d,0}^{\text{conv}} \mathbf{A}_0 \mathbf{F}_0^{\mathcal{H}}$ results in $\text{diag}(H_{d,0})$, where $\mathbf{F}_u \in \mathbb{C}^{N\times N}$ denotes the normalized FFT matrix uth user uses in the generation and reception of OFDM symbols. Hence, ignoring the noise, the received symbols $y_{:,d,0} \in \mathbb{C}^{N_0\times 1}$, where $y_{:,d,0} = \mathbf{F}_0 \mathbf{B}_{L_{:,d,0}^{\text{w}}} \mathbf{h}_{d,0}^{\text{conv}} \mathbf{A}_0 \mathbf{F}_0^{\mathcal{H}} \mathbf{Q}_u s_{:,d,0} = \text{diag}(H_{d,0})\, s_{:,d,0} = H_{d,0} \odot s_{:,d,0}$. $y_{:,d,0}$ is equalized using zero forcing (ZF) equalization [68] via a similar Hadamard division by CFR to obtain the symbol estimates $\hat{s}_{:,d,0} \in \mathbb{C}^{N_0\times 1}$:

$$\hat{s}_{:,d,0} = \mathbf{Q}_u^{\mathcal{H}} \left(y_{:,d,0} \oslash \hat{H}_{d,0}\right), \quad (2.5)$$

where $\hat{H}_{d,0}$ is the desired OFDM symbol's CFR estimated at the receiver.

In this work, although there would be residual ISI as eq. (2.3) is invalid, equalization will still be performed as in eq. (2.5) and no interference cancellation technique other than receiver windowing is applied to reduce the ACI and residual ISI. In the scenario of interest, the received signal consists of the distorted desired signal and interference from other signals, including ISI from the previous symbol, and ACI from signals in adjacent bands. The aim of this study is to minimize the aggregation of the distortion of desired signal and interference.

The distortion of the desired signal can be calculated by calculating the difference between the signal that would have been received if eq. (2.3) was satisfied, and the actual received signal. If eq. (2.3) was satisfied, the channel convolution matrix would have been perfectly circular, and received signal would be $y_{:,d,0} = \mathbf{F}_0 \mathbf{h}_{d,0}^{\text{circ}} \mathbf{F}_0^{\mathcal{H}} \mathbf{Q}_u s_{:,d,0}$. Then, the difference between the perfect and effective circular channel convolution matrices when CP is added using eq. (2.1) and removed using eq. (2.2), forms the distortion matrix $\mathbf{h}_{d,0}^{\text{dist}} \in \mathbb{C}^{N_u\times N_u}$, which is $\mathbf{h}_{d,0}^{\text{dist}} = \mathbf{B}_{L_{n,i}^{\text{w}}} \mathbf{h}^{\text{conv}} \mathbf{A} - \mathbf{h}^{\text{circ}}$. Hence, the distortion in the nth subcarrier of the desired OFDM symbol is found as $y_{n,d,0}^{\text{dist}} = \mathbf{F}_0 \mathbf{h}_{d,0}^{\text{dist}} \mathbf{F}_0^{\mathcal{H}} \mathbf{Q}_u s_{:,d,0}$.

The ISI and ACI from all other signals are calculated by projecting samples of each received OFDM symbol to the corresponding samples of the desired OFDM symbol in this asynchronous scenario. Each received OFDM symbol affects a total of $\frac{\Delta f_0}{\Delta f_u}\left(N_u + K_u + (L_u - 1)\right)$ time samples. The channel output, including the CIR filter tail, is calculated by left multiplying the transmit samples with $\mathbf{h}_{i,u}^{\text{full}} \in \mathbb{C}^{\frac{\Delta f_0}{\Delta f_u}(N_u+K_u+(L_u-1))\times N_u+K_u}$, where

$$\mathbf{h}_{i,u}^{\text{full}} = \text{toep}\left(\begin{bmatrix} h_{i,u} & \mathbf{0}_{1\times N_u+K_u-1}\end{bmatrix}^T, \begin{bmatrix} h_{i,u}(0) & \mathbf{0}_{1\times N_u+K_u-1}\end{bmatrix}\right)\mathbf{R}, \tag{2.6}$$

where $\mathbf{R} \in \mathbb{C}^{\frac{\Delta f_0}{\Delta f_u}(N_u+K_u)\times N_u+K_u}$ is any resampling transform[4]. Let $t_{i,u} \in \mathbb{R}^{\frac{\Delta f_0}{\Delta f_u}(N_u+K_u+(L_u-1))\times 1}$ denote the time indices of the received samples that contains energy from the samples of the ith OFDM symbol of uth user. Then, a projection matrix $\mathbf{\Pi}_{i,u;d,0} \in \mathbb{R}^{N_0+K_0\times\frac{\Delta f_0}{\Delta f_u}(N_u+K_u+(L_u-1))}$ is formed such that the misaligned, asynchronous samples are projected onto the received symbol:

$$\mathbf{\Pi}_{i,u;d,0}(g,j) = \begin{cases} 1 & , t_{d,0}(g) = t_{i,u}(j) \\ 0 & , \text{o.w.} \end{cases} \tag{2.7}$$

Thus, the aggregate interference on the nth subcarrier of the desired symbol is found as:

$$y_{n,d,0}^{\text{int}} = y_{n,d,0}^{\text{dist}} + \sum_{\substack{u \\ \{i,u\}\neq\{d,0\}}}\sum_{i} \mathbf{F}_0\mathbf{B}_{L_{n,d,0}^{\text{w}}}\mathbf{\Pi}_{i,u;d,0}\mathbf{h}_{i,u}^{\text{full}}\mathbf{A}_u\mathbf{F}_u^{\mathcal{H}}\mathbf{Q}_u s_{:,i,u} \tag{2.8}$$

Using this formulation, the instantaneous interference power is calculated easily if all parameters are known. However, practically, information symbols of all users are unknown at the time of reception, and an estimate of the expected interference power is needed. To calculate this value, the following statistical conjecture is used:

Conjecture 1. *The symbols transmitted using any subcarrier of any OFDM symbol of any user are independent from each other and the used modulation is unit average power, i.e.,* $\mathbb{E}\left\{s_{n,i,u}s_{n',i',u'}^*\right\} = \delta(n-n')\,\delta(i-i')\,\delta(u-u')\;\forall n,n',i,i',u,u'.$

[4]In the numerical verification of this work, sampling rates are matched using Fourier interpolation, implying a Dirichlet kernel.

Conjecture 1 implies that, for practical number of subcarriers, the variance of their sum is the sum of their variances by the law of large numbers [69]. Each column of $\mathbf{F}^{\mathcal{H}}$ contains the phase rotation of a normal random variable and the sum of variances of all columns yields the total interference power contributed to the symbol. Thus, the expected aggregate interference to the nth received subcarrier of the desired user is given in the nth column of

$$\mathbb{E}_s\left\{\mathbf{P}^{\text{int}}_{:,d,0}\right\} = 1_{1\times N}\left(\left|\mathbf{F}_0\mathbf{h}^{\text{dist}}_{d,0}\mathbf{F}_0^{\mathcal{H}}\right|^{\odot 2}\right)^T + \sum_{\substack{u\\ \{i,u\}\neq\{d,0\}}}\sum_{i} 1_{1\times N}\left(\left|\mathbf{F}_0\mathbf{B}_{L^{\text{w}}_{n,d,0}}\mathbf{\Pi}_{i,u;d,0}\mathbf{h}^{\text{full}}_{i,u}\mathbf{A}_u\mathbf{Q}_u\mathbf{F}_u^{\mathcal{H}}\right|^{\odot 2}\right)^T \tag{2.9}$$

where the nth column of $1_{1\times N}\mathbf{X}^T$ contains the sum of all elements in the nth row of $\mathbf{X}$.

2.2 Proposed Method

The receiver is to solve either of

$$\hat{L^{\text{SSW}}_{n,i,u}} = \arg\min_{L^{\text{w}}_{n,d,u}} \quad \mathbb{E}_s\left\{\mathbf{P}^{\text{int}}_{n,d,u}\right\} \tag{2.10}$$

$$\hat{L^{\text{avs}}_{n,u}} = \arg\min_{L^{\text{w}}_{n,i,u}} \quad \mathbb{E}_i\left\{\mathbb{E}_s\left\{\mathbf{P}^{\text{int}}_{n,i,u}\right\}\right\} \tag{2.11}$$

$$\hat{L^{\text{fix}}_{d,u}} = \arg\min_{L^{\text{w}}_{n,d,u}} \quad \mathbb{E}_n\left\{\mathbb{E}_s\left\{\mathbf{P}^{\text{int}}_{n,d,u}\right\}\right\} \tag{2.12}$$

$$\hat{L^{\text{avf}}_{u}} = \arg\min_{L^{\text{w}}_{n,i,u}} \quad \mathbb{E}_i\left\{\mathbb{E}_n\left\{\mathbb{E}_s\left\{\mathbf{P}^{\text{int}}_{n,i,u}\right\}\right\}\right\} \tag{2.13}$$

$$\text{subject to} \quad L^{\text{w}}_{n,i,u} \in \{0,1,\ldots,K_u\} \tag{2.14}$$

to find

1. optimal SSWs lengths for known CIRs
2. average SSW lengths depending on users' PDPs
3. optimal window length for conventional "fixed" receiver windowing using the same window lengths for all subcarriers for known CIRs

4. average fixed length depending on users' PDPs

where required computational complexity decreases along with performance as we get to the bottom of the options. The solutions to window length calculations are not provided but performance gain will be shown. Provided the solutions are known, SSW requires additional $\sum_{L^{\mathrm{w}} \in L^{\hat{\mathrm{SSW}}} \setminus L_i^{\hat{\mathrm{fix}}}} \left(4L^{\mathrm{w}} + \frac{N}{2} \log_2 N\right)$ multiplications and $\sum_{L^{\mathrm{w}} \in L^{\hat{\mathrm{SSW}}} \setminus L_i^{\hat{\mathrm{fix}}}} \left(2L^{\mathrm{w}} + N \log_2 N\right)$ additions on top of fixed windowing, due to additional overlapping (first terms) and FFT operations (second terms).

2.3 Numerical Verification

A system with the following parameters was simulated to demonstrate the gains of the proposed algorithm. α_u, CIRs and time offset between users are randomized at each run. $\hat{\mathbf{H}}_{i,u} = \mathbf{H}_{i,u} \forall i, u$ and $\mathbb{E}_i \left\{ \mathbf{h}_{i,u} \mathbf{h}^*_{i-\Delta i,u} \right\} = P_u \delta(\Delta i)$. $P_{-1} = P_1$ always, and are equal to $2P_0$ in the remaining figures except Figure 2.6. There is no guard band between any user, first subcarrier of the user with narrower bandwidth is located at the first null of the adjacent user's edge-most subcarrier. $2\Delta f_{-1} = \Delta f_0 = \Delta f_1/2$, where user indices distinguishes their order in the spectrum. The rest of the variables are given in the sampling rate of user 0. $N_{\{-1,0,1\}} = \{512, 256, 128\}$, $M_{\{-1,0,1\}} = \{123, 127, 31\}$, and $K_{\{-1,0,1\}} = \{36, 18, 9\}$ whereas $L_{\{-1,0,1\}} = \{64, 32, 16\}$. The post-equalization expected aggregate interference for unknown signals and the actual interference for known signals for a single realization of the aforementioned setup is shown in Figure 2.1. The expected interference calculations are accurate in determining the actual interference, but a slight mismatch occurs due to dependance of ACI on interfering users' signals.

The ISI power (consisting of both the distortion of the symbol in interest and the leakage from preceding symbol of desired), ACI power and the combined interference power at the subcarriers of the desired signal are shown in Figures 2.2 and 2.3. In case of a single realization shown in Figure 2.2, the dependency to the instantaneous channels of interfering users can be observed by the power offset at edge subcarriers although both interferers have the same transmit powers. As the

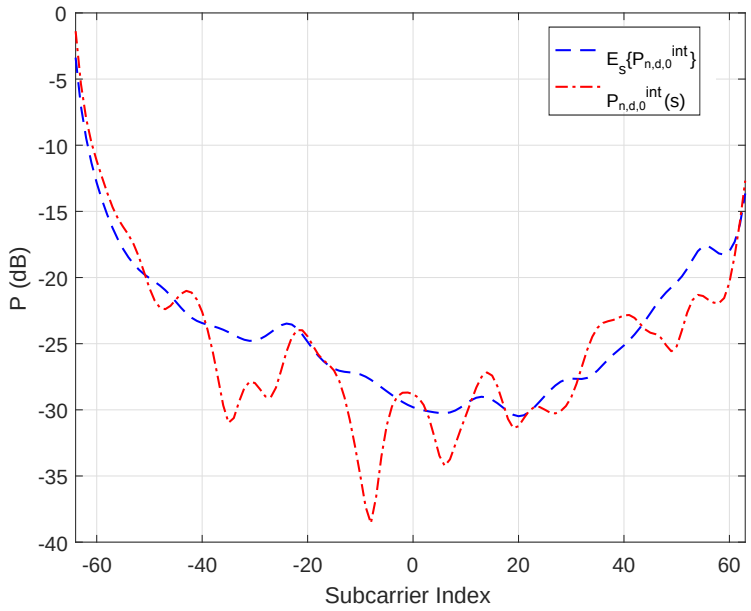

Figure 2.1: Post-equalization $\mathbb{E}_s\left\{\mathbf{P}^{\text{int}}_{n,d,0}\right\}$ and $\mathbf{P}^{\text{int}}_{n,d,0}(\mathbf{s})$ for a realization, for $L^{\text{w}}_{n,d,0} = 0 \forall n$.

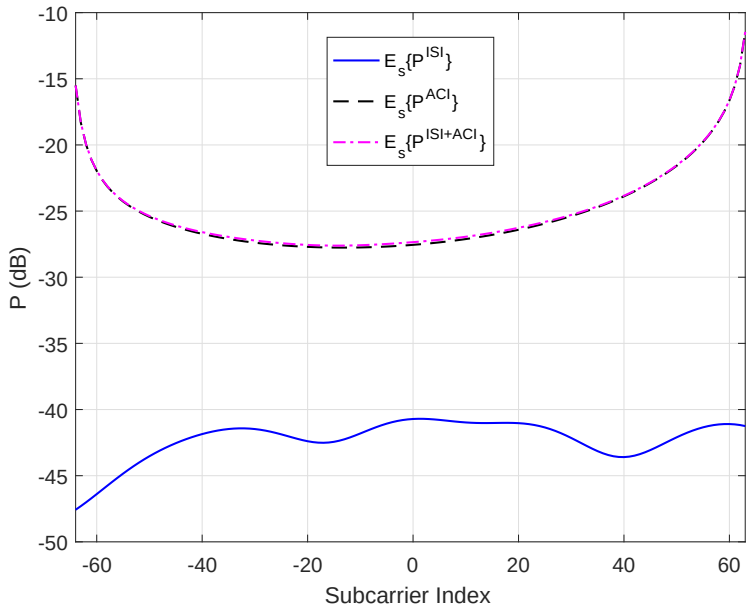

Figure 2.2: One realization of pre-window interference power in desired user's signal.

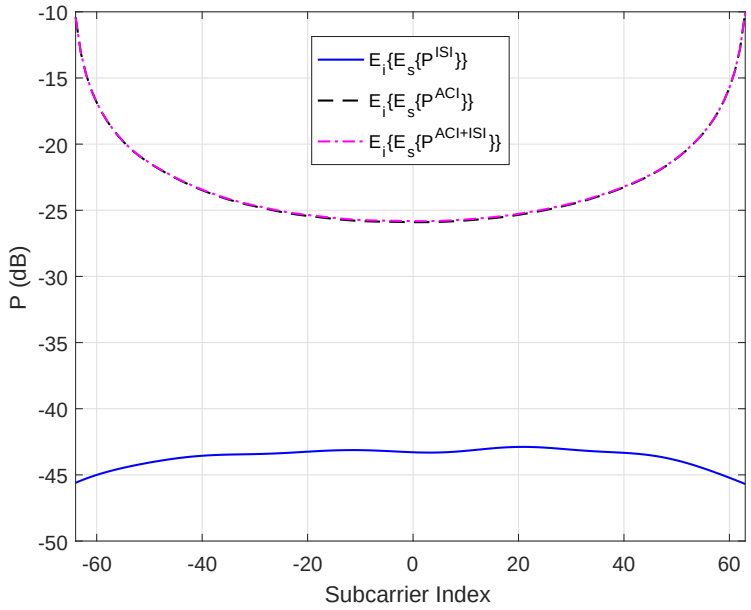

Figure 2.3: Pre-window interference power in desired user's signal.

results are averaged over many realizations as shown in Figure 2.3, ISI becomes uniform throughout the subcarriers and ACI becomes stronger at edges and weaker in inner subcarriers.

The results of the grid search for optimal SSW length satisfying eq. (2.10) are shown in Figures 2.4 and 2.5 for the same realization depicted in Figure 2.4, which agrees with channel dependency of optimal SSW lengths. As shown in Figure 2.5, longer window lengths are required at edge subcarriers.

SIR gain of receivers with $L^{\mathrm{w}}_{n,i,u} = \left\{ L^{\hat{\mathrm{fix}}}_{i-1,u}, L^{\hat{\mathrm{avf}}}_{u}, L^{\hat{\mathrm{fix}}}_{i,u}, L^{\mathrm{SS}\hat{\mathrm{W}}}_{n,i-1,u}, L^{\hat{\mathrm{avs}}}_{n,u}, L^{\mathrm{S}\hat{\mathrm{SW}}}_{n,i,u} \right\}$ over no windowing for different interferer power offsets is presented in Figure 2.6. SSW guarantees higher gain than fixed windowing with current and average optimal length, and outdated lengths become robust as interferers become more powerful. Most carriers are still windowed efficiently albeit fluctuations around the expected interference trend with outdated CIRs and PDPs, but the performance recedes compared to current lengths due to the non-optimal windowing as the CIRs of all users may have changed drastically.

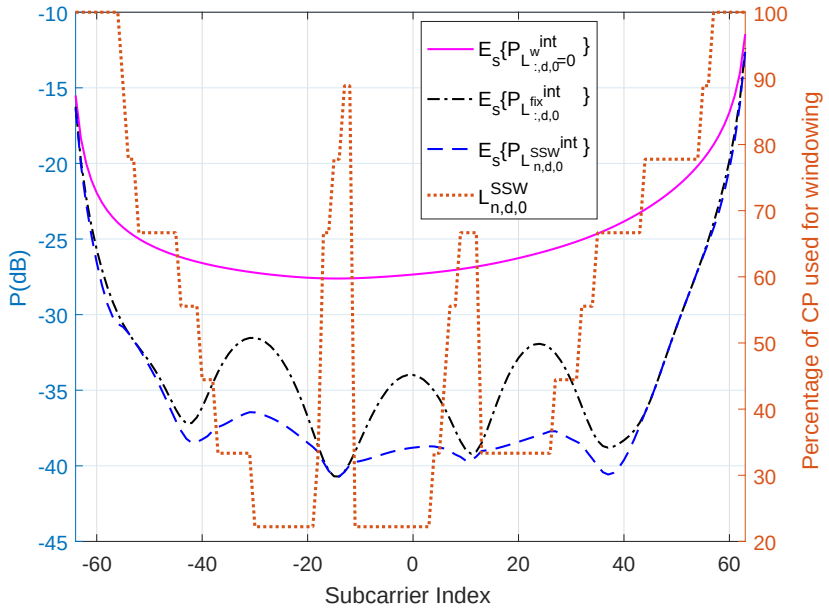

Figure 2.4: $L_{n,i}^{\hat{\mathrm{SSW}}}/K$ and $\mathbb{E}_s\left\{\mathbf{P}_{n,d,0}^{\mathrm{int}}\right\}$ for $L_{n;d,0}^{\mathrm{w}} = \left\{0, L_d^{\hat{\mathrm{fix}}}, L_{n,d}^{\hat{\mathrm{SSW}}}\right\}$.

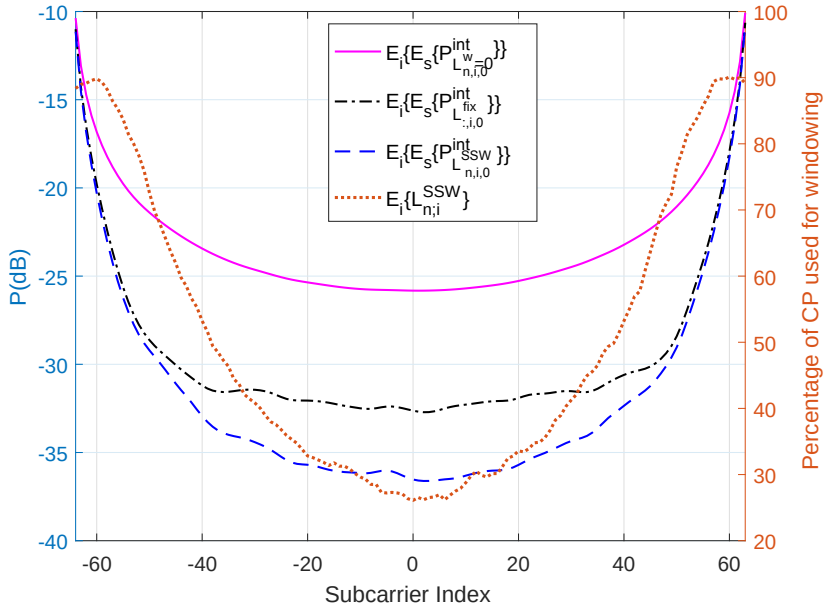

Figure 2.5: $L_n^{\hat{\mathrm{avs}}}/K$, and $\mathbb{E}_i\left\{\mathbb{E}_s\left\{\mathbf{P}_{n,i,0}^{\mathrm{int}}\right\}\right\}$ for $L_{n,i,0}^{\mathrm{w}} = \left\{0, L_i^{\hat{\mathrm{fix}}}, L_{n,i}^{\hat{\mathrm{SSW}}}\right\}$.

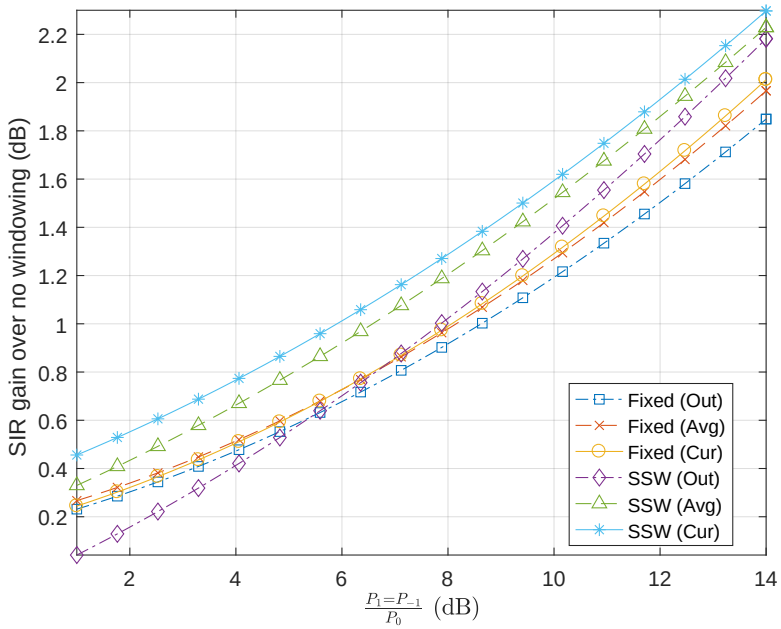

Figure 2.6: The SIR gains of seven different receivers over no windowing as a function of power offsets.

Chapter 3: Extensionless Adaptive Transmitter and Receiver Windowing of Beyond 5G Frames

The following notation is used throughout this Chapter[5]: $(\cdot)^{\mathsf{T}}$, $(\cdot)^{*}$ and $(\cdot)^{\mathsf{H}}$ denote the transpose, conjugate and Hermitian operations, $\boldsymbol{A}[a,b]$ is the element in the ath row and bth column of matrix $\boldsymbol{A}$, $\boldsymbol{A}[a,:]$ and $\boldsymbol{A}[:,b]$ are each row and column vectors containing the ath row and bth column of matrix $\boldsymbol{A}$, respectively, $\mathrm{vec}(\boldsymbol{A}) = \begin{bmatrix} \boldsymbol{A}[:,1]^{\mathsf{T}} & \boldsymbol{A}[:,2]^{\mathsf{T}} & \dots \end{bmatrix}^{\mathsf{T}}$ is the vectorization operator, $\boldsymbol{A} \odot \boldsymbol{B}$ and $\boldsymbol{A} \oslash \boldsymbol{B}$ correspond to Hadamard multiplication and division of matrices $\boldsymbol{A}$ and $\boldsymbol{B}$ and $\boldsymbol{A}$ by $\boldsymbol{B}$, $\boldsymbol{0}_{A\times B}$ denotes matrices of zeros with A rows and B columns, $\mathcal{CN}\left(\mu,\sigma^2\right)$ represents complex Gaussian random processes with mean μ and variance σ^2, $\#\mathbb{S}$ denotes the cardinality of set $\mathbb{S}$, $\mathbb{E}_x\{\boldsymbol{y}\}$ is the expected value of random vector $\boldsymbol{y}$ with respect to variable x, and $\jmath = \sqrt{-1}$.

3.1 System Model

In this chapter, we assume that there is a node, referred to as the gNB, that conveys information to all other nodes in the system and all other nodes aim to convey information solely to the gNB during processes referred to as DL and UL, respectively. There are U nodes other than the gNB, hereinafter referred to as UEs, sharing a total bandwidth B to communicate with the gNB using OFDM. Each UE u samples this whole band band using an N_u-point FFT, such that the frequency spacing between the points at the FFT output becomes $\Delta f_u = B/N_u$. The quantity Δf_u is referred to as the subcarrier spacing of UE u. Bi-directional communication takes place in a TDD fashion and frequency division multiple accessing (FDMA) is used for multiple accessing; UEs solely receive and do not transmit during gNB's transmission, i.e. DL, whereas all UEs transmit simultaneously in adjacent but non-overlapping frequency bands in the UL. UL is assumed to take place before DL and is crucial to the work, but we focus on modeling the details of the DL necessary for the proposed

[5]Part of this chapter was published in [70] and patented [71]. Permission is included in Appendix A.

methods for sake of brevity, while necessary details regarding UL are provided in numerical verification. The data of each UE u is conveyed in M_u consecutive subcarriers of L_u consecutive OFDM symbols, with contiguous indices $\{M_{u,1}, \ldots, M_{u,M_u}\}$ out of the possible N_u, while the remaining subcarriers are left empty for use by other UEs. Although the algorithms presented and performed analysis are directly compatible with OFDMA, for the sake of simplifying the notation throughout this work, we assume pure FDMA, that is, $L_{u_1} N_{u_1} = L_{u_2} N_{u_2}\,, \forall u_1, u_2 \in \mathbb{N}^*_{\leq U}$.

Symbols known by receiving nodes, commonly referred to as pilot or demodulation reference signal (DMRS), are transmitted in some REs for time synchronization and channel estimation purposes in both UL and DL. The DMRS transmitted to UE u are contained in the sparse matrix $\boldsymbol{P}_u \in \mathbb{C}^{M_u \times L_u}$. The SC data symbols transmitted to UE u are contained in $\boldsymbol{D}_u \in \mathbb{C}^{M_u \times L_u}$, of which nonzero elements do not overlap with that of $\boldsymbol{P}_u$.

A CP of length K_u samples is appended to the each time domain OFDM symbol to mitigate multipath propagation and prevent ISI, where K_u / L_u equals to the same constant for all UEs of the network and is referred to as the CP rate. The OFDM symbol samples, preceded their respective CP samples to be broadcasted to all users can be obtained as

$$\breve{\boldsymbol{x}} = \sum_{u=1}^{U} \operatorname{vec}\left(\begin{bmatrix} \boldsymbol{0}_{K_u \times (N_u - K_u)} & \boldsymbol{I}_{K_u} \\ & \boldsymbol{I}_{N_u} \end{bmatrix} \boldsymbol{F}_{N_u} \boldsymbol{Q}_u \left(\boldsymbol{P}_u + \boldsymbol{D}_u \right) \right), \tag{3.1}$$

where $\breve{\boldsymbol{x}} \in \mathbb{C}^{(N_u + K_u) L_u \times 1, \forall u}$ is the basic baseband sample sequence, $\boldsymbol{Q}_u \in \mathbb{R}^{N_u \times M_u}$ is the resource mapping matrix of uth UE that maps the data elements to the scheduled resources, and $\boldsymbol{F}_{N_u} \in \mathbb{C}^{N_u \times N_u}$ is the normalized N_u-point FFT matrix. Some CP samples may also be used for transmitter windowing to limit the OOB emission as described in [44, 46]. Different transmitter window durations may be utilized for each RE to be transmitted to each UE. The transmitter window durations associated with uth UE's REs are given in $\boldsymbol{T}_u \in \mathbb{N}^{M_u \times L_u}_{\leq K_u}$ and calculated according to Subsection 3.2.1. Let $\boldsymbol{x} \in \mathbb{C}^{((K_u + N_u) L_u) \times 1}$ denote the per-RE transmitter windowed baseband sample sequence, calculated computationally efficiently as described in Subsection 3.2.1.

The waveform is then transmitted over the multiple access multipath channel. The complex channel gain of the cluster that arrives at the uth UE at the tth sample after a delay of τ samples is denoted by the complex coefficient $h_{u,\tau,t}$. We assume that these channel gains are normalized such that $\mathbb{E}_t\left[\sum_{\tau=0}^{t-\Delta_{t,u}-1}\left|h_{u,\tau,t}\right|^2\right] = 1$ and that they vary at each sample instant where the mobility of each UE is independent of all others. Then, the tth sample received at uth UE is written as

$$\boldsymbol{y}_u\left[t\right] = \tilde{n} + \sqrt{\gamma_u}\sum_{\tau=0}^{t-\Delta_{t,u}-1} h_{u,\tau,t}\boldsymbol{x}\left[t-\Delta_{t,u}-\tau\right],\ t \in \mathbb{N}^*, \tag{3.2}$$

where $\boldsymbol{x}\left[t\right] \coloneqq 0, \forall t \in \mathbb{N}_{>(K_u+N_u)L_u} \cup \mathbb{Z}^-$, $\tilde{n} \sim \mathcal{CN}\left(0,1\right)$ is the background additive white Gaussian noise (AWGN), γ_u is the overall SNR of uth UE and $\Delta_{t,u}$ is the propagation delay for uth UE in number of samples. Each UE then synchronizes to their signal by correlating the received samples with samples generated only using their $\boldsymbol{P}_u$ and estimates $\hat{\Delta_{t,u}}$ [72]. The samples estimated to contain uth UE's lth OFDM symbol and its corresponding CP is denoted by vector $\boldsymbol{y}_{l,u} \in \mathbb{C}^{(K_u+N_u)\times 1}$, where $\boldsymbol{y}_{l,u}\left[s\right] = \boldsymbol{y}_u\left[\left(l-1\right)\left(N_u+K_u\right)+\hat{\Delta_{t,u}}+s\right],\ s \in \mathbb{N}^*_{\leq(K_u+N_u)}$. Before the receiver windowing operations are performed, uth UE first performs regular OFDM reception and calculates the received SC symbols from the OFDM symbol samples as

$$\boldsymbol{Y}_u\left[:,l,0\right] = \boldsymbol{Q}_u{}^{\mathsf{T}}\boldsymbol{F}_{N_u}\begin{bmatrix}\boldsymbol{0}_{N_u\times K_u} & \boldsymbol{I}_{N_u}\end{bmatrix}\boldsymbol{y}_{l,u}, \tag{3.3}$$

where the first plane of $\boldsymbol{Y}_u \in \mathbb{C}^{M_u\times L_u\times(K_u+1)}$ are the received base SC symbols. Each UE uses a different receiver window duration to receive each RE. The receiver window durations associated with uth UE's REs are given in $\boldsymbol{R}_u \in \mathbb{N}^{M_u\times L_u}_{\leq K_u}$ and are calculated according to Subsection 3.2.2, wherein also the calculation of the receiver windowed SC symbols $\hat{\boldsymbol{Y}}_u \in \mathbb{C}^{M_u\times L_u}$ are demonstrated. CFR coefficients at DMRS locations are first estimated as

$$\check{\boldsymbol{H}}_u\left[m,l\right] = \hat{\boldsymbol{Y}}_u\left[m,l\right] \oslash \boldsymbol{P}_u\left[m,l\right] \tag{3.4}$$

using nonzero elements of $\mathbf{P}_u$. Then, a transform domain channel estimator [73, (33)] is applied and estimated CIRs are reduced to their first K_u coefficients. The CIR coefficients of non-pilot carrying symbols are interpolated and extrapolated [74], and all CFR coefficient estimates $\hat{\boldsymbol{H}}_u$ are obtained [73, (33)]. Finally, data symbols are equalized as described in [75] for nonzero elements of $\mathbf{D}_u$ and the received symbols are estimated as

$$\hat{\mathbf{D}}_u = \frac{\hat{\boldsymbol{Y}}_u \odot \hat{\boldsymbol{H}}_u^*}{\hat{\boldsymbol{\sigma}}_{\mathrm{n},u}^2 + \hat{\boldsymbol{H}}_u \odot \hat{\boldsymbol{H}}_u^*}, \tag{3.5}$$

where $\hat{\boldsymbol{\sigma}}_{\mathrm{n},u}^2 \in \mathbb{R}^{M_u \times L_u}$ is the variance estimated by uth UE for noise, various interference sources and other disruptions.

3.2 Proposed Method

The idea proposed in this work involves determination of $\boldsymbol{T}_u$ and $\boldsymbol{R}_u$ for all UEs that maximizes the fair-proportional network capacity. Because these concepts are implemented independently, they are discussed separately.

3.2.1 Estimation of Optimum Transmitter Window Durations

This subsubsection first discusses efficient differential calculation of per-RE transmitter windowed samples to prove the optimum transmitter window durations calculations feasible. The optimization metric, fair proportional network capacity, is then defined. An algorithm to effectively maximize the fair proportional network capacity is provided. Finally, the computational complexity of the provided algorithm is calculated and discussed.

3.2.1.1 Converting Conventional CP-OFDM Samples to Per-RE TW-OFDM Samples

The transmit pulse shape of the mth subcarrier of lth OFDM symbol to be transmitted to UE u in accordance with $\boldsymbol{T}_u[m, l]$ is contained in the vector $\boldsymbol{t}_{m,l,u} \in \mathbb{R}^{(K_u+N_u+T_u)\times 1}$ of which indexing is demonstrated in Figure 3.1 and is calculated per [46] to contain the energy of that subcarrier

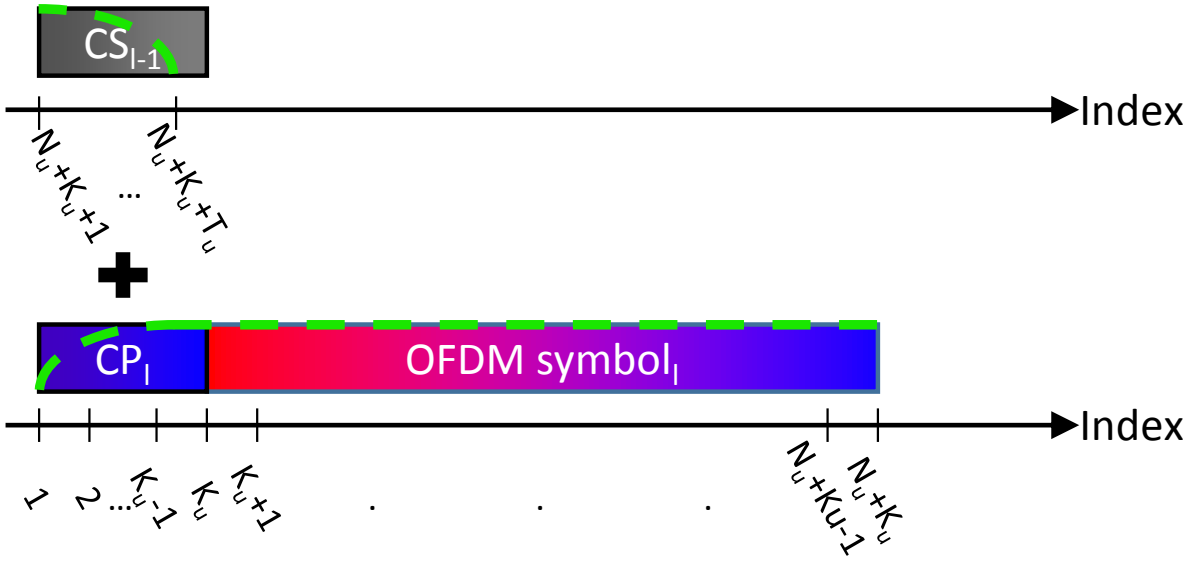

Figure 3.1: Indexing of $\boldsymbol{t}$ within a demonstration of how transmitter windowed samples are generated by overlapping scaled CP of current and CS of preceding OFDM symbols of which indices are given in the subscripts.

within the band assigned to the UE. Investigating (3.1), if no transmitter windowing is applied, i.e. the generation of a regular CP-OFDM sample sequence $\breve{\boldsymbol{x}}$, the contribution from the symbol in the mth subcarrier of the lth OFDM symbol of uth user to the $k \leq K_u$th sample of that OFDM symbol is $\exp\left(-\jmath 2\pi M_{u,m}\left(k-K_U-1\right)/N_u\right)\left(\boldsymbol{D}_u\left[m,l\right]+\boldsymbol{P}_u\left[m,l\right]\right)/\sqrt{N_u}$. If transmitter windowing is applied to the RE in interest, the contribution at $k \leq \boldsymbol{T}_u\left[m,l\right]$th sample would instead become

$$\begin{aligned}
&\left(\boldsymbol{t}_{m,l,u}\left[k\right]\exp\left(-\jmath\tfrac{2\pi M_{u,m}(k-1-K_U)}{N_u}\right)\left(\boldsymbol{D}_u\left[m,l\right]+\boldsymbol{P}_u\left[m,l\right]\right)\right. \\
&\left.+\,\boldsymbol{t}_{m,l,u}\left[k+N_u+K_u\right]\exp\left(-\jmath\tfrac{2\pi M_{u,m}(k-1)}{N_u}\right)\left(\boldsymbol{D}_u\left[m,l-1\right]+\boldsymbol{P}_u\left[m,l-1\right]\right)\right)/\sqrt{N_u} \\
&=\frac{\exp\left(-\jmath\frac{2\pi M_{u,m}(k-1)}{N_u}\right)}{\sqrt{N_u}}\left(\boldsymbol{t}_{m,l,u}\left[k\right]\exp\left(\jmath\tfrac{2\pi M_{u,m}K_U}{N_u}\right)\left(\boldsymbol{D}_u\left[m,l\right]+\boldsymbol{P}_u\left[m,l\right]\right)\right. \\
&\qquad\left.+\,\boldsymbol{t}_{m,l,u}\left[k+N_u+K_u\right]\left(\boldsymbol{D}_u\left[m,l-1\right]+\boldsymbol{P}_u\left[m,l-1\right]\right)\right).
\end{aligned} \tag{3.6}$$

Noting that $\boldsymbol{t}_{m,l,u}\left[k\right] := 1-\boldsymbol{t}_{m,l,u}\left[k+N_u+K_u\right], \forall k \in \mathbb{Z}^+_{\leq N_u+K_u}$ [44, 46], the $k \leq T_u\left[m,l\right]$th sample of uth user's lth OFDM symbol's per-RE transmitter windowed mth subcarrier can be converted from that generated using a conventional CP-OFDM procedure as

$$\boldsymbol{x}\left[(l-1)\left(N_u+K_u\right)+k\right]=\breve{\boldsymbol{x}}\left[(l-1)\left(N_u+K_u\right)+k\right] + \frac{\boldsymbol{t}_{m,l,u}[k+N_u+K_u]\exp\left(-\jmath\frac{2\pi M_{u,m}(k-1)}{N_u}\right)}{\sqrt{N_u}}\left(\left(\boldsymbol{D}_u\left[m,l-1\right]+\boldsymbol{P}_u\left[m,l-1\right]\right) - \exp\left(\jmath\frac{2\pi M_{u,m}K_U}{N_u}\right)\left(\boldsymbol{D}_u\left[m,l\right]+\boldsymbol{P}_u\left[m,l\right]\right)\right). \tag{3.7}$$

$\boldsymbol{x}$ can be obtained by converting all $T_u\left[m,l\right]$ samples of $\breve{\boldsymbol{x}}$ to per-RE transmitter windowed samples, and this is implied in all further references to eq. (3.7).

3.2.1.2 Estimation of Fair Proportional Network Capacity

In order to estimate the optimum transmitter window durations, the gNB first estimates the SINR and corresponding capacity for each RE of each user prior to transmission, calculates the fair proportional network capacity, and tries to increase it iteratively. The samples to be received at the uth UE are first estimated as

$$\hat{\boldsymbol{y}}_u\left[t\right]=\sum_{\tau=0}^{t-1}\hat{h}_{u,\tau,t}\boldsymbol{x}\left[t-\tau\right],\ t\in\mathbb{N}^*_{\leq(K_u+N_u)L_u}, \tag{3.8}$$

where $\hat{h}_{u,\tau,t}$ are the CIR coefficient predictions [74] at the gNB prior to transmission[6]. The samples are regrouped accordingly to L_u groups of K_u+N_u samples each and receiver processed as described in Section 3.1, that is, CPs are removed from all symbols, FFTs are applied, and receiver windowing is performed if the gNB is aware that the receiver in current interest does so. Results for various cases of receiver windowing are provided in Section 3.3, but for the sake of brevity, we assume that the gNB assumes none of the UEs perform receiver windowing in the remainder of this subsubsection. The gNB estimate at the FFT output, $\tilde{\boldsymbol{Y}}_u\in\mathbb{C}^{M_u\times L_u}$, is formulated as

$$\tilde{\boldsymbol{Y}}_u\left[m,l\right]=\tilde{\boldsymbol{H}}_u\left[m,l\right]\left(\mathbf{D}_u\left[m,l\right]+\tilde{\mathbf{D}}_u\left[m,l\right]\right), \tag{3.9}$$

where $\tilde{\boldsymbol{H}}_u\left[m,l\right]$ is the CFR coefficient prediction of the mth subcarrier of the lth OFDM symbol of uth user, the first term inside parentheses is due to the data itself, and the second term inside

[6] $\hat{h}_{u,\tau,t}$ inherits $\sqrt{\gamma_u}$ in the channel estimation phase.

parentheses shown as $\tilde{\mathbf{D}}_u$ is the cumulative ACI, ICI and ISI. Note that since the source samples for all these effects are summed with that of data at the gNB and are passed through the same channel, this cumulative disruption is also scaled with the same channel gain. Accordingly, the number of bits that can be conveyed in the actual noisy transmission channel using the data carrying mth subcarrier of the lth OFDM symbol of uth UE is [76]

$$\begin{aligned}\breve{\boldsymbol{\eta}}_u[m,l] &= \log_2\left(1+\frac{\left|\tilde{\boldsymbol{H}}_u[m,l]\right|^2}{1+\left|\tilde{\boldsymbol{H}}_u[m,l]\right|^2\left|\tilde{\mathbf{D}}_u[m,l]\right|^2}\right)\\ &= \log_2\left(1+\frac{\left|\tilde{\boldsymbol{H}}_u[m,l]\right|^2}{1+\left|\tilde{\boldsymbol{Y}}_u[m,l]-\tilde{\boldsymbol{H}}_u[m,l]\,\mathbf{D}_u[m,l]\right|^2}\right).\end{aligned} \tag{3.10}$$

If the RE under investigation is scheduled to use a certain modulation and coding scheme (MCS) to carry $\boldsymbol{b}_u[m,l]$ bits, (3.10) is in fact capped as

$$\boldsymbol{\eta}_u[m,l] = \min\left(\boldsymbol{b}_u[m,l], \breve{\boldsymbol{\eta}}_u[m,l]\right). \tag{3.11}$$

The mean number of bits conveyable to uth UE per RE is

$$\bar{\eta}_u = \mathbb{E}_{[}\{m\}]\mathbb{E}_{[}\{l\}]\boldsymbol{\eta}_u[m,l], \tag{3.12}$$

and we define the fair proportional network capacity as the geometric mean of the mean capacities of all UEs in the network

$$\eta = \sqrt[U]{\prod_{u=1}^{U}\bar{\eta}_u}. \tag{3.13}$$

3.2.1.3 Optimum Transmitter Window Duration Estimation Algorithm

Given the discrete nature of possible window durations in digital pulse shaping and the lack of a relation between window duration and amount of interference incurred on a victim subcarrier for optimum window functions used in this work [46] for the time-varying multipath multiple access channel, an analytical solution to this multivariate integer optimization problem with such a

nonlinear utility function is not obvious at the time of writing. The choice of transmitter window duration of any RE must balance the SINR degradation to the REs caused by induced ISI, and the SINR improvement to all other REs, particularly those of other UEs. The transmitter window duration affects the whole network, hence, must be calculated keeping the whole network in mind, meaning (3.13) must be calculated and optimized at the gNB prior to transmission. However, explicitly calculating eqs. (3.7) to (3.13) every time for each RE is computationally exhaustive. The aforementioned equations are provided to provide the necessary understanding, but the following equations will be used in the computationally efficient estimation of optimum transmitter window durations. Consider that we wish to test whether setting the transmitter window duration of the RE in the $\dot{m}$th subcarrier of the $\dot{l}$th OFDM symbol of $\dot{u}$th user to $\boldsymbol{T}_{\dot{u}}\left[\dot{m},\dot{l}\right]$ improves the fair proportional network capacity or not. Assume the transmitter windowed samples are calculated per (3.7). To keep expressions clear, let us refer to the difference in the kth CP sample in interest per (3.7) as

$$\dot{x}_k \coloneqq \boldsymbol{x}\left[\left(\dot{l}-1\right)\left(N_{\dot{u}}+K_{\dot{u}}\right)+k\right]-\breve{\boldsymbol{x}}\left[\left(\dot{l}-1\right)\left(N_{\dot{u}}+K_{\dot{u}}\right)+k\right] \tag{3.14}$$

$$\begin{aligned}=\frac{\boldsymbol{t}_{\dot{m},\dot{l},\dot{u}}[k+N_{\dot{u}}+K_{\dot{u}}]\exp\left(-\jmath\frac{2\pi M_{\dot{u},\dot{m}}(k-1)}{N_{\dot{u}}}\right)}{\sqrt{N_{\dot{u}}}}\Big(\left(\boldsymbol{D}_{\dot{u}}\left[\dot{m},\dot{l}-1\right]+\boldsymbol{P}_{\dot{u}}\left[\dot{m},\dot{l}-1\right]\right)\\ -\exp\left(\jmath\frac{2\pi M_{\dot{u},\dot{m}}K_{\dot{U}}}{N_{\dot{u}}}\right)\left(\boldsymbol{D}_{\dot{u}}\left[\dot{m},\dot{l}\right]+\boldsymbol{P}_{\dot{u}}\left[\dot{m},\dot{l}\right]\right)\Big).\end{aligned} \tag{3.15}$$

The next step is to regenerate (3.9) for all UEs. However, as the number of changed symbols is limited, whole sample sequences do not need regeneration, but only the received samples that are affected by the changed samples, and fall into a valid receiver window must be recalculated. For example, assuming a conventional rectangular receiver window is utilized at the receivers, which will be assumed in the rest of this subsection, any changes to CP samples will be discarded as they fall outside the receiver window, hence need not be calculated. In this case, first $\boldsymbol{T}_{\dot{u}}\left[\dot{m},\dot{l}\right]$ modified samples that the channel would leak into the symbol duration must be calculated for each UE, and the kth sample (per indexing of Figure 3.1) of the transmitter windowed received sample sequence

$\boldsymbol{y}_u\widehat{\boldsymbol{y}_u}$ can be written as

$$\boldsymbol{y}_u\widehat{\boldsymbol{y}_u}\left[\left(\dot{l}-1\right)\left(N_{\dot{u}}+K_{\dot{u}}\right)+k\right]=\sum_{\tau=0}^{K_u}\hat{h}_{u,\tau,\left(\dot{l}-1\right)\left(N_{\dot{u}}+K_{\dot{u}}\right)+k}\boldsymbol{x}\left[\left(\dot{l}-1\right)\left(N_{\dot{u}}+K_{\dot{u}}\right)+k-\tau\right] \quad (3.16)$$

$$=\sum_{\tau=0}^{K_u}\hat{h}_{u,\tau,\left(\dot{l}-1\right)\left(N_{\dot{u}}+K_{\dot{u}}\right)+k}\left(\check{\boldsymbol{x}}\left[\left(\dot{l}-1\right)\left(N_{\dot{u}}+K_{\dot{u}}\right)+k-\tau\right]+\dot{x}_{k-\tau}\right)$$

$$=\hat{\boldsymbol{y}}_u\left[\left(\dot{l}-1\right)\left(N_{\dot{u}}+K_{\dot{u}}\right)+k\right]+\sum_{\tau=k-\boldsymbol{T}_{\dot{u}}\left[\dot{m},\dot{l}\right]}^{K_u}\hat{h}_{u,\tau,\left(\dot{l}-1\right)\left(N_{\dot{u}}+K_{\dot{u}}\right)+k}\dot{x}_{k-\tau}.$$

Let us similarly refer to the difference in the kth relevant (belonging to the OFDM symbol affected by the windowing operation) sample to be received by the uth UE as

$$\dot{y}_{u,k}=\boldsymbol{y}_u\widehat{\boldsymbol{y}_u}\left[\left(\dot{l}-1\right)\left(N_{\dot{u}}+K_{\dot{u}}\right)+k\right]-\hat{\boldsymbol{y}}_u\left[\left(\dot{l}-1\right)\left(N_{\dot{u}}+K_{\dot{u}}\right)+k\right] \quad (3.17)$$

$$=\sum_{\tau=k-\boldsymbol{T}_{\dot{u}}\left[\dot{m},\dot{l}\right]}^{K_u}\hat{h}_{u,\tau,\left(\dot{l}-1\right)\left(N_{\dot{u}}+K_{\dot{u}}\right)+k}\dot{x}_{k-\tau}. \quad (3.18)$$

The FFT outputs also only need to be updated for a few samples and taking the FFT of the whole OFDM symbol is not necessary. Using the previously calculated received symbol estimates, if there is an update to symbol estimate in the mth subcarrier of the lth OFDM symbol of uth user, the new symbol can be estimated by adding the contribution from the updated samples and removing the contribution from the original samples as

$$\boldsymbol{Y}_u\widetilde{\boldsymbol{Y}_u}\left[m,l\right]=\tilde{\boldsymbol{Y}}_u\left[m,l\right]+\sum_{k=K_u+1}^{K_u+\boldsymbol{T}_{\dot{u}}\left[\dot{m},\dot{l}\right]}\frac{\exp\left(\jmath\frac{2\pi M_{u,m}\left(k-K_u-1\right)}{N_u}\right)}{\sqrt{N_u}}\dot{y}_{u,k}. \quad (3.19)$$

The difference in the updated symbol estimate in uth user's lth OFDM symbol's mth subcarrier due to the proposed window is denoted by

$$\dot{Y}_{u,l,m}=\boldsymbol{Y}_u\widetilde{\boldsymbol{Y}_u}\left[m,l\right]-\tilde{\boldsymbol{Y}}_u\left[m,l\right] \quad (3.20)$$

$$=\sum_{k=K_u+1}^{K_u+\boldsymbol{T}_{\dot{u}}\left[\dot{m},\dot{l}\right]}\frac{\exp\left(\jmath\frac{2\pi M_{u,m}\left(k-K_u-1\right)}{N_u}\right)}{\sqrt{N_u}}\dot{y}_{u,k}. \quad (3.21)$$

Accordingly, new channel capacity becomes

$$\boldsymbol{\eta}_u \widetilde{\boldsymbol{\eta}}_u [m,l] = \log_2 \left(1 + \frac{\left| \tilde{\boldsymbol{H}}_u [m,l] \right|^2}{1 + \left| \boldsymbol{Y}_u \widetilde{\boldsymbol{Y}_u} [m,l] - \tilde{\boldsymbol{H}}_u [m,l] \, \mathbf{D}_u [m,l] \right|^2} \right) \tag{3.22a}$$

$$= \log_2 \left(1 + \frac{\left| \tilde{\boldsymbol{H}}_u [m,l] \right|^2}{1 + \left| \dot{Y}_{u,l,m} + \tilde{\boldsymbol{Y}}_u [m,l] - \tilde{\boldsymbol{H}}_u [m,l] \, \mathbf{D}_u [m,l] \right|^2} \right). \tag{3.22b}$$

Note that the term $\tilde{\boldsymbol{Y}}_u [m,l] - \tilde{\boldsymbol{H}}_u [m,l] \, \mathbf{D}_u [m,l]$ was previously calculated in (3.10) and the introduced difference term can simply be added to the previously calculated sum. Notice that the capacities of only the RE of which transmit pulses overlap with that of the RE under investigation are changed, and only these need to be compared. Accordingly, assuming that the MCSs are not decided yet, it is to the network's advantage to transmitter window the RE under investigation with the according window duration if the following is positive:

$$\eta_\Delta = \prod_{u=1}^{U} \left(\sum_{m=1}^{M_u} \boldsymbol{\eta} \widetilde{\boldsymbol{\eta}}_u \left[m, \left\lceil \frac{\dot{l} N_{\dot{u}}}{N_u} \right\rceil \right] \right) - \prod_{u=1}^{U} \left(\sum_{m=1}^{M_u} \check{\boldsymbol{\eta}}_u \left[m, \left\lceil \frac{\dot{l} N_{\dot{u}}}{N_u} \right\rceil \right] \right). \tag{3.23}$$

Or if the MCSs are already decided, η_Δ becomes

$$\begin{aligned} \eta_\Delta = & \prod_{u=1}^{U} \left(\sum_{m=1}^{M_u} \min \left(\boldsymbol{b}_u \left[m, \left\lceil \frac{\dot{l} N_{\dot{u}}}{N_u} \right\rceil \right], \boldsymbol{\eta} \widetilde{\boldsymbol{\eta}}_u \left[m, \left\lceil \frac{\dot{l} N_{\dot{u}}}{N_u} \right\rceil \right] \right) \right) \\ & - \prod_{u=1}^{U} \left(\sum_{m=1}^{M_u} \min \left(\boldsymbol{b}_u \left[m, \left\lceil \frac{\dot{l} N_{\dot{u}}}{N_u} \right\rceil \right], \check{\boldsymbol{\eta}}_u \left[m, \left\lceil \frac{\dot{l} N_{\dot{u}}}{N_u} \right\rceil \right] \right) \right). \end{aligned} \tag{3.24}$$

Consequently, Algorithm 1 is proposed to iteratively calculate the optimum transmitter windowing duration at the gNB. The variable introduced in Algorithm 1, $\boldsymbol{\lambda}_u \in \mathbb{R}^{M_u \times L_u}$, corresponds to the excess SNR of the RE if MCSs are determined, or to the SNR of the RE if not. On par with the motivation behind Algorithm 1, the REs that have higher excess SNR are more likely to have longer windowing durations resulting in more significant overall interference reduction before those with lesser impact are pursued. Since there is no additional extension to CP, which is currently designed only to support the multipath channel, all REs are assumed to have a zero transmitter windowing duration initially. The duration is incremented instead of a binary search as the expected window

Algorithm 1: Estimate $\boldsymbol{T}_u$, $\forall u \in \mathbb{N}^*_{\leq U}$ & Calculate $\boldsymbol{x}$

$\boldsymbol{T}_u \leftarrow 0,\ \forall u \in \mathbb{N}^+_{\leq U}$
$\check{\boldsymbol{x}} \leftarrow$ (3.1)
for all $u \in \mathbb{N}^*_{\leq U}$, $\tau \in \mathbb{N}_{\leq K_u}$, $t \in \mathbb{N}^*_{\leq (N_u+K_u)L_u}$ **do**
    Predict DL CIRs $\tilde{\boldsymbol{h}}_{u,\tau,t}$ and CFRs $\tilde{\boldsymbol{H}}_u$
for all $u \in \mathbb{N}^*_{\leq U}$, $m \in \mathbb{N}^*_{\leq M_u}$, $l \in \mathbb{N}^*_{\leq L_u}$ **do**
    Calculate eqs. (3.8) to (3.10)
    $\boldsymbol{\lambda}_u[m,l] \leftarrow$ (3.10)
    if MCSs fixed **then**
        $\boldsymbol{\lambda}_u[m,l] \leftarrow \boldsymbol{\lambda}_u[m,l] - \boldsymbol{b}_u[m,l]$
for $\dot{m},\dot{l},\dot{u} \leftarrow \arg\max_{m,l,u} \boldsymbol{\lambda}_u[m,l], \arg\min_{m,l,u} \boldsymbol{\lambda}_u[m,l]$ **do**
    for $\boldsymbol{T}_{\dot{u}}\left[\dot{m},\dot{l}\right] \leftarrow 1, K_u$ **do**
        $\eta_\Delta \leftarrow$ (3.23) or (3.24)
        if $\eta_\Delta > 0$ **then**
            for all $u \in \mathbb{N}^*_{\leq U}, m \in \mathbb{N}^*_{\leq M_u}$ **do**
                $\check{\boldsymbol{\eta}}_u\left[m, \left\lceil \frac{\dot{l}N_{\dot{u}}}{N_u} \right\rceil\right] \leftarrow \boldsymbol{\eta}\tilde{\boldsymbol{\eta}}_u\left[m, \left\lceil \frac{\dot{l}N_{\dot{u}}}{N_u} \right\rceil\right]$
        else
            $\boldsymbol{T}_{\dot{u}}\left[\dot{m},\dot{l}\right] \leftarrow \boldsymbol{T}_{\dot{u}}\left[\dot{m},\dot{l}\right] - 1$
            if $\boldsymbol{T}_{\dot{u}}\left[\dot{m},\dot{l}\right] > 0$ **then**
                for all $k \in \mathbb{N}^*_{\leq \boldsymbol{T}_{\dot{u}}\left[\dot{m},\dot{l}\right]}$ **do**
                    $\check{\boldsymbol{x}}\left[\left(\dot{l}-1\right)\left(N_{\dot{u}}+K_{\dot{u}}\right)+k\right] \leftarrow$ (3.7)
                break

durations are short and calculation of shorter durations are computationally less exhaustive as will be described in paragraph 3.2.1.4. The algorithm is provided in a recursive manner for brevity, but the equations invoked by (3.23)/(3.24). It should also be noted that Algorithm 1 runs only at the gNB which virtually has no computational complexity and power limitations while the UEs are unaware of the process and are not passed any information. This makes Algorithm 1 forward and backward compatible with all communication standards.

3.2.1.4 Computational Complexity

Channel prediction, and mean SNR and capacity estimation for each user is assumed to be performed for link adaptation purposes [74] regardless of Algorithm 1 and is not considered in the computational complexity of proposed algorithm. There are many computational complexity reducing implementation tricks used in paragraph 3.2.1.3. The computational complexity of the algorithm is derived by counting the number of operations performed for each step and how many times those steps were invoked. Table 3.1 shows the number of real additions and multiplications required to test whether windowing an RE at the transmitter with a duration of T is beneficial, i.e. executing line 12 of Algorithm 1, how many times each equation is invoked, and the total number of necessary operations. It is shown that each test requires (3.25) real additions and (3.26) real multiplications. Accordingly determining the optimum transmitter window durations for all REs in the transport block, and windowing the sample sequence accordingly results in $\sum_{u=1}^{U}\sum_{l=1}^{L_u}\sum_{m=1}^{M_u}\left(2\boldsymbol{T}_u\left[m,l\right]+\sum_{T=1}^{\min(\boldsymbol{T}_u[m,l]+1,K_u)}(3.25)\right)$ real additions and $\sum_{u=1}^{U}\sum_{l=1}^{L_u}\sum_{m=1}^{M_u}\sum_{T=1}^{\min(\boldsymbol{T}_u[m,l]+1,K_u)}(3.26)$ real multiplications. Other than this, Algorithm 1 also needs the calculate the fair proportional network capacity for the nonwindowed case, requiring $\sum_{u=1}^{U}\left(M_u-1\right)L_u$ real additions, and $\max L_u$ real multiplications if there are only 2 different subcarrier spacings or $\frac{3}{2}\max L_u$ real multiplications if all three subcarrier spacing possibilities for the band is used. Statistics regarding the distribution of T and according number of calculations for the evaluated scenarios are provided in Section 3.3. Regarding the timewise complexity, it should be noted that the calculation can be done in parallel for the $\min L_u$ independent symbol groups, and

Table 3.1: Computational complexity of each call to to (3.23)/(3.24)

Eq.	#Add	#Mult.	#Inv.
(3.15)	$6T$	$10T$	1
(3.18)	$2T^2$	$2T^2 + 2T$	U
(3.21)	$4T - 2$	$4T$	$\sum_{u=1}^{U} M_u$
(3.22b)	3	3	$\sum_{u=1}^{U} M_u$
(3.23) /(3.24)	$1 + \sum_{u=1}^{U} (M_u - 1)$	$U - 1$	1
Total	$2UT^2 + T\left(4\sum_{u=1}^{U} M_u + 6\right) + 2\sum_{u=1}^{U} M_u + 1 - U$ (3.25)	$2UT^2 + T\left(2U + 4\sum_{u=1}^{U} M_u + 10\right) + U + 3\sum_{u=1}^{U} M_u - 1$ (3.26)	

therefore the worst-case time complexity of the described computationally efficient implementation is $\mathcal{O}\left(\sum_u M_u K_u^2\right)$, whereas a more operation count- and memory-wise exhaustive implementation can complete in $\mathcal{O}\left(\max\left(K_u\right) + \max\left(M_u\right)\right)$, which may be feasible at the gNB. Further operational and timewise computational complexity reduction can be obtained if the Algorithm is only run for a subset of subcarriers such as [45].

3.2.2 Estimation of Optimum Receiver Window Durations

A theoretical approach requiring knowledge regarding channel conditions of at least the UEs utilizing adjacent bands was proposed in [64]. Although the approach in [64] is theoretically optimal, it is not feasible for use especially in the DL due to the extent of required data (at least PDPs, or better yet, CIRs between the transmitters of signals occupying adjacent bands and the receiver) at the UEs. In this work, we propose calculating receiver window duration solely using the statistics of the received signal. Sole dependence on statistics allows each UE to perform their own estimation in a decentralized manner without the need for network-wide channel and data knowledge required in [64]. Since calculations are done only by the intended receiver and receiver

windowing only affects the SINR of the RE that the operation is applied to, there is no need to convey any information to and from other nodes and maximization of fair-proportional network capacity is achieved by independently maximizing the capacity of each RE. This makes the proposed algorithm backward and forward compatible with any communication standard and protocol. Furthermore, computationally efficient receiver windowing of OFDM symbols for multiple receiver window durations are discussed and the computational complexity of the proposed technique is derived.

3.2.2.1 Converting Conventionally Received CP-OFDM Symbols to Per-RE RW-OFDM Symbols

Assume uth UE uses the receiver windowing pulse shape $\boldsymbol{r}_{m,l,u} \in \mathbb{R}^{(N_u+K_u)\times 1}$ of which indexing is shown in Figure 3.2 calculated according to [46] to reject the energy outside the UE's band with a receiver windowing duration of $\boldsymbol{R}_u[m,l]$ to receive the mth subcarrier of lth OFDM symbol. As also discussed in [46], a visual investigation of Figure 3.2 reveals that the analyzed receiver windowed single carrier symbols differ from that of the FFT output by the last $\boldsymbol{R}_u[m,l]$ samples. The contribution from the $s \in \mathbb{N}^*_{K_u<s\leq K_u+N_u}$th sample to the FFT output, if windowing is not performed, is, $\boldsymbol{y}_{l,u}[s]\exp\left(\jmath 2\pi M_{u,m}\left(s-K_u-1\right)/N_u\right)/\sqrt{N_u}$. If windowing is applied, for $s \in \mathbb{N}^*_{N_u<s\leq K_u+N_u}$, the contribution instead becomes

$$\left(\boldsymbol{y}_{l,u}[s]\,\boldsymbol{r}_{m,l,u}[s]+\boldsymbol{y}_{l,u}[s-N_u]\,\boldsymbol{r}_{m,l,u}[s-N_u]\right)\frac{\exp\left(\jmath\frac{2\pi M_{u,m}(s-K_u-1)}{N_u}\right)}{\sqrt{N_u}}. \tag{3.27}$$

Accordingly, by removing the non-windowed contribution from all windowed samples and adding their respective windowed contribution to the FFT output, the SC symbol that is receiver windowed with window duration $0<r\leq K_u$ can be written as

$$\begin{aligned}\boldsymbol{Y}_u[m,l,r]=\boldsymbol{Y}_u[m,l,0]+\sum_{s=N_u+K_u-r+1}^{N_u+K_u}\Big(&\boldsymbol{y}_{l,u}[s]\left(\boldsymbol{r}_{m,l,u}[s]-1\right)\\&+\boldsymbol{y}_{l,u}[s-N_u]\,\boldsymbol{r}_{m,l,u}[s-N_u]\Big)\frac{\exp\left(\jmath\frac{2\pi M_{u,m}(s-K_u-1)}{N_u}\right)}{\sqrt{N_u}}.\end{aligned} \tag{3.28}$$

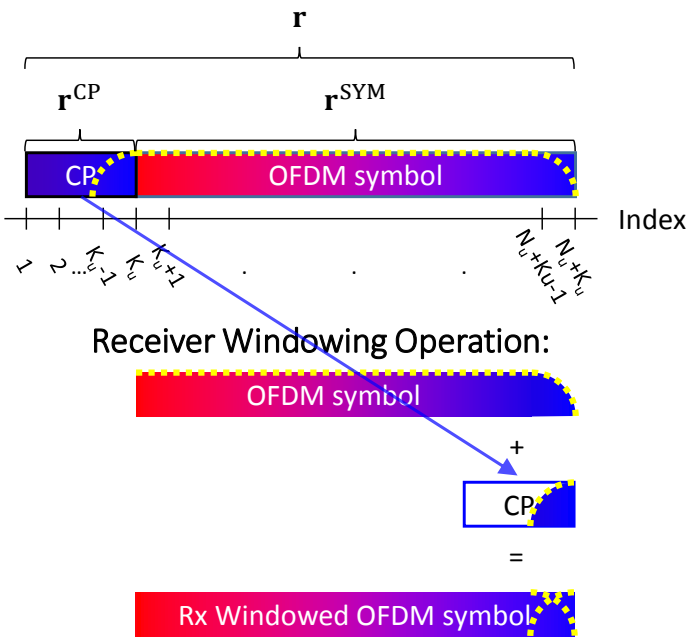

Figure 3.2: Indexing of $\boldsymbol{r}$ and identification of its parts $\boldsymbol{r}^{\mathrm{CP}}$ and $\boldsymbol{r}^{\mathrm{SYM}}$ within a demonstration of how receiver windowing operation is performed.

Plugging $\boldsymbol{r}_{m,l,u}[s] = 1 - \boldsymbol{r}_{m,l,u}[s - N_u]$ for the windowed region per [44, 46], (3.28) can be simplified to

$$\boldsymbol{Y}_u[m,l,r] = \boldsymbol{Y}_u[m,l,0] + \sum_{s=N_u+K_u-r+1}^{N_u+K_u} \left(\boldsymbol{y}_{l,u}[s-N_u] - \boldsymbol{y}_{l,u}[s]\right) \boldsymbol{r}_{m,l,u}[s - N_u] \frac{\exp\left(\jmath \frac{2\pi M_{u,m}(s-K_u-1)}{N_u}\right)}{\sqrt{N_u}}, \tag{3.29}$$

which allows computing the receiver windowed symbols with reduced computational complexity.

3.2.2.2 Optimum Receiver Windowing Duration Estimation Algorithm

The optimum receiver windowing duration similarly maximizes (3.10). However, unlike the gNB that has predicted the CFR coefficients and already knows the payload, the UEs know neither. However, there are other higher order statistics that can be exploited by the UEs. Similar to (3.9), one can write

$$\boldsymbol{Y}_u[m,l,r] = \boldsymbol{H}_u[m,l]\left(\boldsymbol{D}_u[m,l] + \boldsymbol{P}_u[m,l]\right) + \tilde{\boldsymbol{N}}_u[m,l,r] + \tilde{n}_u[m,l,r], \tag{3.30}$$

where $\boldsymbol{H}_u[m,l]$ is the actual CFR coefficient affecting the mth subcarrier of lth OFDM symbol of uth user, $\tilde{\boldsymbol{N}}_u[m,l,r]$ is the combined ACI, ICI and ISI[7] affecting the aforementioned RE if receiver window duration r is used, and $\tilde{n}_u[m,l,r]$ is the noise value affecting the aforementioned RE. Let the 2-tuple elements of the set $\mathbb{P}_u\left[\dot{m},\dot{l}\right]$ refer to the subcarrier and OFDM symbol indices of P REs that are statistically expected to experience the channels most correlated with $\boldsymbol{H}_u\left[\dot{m},\dot{l}\right]$ [77]. To keep equations concise, we will only use $\boldsymbol{D}_u[m,l]$ to refer to $\boldsymbol{D}_u[m,l]+\boldsymbol{P}_u[m,l]$ from this point onward. Even though no element other than $\boldsymbol{P}_u[m,l]$ in the equation is known, the UE can still obtain

$$\check{\boldsymbol{Y}}_u\left[\dot{m},\dot{l},r\right] \coloneqq \mathrm{var}\left[\left\{\boldsymbol{Y}_u[m,l,r],(m,l)\in\mathbb{P}_u\left[\dot{m},\dot{l}\right]\right\}\right] \tag{3.31a}$$

$$= \mathrm{var}\left[\left\{\boldsymbol{H}_u[m,l]\,\boldsymbol{D}_u[m,l]+\tilde{\boldsymbol{N}}_u[m,l,r]+\tilde{n}_u[m,l,r]\right\}\right] \tag{3.31b}$$

$$= \mathrm{var}\left[\left\{\boldsymbol{H}_u[m,l]\,\boldsymbol{D}_u[m,l]\right\}\right]+\mathrm{var}\left[\left\{\tilde{n}_u[m,l,r]\right\}\right]+\mathrm{var}\left[\left\{\tilde{\boldsymbol{N}}_u[m,l,r]\right\}\right], \tag{3.31c}$$

where the set definitions $(m,l)\in\mathbb{P}_u\left[\dot{m},\dot{l}\right]$ were removed after the first line to keep equations concise, but are always implied throughout the rest of this subsection for all mean and variance operations, and an equal-weight variance is assumed, or in probability terms, all elements are assigned the same $1/P$ probability. Weighting elements with the correlation between $\boldsymbol{H}_u[m,l]$ and $\boldsymbol{H}_u\left[\dot{m},\dot{l}\right]$ [78] is optimum [79], however, the equiweight implementation drastically reduces the computational complexity as will be shown below, without an observable performance loss. Note that since $\tilde{n}_u[m,l,r]\sim\mathcal{CN}(0,1)\,\forall u,m,l,r$, although the noise value itself changes with windowing, the noise variance remains unity. Furhermore, as ICI and ISI are separated, the variance in the actual channel coefficients can be assumed to remain constant regardless of window duration as well. Thus, the CFR coefficient, transmitted data and noise variance remain constant regardless of applied window, but the combined interference and its variance varies with the windowing operation. Although it is impossible to distinguish between these components by looking at the effects of windowing on a single received symbol, the spectrotemporal correlation of channel and interference can be exploited to identify the amount of combined interference in a group of REs.

[7]Although this element consists of the sum of each of these components scaled with different coefficients, all varying with used window, only this combined element will be referred to for the sake of brevity as future analysis only involves the sum.

Algorithm 2: Estimate $\boldsymbol{R}_u$ & $\hat{\boldsymbol{Y}}_u$

$\boldsymbol{R}_u \leftarrow 0$
for all $m \in M_u, l \in L_u$ **do**
  $\check{\boldsymbol{Y}}_u[m,l,0] \leftarrow$ (3.34b)
  for $r \leftarrow 1, K_u$ **do**
    $\check{\boldsymbol{Y}}_u[m,l,r] \leftarrow$ (3.34c)
    if $\check{\boldsymbol{Y}}_u[m,l,r] > \check{\boldsymbol{Y}}_u[m,l,r-1]$ **then**
      $\boldsymbol{R}_u[m,l] \leftarrow r-1$
      break
  $\hat{\boldsymbol{Y}}_u[m,l] \leftarrow$ (3.29)

That is, although $\mathrm{var}\left[\left\{\tilde{\boldsymbol{N}}_u[m,l,r], (m,l) \in \mathbb{P}_u\left[\dot{m},\dot{l}\right]\right\}\right]$ can not be found explicitly, one can conclude that

$$\arg\min_r \check{\boldsymbol{Y}}_u\left[\dot{m},\dot{l},r\right] \triangleq \arg\min_r \mathrm{var}\left[\left\{\tilde{\boldsymbol{N}}_u[m,l,r]\right\}\right]. \tag{3.32}$$

The optimum receiver windowing duration calculation algorithm utilizes (3.32) to minimize the combined interference energy and maximize capacity. With similar reasoning to Algorithm 1, Algorithm 2 also starts with the assumption of zero initial window duration, and checks to see whether longer window durations are beneficial for each RE. Let us now investigate a possible reduced complexity implementation of this idea, particularly utilizing the relation between $\boldsymbol{Y}_u[m,l,0]$ and $\boldsymbol{Y}_u[m,l,r]$ as shown in (3.28). Let us first define

$$\ddot{y}_u[m,l,r] = \boldsymbol{Y}_u[m,l,r] - \boldsymbol{Y}_u[m,l,0] \tag{3.33a}$$

$$= \sum_{s=N_u+K_u-r+1}^{N_u+K_u} \left(\boldsymbol{y}_{l,u}[s-N_u] - \boldsymbol{y}_{l,u}[s]\right) \boldsymbol{r}_{m,l,u}[s-N_u] \frac{\exp\left(\jmath\frac{2\pi M_{u,m}(s-K_u-1)}{N_u}\right)}{\sqrt{N_u}} \tag{3.33b}$$

to keep following equations concise. Then

$$\check{\boldsymbol{Y}}_u\left[\dot{m},\dot{l},r\right] = \sum_{(m,l)\in\mathbb{P}_u\left[\dot{m},\dot{l}\right]} \frac{\left|\boldsymbol{Y}_u[m,l,r] - \sum_{(\ddot{m},\ddot{l})\in\mathbb{P}_u\left[\dot{m},\dot{l}\right]} \boldsymbol{Y}_u\left[\ddot{m},\ddot{l},r\right]/P\right|^2}{P} \tag{3.34a}$$

$$= \frac{1}{P^3} \sum_{(m,l)\in\mathbb{P}_u\left[\dot{m},\dot{l}\right]} \left|\boldsymbol{Y}_u[m,l,r](P-1) - \sum_{(\ddot{m},\ddot{l})\in\mathbb{P}_u\left[\dot{m},\dot{l}\right]\setminus(m,l)} \boldsymbol{Y}_u\left[\ddot{m},\ddot{l},r\right]\right|^2 \tag{3.34b}$$

$$= \frac{1}{P^3} \sum_{(m,l)\in\mathbb{P}_u\left[\dot{m},\dot{l}\right]} \left| \boldsymbol{Y}_u\left[m,l,0\right](P-1) - \sum_{\left(\ddot{m},\ddot{l}\right)\in\mathbb{P}_u\left[\dot{m},\dot{l}\right]\setminus(m,l)} \boldsymbol{Y}_u\left[\ddot{m},\ddot{l},0\right] \right. \tag{3.34c}$$
$$\left. + \ddot{y}_u\left[m,l,r\right](P-1) - \sum_{\left(\ddot{m},\ddot{l}\right)\in\mathbb{P}_u\left[\dot{m},\dot{l}\right]\setminus(m,l)} \ddot{y}_u\left[\ddot{m},\ddot{l},r\right] \right|^2$$

demonstrates that once

$$\boldsymbol{Y}_u\left[m,l,0\right](P-1) - \sum_{\left(\ddot{m},\ddot{l}\right)\in\mathbb{P}_u\left[\dot{m},\dot{l}\right]\setminus(m,l)} \boldsymbol{Y}_u\left[\ddot{m},\ddot{l},0\right] \tag{3.35}$$

is calculated, the variance of the windowed cases can be calculated by adding the window differences and summing the squared magnitudes. The advantage of the equiweight assumption becomes clear at this point, a simple investigation reveals that once $\check{\boldsymbol{Y}}_u\left[\dot{m},\dot{l},r\right]$ is calculated for an RE, the same calculation for neighboring REs only require adding and removing contributions from few REs. More information on computational complexity is provided in paragraph 3.2.2.3.

3.2.2.3 Computational Complexity

Calculating (3.35) for $(m,l) \leftarrow (m_1,l_1) \in \mathbb{P}_u\left[\dot{m},\dot{l}\right]$ for a single RE requires $2P$ real additions and 2 real multiplications. The result of the same equation for another RE with indices $(m,l) \leftarrow (m_2,l_2) \in \mathbb{P}_u\left[\dot{m},\dot{l}\right]$ can be obtained by adding $P\left(\boldsymbol{Y}_u\left[m_2,l_2,0\right] - \boldsymbol{Y}_u\left[m_1,l_1,0\right]\right)$ to the previously calculated value, resulting in 4 real additions and 2 real multiplications. Thus, calculating (3.35) $\forall\,(m,l) \in \mathbb{P}_u\left[\dot{m},\dot{l}\right]$ requires a total of $6P-4$ real additions and $2P$ real multiplications.

Trials show that the subsets $\mathbb{P}_u\left[\dot{m},\dot{l}\right]$ differ at most by $\log\left(c+P\right)$ individual REs for neighbor REs under vehicular channels [80] for statistically meaningful P values, where c is a small positive constant. While the mean subset difference is well below that for the possible transmission time interval (TTI) durations and bandwidth part configurations in NR, $\log\left(P\right)$ will be assumed for all REs as the mean asymptotically reaches this number with increasing number of allocated slots and

RBs, and to mitigate c. Thus, after (3.35) is calculated for an RE for $\mathbb{P}_u\left[\dot{m}_1, \dot{l}_1\right]$, the results can be generalized for the same RE for another $\mathbb{P}_u\left[\dot{m}_2, \dot{l}_2\right], \left(\dot{m}_2, \dot{l}_2\right) \leftarrow \exists\left\{\left(\dot{m}_1 \pm 1, \dot{l}_1\right), \left(\dot{m}_1, \dot{l}_1 \pm 1\right)\right\}$ by adding $P\left(\sum_{\left(\ddot{m}, \ddot{l}\right) \in \mathbb{P}_u\left[\dot{m}_2, \dot{l}_2\right]} \boldsymbol{Y}_u\left[\ddot{m}, \ddot{l}, 0\right] - \sum_{\left(\ddot{m}, \ddot{l}\right) \in \mathbb{P}_u\left[\dot{m}_1, \dot{l}_1\right]} \boldsymbol{Y}_u\left[\ddot{m}, \ddot{l}, 0\right]\right)$ to the previous findings, which requires $4\log\left(P\right)$ real additions and 2 real multiplications. The findings can then similarly propagate to other REs $\in \mathbb{P}_u\left[\dot{m}_2, \dot{l}_2\right]$ by performing 4 real additions and 2 real multiplications each as described above. Therefore, number of operations required to obtain (3.35) $\forall\left(m, l\right), \forall\left(\dot{m}, \dot{l}\right)$ is upper bounded by $4\left(M_u L_u\left(P + \log\left(P\right) - 1\right) - \log\left(P\right)\right) + 2P$ real additions and $2PM_uL_u$ real multiplications.

A direct investigation reveals that each (3.33b) calculation requires $6r - 2$ real additions and $6r$ real multiplications to obtain the symbol windowed with window duration r. Once the relevant (3.33b) values are calculated, the number of equations required to calculate the difference $\ddot{y}_u\left[m, l, r\right]\left(P - 1\right) - \sum_{\left(\ddot{m}, \ddot{l}\right) \in \mathbb{P}_u\left[\dot{m}, \dot{l}\right] \setminus (m,l)} \ddot{y}_u\left[\ddot{m}, \ddot{l}, r\right]$ in (3.34c) is the same as the number of operations required to obtain (3.35). It should be noted that these values are only required for $(m, l) \in \mathbb{P}_u\left[\dot{m}, \dot{l}\right]$ if $\check{\boldsymbol{Y}}_u\left[\dot{m}, \dot{l}, r\right]$ is being calculated, which is not always needed.

After both differences in (3.34c) is obtained, the sum of the squared magnitudes of the sum of differences can be calculated to finalize (3.34c) calculation. This requires $3P - 1$ real additions and $2P$ real multiplications. If $\boldsymbol{R}_u\left[m, l\right] = R$, (3.34c) must be calculated $\forall r \in \mathbb{N}^*_{\leq \min(R+1, K_u)}$. Once $\boldsymbol{R}_u$ is found, (3.29) is performed to obtain windowed symbols to continue reception, which requires only $2\#\left\{\boldsymbol{R}_u \neq 0\right\}$ real additions and no multiplications. Some statistics for $\boldsymbol{R}_u$ and number of operations performed for vehicular channel conditions are provided in Section 3.3. It should also be noted that the worst case time complexity of the described efficient implementation is on the order of $\mathcal{O}\left(K_u^2 P M_u L_u\right)$, while a more straightforward operation count- and memory-wise exhaustive implementation can run within $\mathcal{O}\left(P + K_u\right)$.

3.2.3 Further Notes on Computational Complexity

The algorithms presented in Section 3.2 are computationally tailored around the basic assumption that both transmitter and receiver window durations are expected to be short as the utilized

extension was solely intended for the channel. While Section 3.3 shows that this assumption holds, there are also other characteristics that can be exploited, such as the spectrotemporal correlation of window durations, and a non-obvious but comprehensible peak in the statistical receiver window duration probability distribution, all of which are presented and discussed in Section 3.3. This subsection was aimed to describe the basic ideas and only simple, universal algorithmic implementation specific details in the most comprehensible manner. Further possible reductions in computational complexity are mentioned along with numerical findings in Section 3.3.

3.3 Numerical Verification

Although the proposed method is formulated for networks with any number of UEs, in this work, a simple network limited to a BS and two UEs equally sharing a 7.68 MHz system bandwidth is considered for the sake of simplicity, as done in other similar works such as [81]. This also allows clearer presentation of the results. This network is realized numerous times with independent and random user data and instantaneous channels, and all presented results are the arithmetic means of all realizations unless otherwise specified. The parameters provided in [82] for link level waveform evaluation under 6 GHz were used when possible. One of the UEs is a high mobility node experiencing a channel that has 30 ns RMS delay spread and 120 km/h mobility, hereinafter referred to as the "'f'ast user", communicating using 60 subcarriers of an OFDM numerology with subcarrier spacing of $\Delta_{f_f} = 60\,\text{kHz}$. The second UEs is a moderate mobility node experiencing a channel that has 100 ns RMS delay spread and 30 km/h mobility, hereinafter referred to as the "'s'low user", communicating using 120 subcarriers of the $\Delta_{f_s} = 30\,\text{kHz}$ numerology in the adjacent band. The PDP of fast user's channel is 3GPP tapped delay line (TDL)-A [80] in $1/2$, TDL-B in $1/3$ and TDL-C in $1/6$ of the simulations to demonstrate the operability of the algorithm under different channel models. Similarly, the PDP of slow user's channel is 3GPP TDL-B in $1/2$, and TDL-A or TDL-C each in $1/4$ of the simulations. The Doppler spectra of both channels are assumed to be classical Jakes [83] at all times [80]. There is a 240 kHz guard band between users.

The SNR of each user is sweeped from 5 dB to 15 dB during which the SNR of the other user is fixed to 10 dB.

Results are obtained for a duration of one NR format 4 slot [84] in the slow user's reference, where both flexible symbols are utilized for UL. The UL transmission interval of a slot followed by the DL transmission interval of the consecutive slot is investigated. There's a timing offset of 64 samples in the UL, whereas the consequent DL period is synchronous. The UL DMRS received at the gNB, which are physical uplink shared channel (PUSCH) DMRS type B mapped [6], are used to estimate the channel. Only this time invariant estimate is used in Algorithm 2 for the following DL transmission interval. This presents the worst-case performance of especially Algorithm 2 under minimum available information. The rate of performance improvement for increasing number of consecutive slots with the help of channel prediction [74] is left for future work. The DL DMRS configuration is single port single layer mapped with crucial parameters uniquely defining the mapping dmrs-AdditionalPosition 3 and dmrs-TypeA-Position pos2 [6]. No windowing or power control is applied to UL signals as well, reducing the performance of solely the proposed methods making it the worst case scenario.

Unless otherwise specified, both UEs utilize a normal CP overhead of $9/128$ with no additional extension for windowing at all times, thus conserving standard 5G NR symbol structure. For comparison, optimum fixed extension windowing algorithm [46] is also featured utilizing the standard extended CP overhead of 25% and the additional extension is used for either transmitter or receiver windowing, as well as F-OFDM [37, 85] and NC-OFDM [50], the tone offset for the former, in accord with the resource allocation, being 7.5 and 3.5 tones for the slow and fast user, respectively; and the N parameter for the latter being $N_{\text{fast}} = 1$ and $N_{\text{slow}} = 2$ per the original work, and both receivers use the iterative correcting receiver [50, Sec. 3] performing 8 iterations. Link adaptation is omitted in the system, all RBs are assigned the same constant MCS which consists of QPSK modulation and $(21/32) \times (7/15)$ standard [86, 87] and extended [88] Bose–Chaudhuri–Hocquenghem (BCH) Turbo product code [89] for the slow user and $(7/16) \times (7/15)$ for the fast user at all times. The MCSs are chosen such that both users operate slightly

below the target BER at the minimum SNR, thus the SNR difference between the users can be referred to as the excess SNR for the utilized SNR values. $P \leftarrow 33$ for both users in Algorithm 2 so that a meaningful z-test can be performed.

The OOB emission of investigated waveforms are depicted in Figure 3.3, where the lines denoted with $\Delta\gamma$ is the results for Algorithm 1, for which the windowed user's average SNR is greater than that of the victim by the provided value; and the sampling points of the victim subcarriers are marked to distinguish between modulations and to provide means to understand the unorthodox frequency localization characteristics of F-OFDM [85] and optimum fixed extension transmitter windowing (ETW) algorithm [46] to unfamiliar readers. Both F-OFDM and ETW-OFDM have unmatched interference performance in the victim's band, but F-OFDM requires the receiver to perform matched filtering, and ETW-OFDM requires an extension that may disturb the standard frame structure, or reduced throughput if the standard extensions are used in vehicular channels as seen in Table 3.2. The interference performance of NC-OFDM at the edge subcarriers also outperforms all cases of Algorithm 1, but Algorithm 1 takes over in the band center subcarriers for high excess SNR. Furthermore, NC-OFDM also requires receiver-side operations, thus has no advantage over F-OFDM. It is seen that while Algorithm 1 has little advantage if the windowing user has no excess SNR, the level of interference decreases further as the window duration is able to increase when the user has excess SNR. Although the proposed algorithm uses the same window design used in ETW-OFDM, the fact that not all REs are windowed prevents the same localization from surfacing. It should also be noted that the gains are a significant function of channel responses of both UEs, and the transmit OOB emission is unable to demonstrate the gains clearly. The fair proportional network throughput, calculated similar to network proportional network capacity using the geometric means of throughput of each user, can be seen in Table 3.2 for optimum fixed extension transmitter and receiver windowed OFDM [46], NC-OFDM, conventional CP-OFDM, adaptive transmitter windowed with estimates obtained using Algorithm 1, adaptive transmitter windowed with optimum durations, F-OFDM, adaptive receiver windowed using durations calculated using Algorithm 2, adaptive transmitter and receiver windowed with transmitter windowing durations

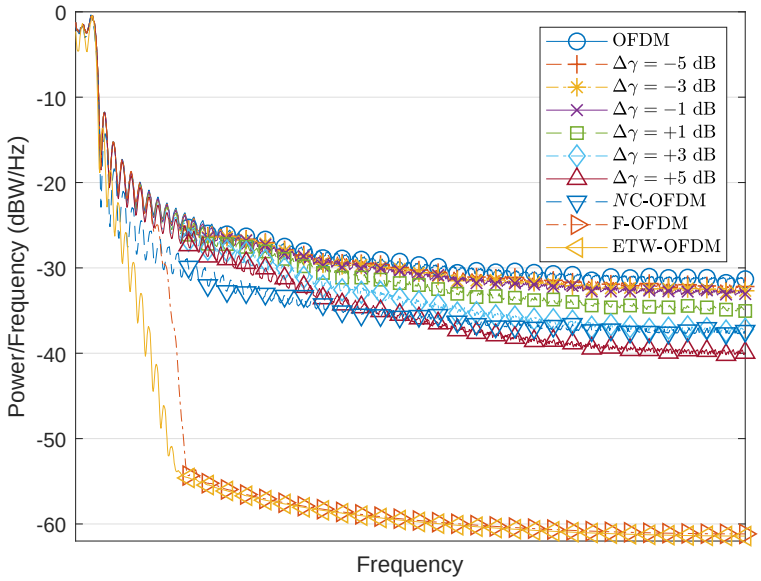

Figure 3.3: OOB emission of investigated modulations.

calculated using Algorithm 1 without knowing receivers are applying Algorithm 2 followed by Algorithm 2 at the receivers, Algorithm 2 applied to the signals that are adaptive transmitter windowed with optimum durations, adaptive transmitter and receiver windowed with transmitter windowing durations calculated using Algorithm 1 knowing receivers are applying Algorithm 2 followed by Algorithm 2 at the receivers, and adaptive transmitter and receiver windowed with durations optimized jointly. The optimum values were obtained by maximizing the fair proportional network throughput using an evolutionary integer genetic algorithm [90] to find the optimum inputs to Algorithms 1 and/or 2 under actual time-varying channels. It can be seen that although previously proposed extended windowing algorithms improve the BERs, increasing the effective symbol duration by ~18% erases the positive implications on the throughput and reduces it. The artificial noise introduced by the NC-OFDM cannot be resolved at the receivers at these high mobility conditions correctly yielding a decrease in actual throughput. It can be seen that even the featured worst case results of the proposed algorithms increase the throughput and improving algorithm outputs by channel prediction promises further gains closer to optimum. While F-OFDM provides higher throughput compared to Algorithm 1 and adaptive transmitter windowing, it requires that

Table 3.2: Fair proportional network throughput of tested modulations

Modulation	Throughput (Mbps)	Gain over CP-OFDM
ETW-OFDM	1.1949	-15.832%
ERW-OFDM	1.1952	-15.708%
*N*C-OFDM	1.3927	-1.456%
CP-OFDM	1.3985	-
Algorithm 1	1.3986	+0.042%
TW-OFDM (w/o Ext)	1.3987	+0.049%
F-OFDM	1.3988	+0.057%
Algorithm 2	1.3990	+0.071%
Algorithm 1 + Algorithm 2 (independent)	1.3991	+0.078%
TW-OFDM + Algorithm 2 (independent)	1.3992	+0.085%
Algorithm 1 + Algorithm 2 (joint)	1.3996	+0.114%
TW-OFDM+ RW-OFDM (joint)	1.3998	+0.128%

both ends of the communication are aware of the filtering process and apply it [37,38,85]. Although knowledge of such improves the throughput, the proposed algorithms do not require the knowledge and action of the counterpart and this is the strength of the proposed method compared to F-OFDM. To show the dependence of window durations on excess SNR, the ratio of estimated and optimum expected window durations to the CP of the corresponding UEs as a function of the SNR difference between the user in interest and the other user are demonstrated in Figure 3.4. The results are ordered as follows: Receiver windowing durations of only Algorithm 2, Algorithm 2 applied to the signals transmitted after applying Algorithm 1, Algorithm 2 applied to transmitter windowed samples with the optimum duration if the gNB is unaware that receivers employ Algorithm 2, Algorithm 2 applied to to the signals produced Algorithm 1 where gNB knows both receivers also employ Algorithm 2, and Algorithm 2 applied to transmitter windowed samples with the optimum duration calculated knowing that receiver will apply Algorithm 2; as well as transmitter windowing durations estimated by Algorithm 1, optimum adaptive transmitter windowing durations, transmitter windowing duration estimates provided by Algorithm 1 knowing that both receivers also employ Algorithm 2 and optimum transmitter windowing durations calculated if both receivers also employ Algorithm 2. A critical observation is that the transmitter windowing durations, both estimated and

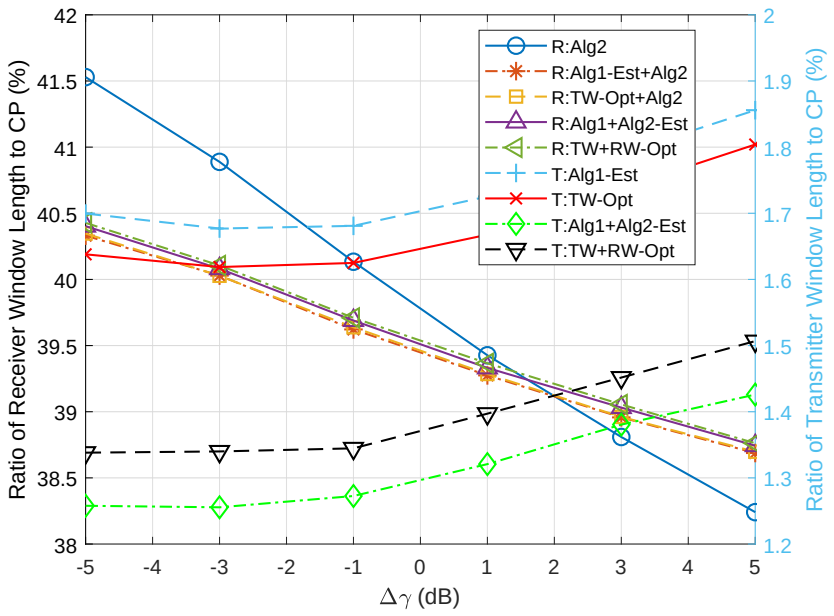

Figure 3.4: $\mathbb{E}\{\boldsymbol{R}_u/K_u\}$ and $\mathbb{E}\{\boldsymbol{T}_u/K_u\}$ against the SNR difference between users.

actual optimum, increase as the SNR of the user increases, whereas the receiver windowing duration decreases. This proves the basic idea behind fair optimization that the ones with excess SNR must focus on their impact on others whereas the ones with lesser SNR must focus on the impact they receive from others. It can also be seen that the optimum durations for each side get shorter once the resources are jointly used, i.e., the gNB knows that receivers utilize Algorithm 2. Figure 3.5 shows the probability of the calculated window duration being a certain amount away from the optimum duration, between Algorithm 1 and optimum transmitter windowing durations, between Algorithm 1 calculated knowing that receivers utilize Algorithm 2 and optimum transmitter window durations obtained when receivers employ Algorithm 2; and receiver windowing durations estimated at the transmitter during calculation of Algorithm 2 and the values obtained at receivers. It can be seen that the guess for both the transmitter and the receiver windowing durations are more accurate for the slower user, proving the dependence on mobility at estimates without channel tracking and prediction. Furthermore, since receiver windowing durations only matter for the RBs in interest as discussed before, receiver windowing durations can be guessed with over 98% probability without making an error. The transmitter windowing estimates have more than 95% probability of being the

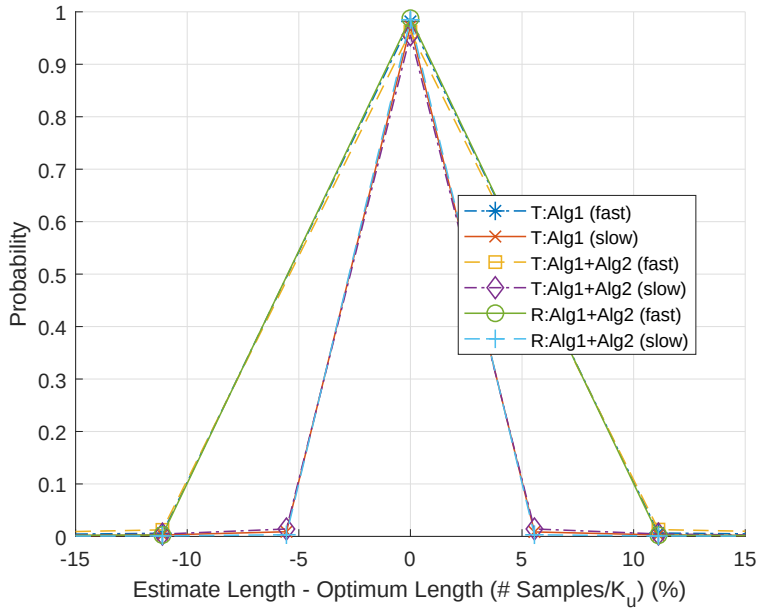

Figure 3.5: Probability of the error between estimated and optimum window lengths being equal to certain percentages of CP.

same as optimum, while overestimating is slightly more probable in the only Algorithm 1 case while underestimating is more probable in the both algorithms utilized case. Figure 3.6 and Figure 3.7 show the amount of receiver and transmitter windowing applied at the band centers and edges and checks the validity of [45] where the window durations are labeled similar to that of Figure 3.4. It can be seen that the amount of transmitter windowing indeed increases at the band edges, and furthermore it is more important that the faster user with the larger subcarrier spacing and less spectral localization to apply more transmitter windowing. This derives from the fact that the PSD of signals with larger subcarrier spacing decay slower than those with smaller subcarrier spacing, hence are more crucial for the interference in the system. It can be seen that the receiver windowing durations are higher at the band centers and higher for the user with lower subcarrier spacing. This occurs partly due to the window function design. The window functions are designed to minimize the absorption outside the the band of interest, however as the pass-band of the window gets smaller, the reduction performance decreases as well [46]. Since the window pass-bands are smaller on the edge subcarriers, the gain from reduced ACI and ICI reduces whereas the performance reduction

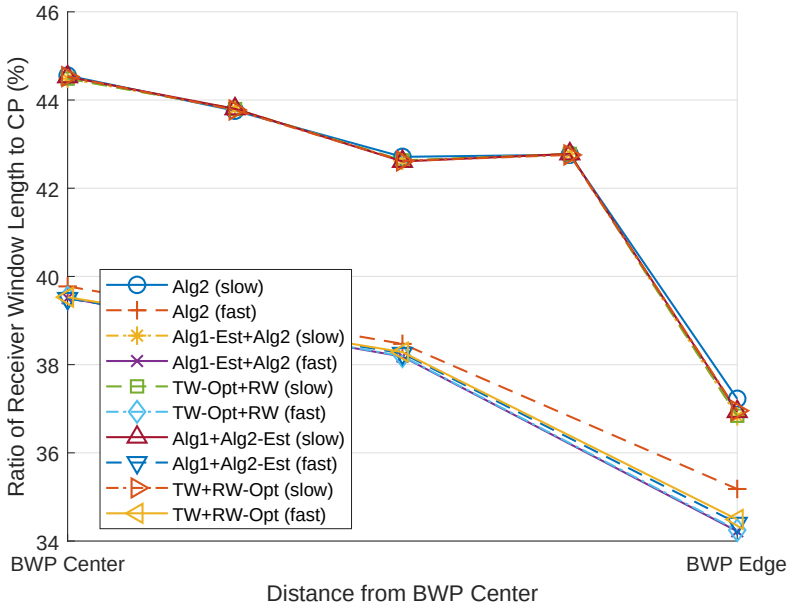

Figure 3.6: Receiver windowing durations as a function of distance from center of the consumed band.

due to increased ISI stays the same. This favors longer window durations at the inner subcarriers where increasing window durations result in significant ICI and ACI reduction. The gain from ICI reduction becomes more prominent for the faster user which observes even higher window lengths at inner subcarriers due to the increased ICI. The gain from either type of windowing reduces for both users as windowing at the counterparty is introduced to the systems, both by reduction of forces driving windowing at a given side and also increase in ISI occurring by applying windowing, as both users observe shorter windowing durations on either side that is more uniformly distributed from band centers to edges. Before the average number of performed operations are provided for presented Algorithms in their current forms and compared, spectrotemporal statistics of window durations are provided to demonstrate that there is room for further computational complexity reductions, which are left for future works. Both experienced channel and amount of interference are highly correlated in both dimensions, which in turn create correlated window durations that can reduce complexity load. For example, Figure 3.8 shows the probability that window durations calculated for adjacent subcarriers differ by a given duration, as a function of CP length. It is seen

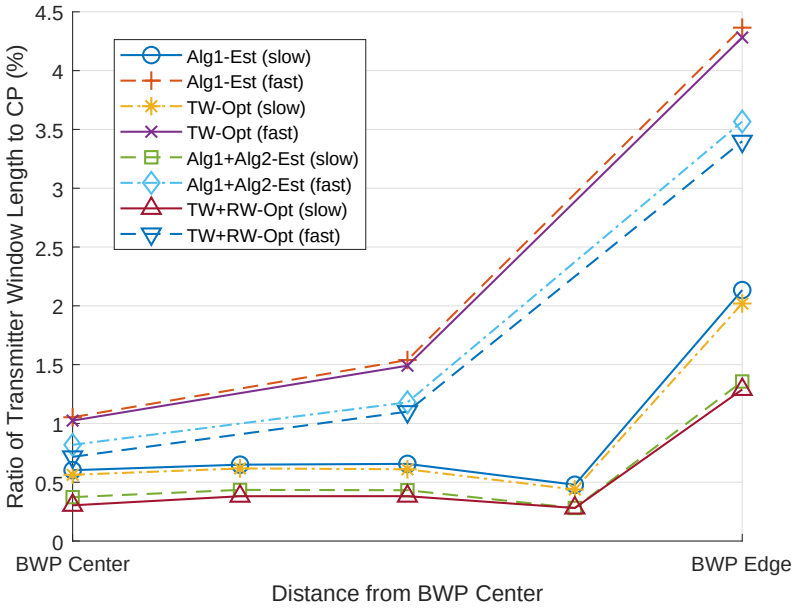

Figure 3.7: Transmitter windowing durations as a function of distance from center of the consumed band.

that no more than 35% CP duration difference occurred at any time. This suggests that if a subcarrier was calculated to have a long window duration, checking brief window durations for the adjacent subcarriers may be skipped at first and the search can start from a higher value. Furthermore, REs may be grouped and processed together. Figure 3.9 presents the same results for Algorithm 2, showing that the differences are even smaller in both time and frequency as the duration is determined using the variance over a group of REs and the RE groups of adjacent RE differ little. It is also worth noting that window durations in adjacent REs of the faster user are more likely to differ by longer durations than that of the slower user, which depends on both increased subcarrier spacing and channel variations. Finally, the computational load of the algorithms in their presented forms is analyzed and compared with F-OFDM. The filter lengths are $N_u/2+1$ per [85], and since filters consist of complex values, the computational complexity of F-OFDM is $(N_u+K_u)\,L_u\,(3N_u/2+2)$ real additions and $(N_u+K_u)\,L_u\,(2N_u+4)$ real multiplications at the UE, and these values summed over all users at the gNB. The computational complexities of the presented algorithms depend on the window duration and side of each RE, of which values have the probability distributions shown

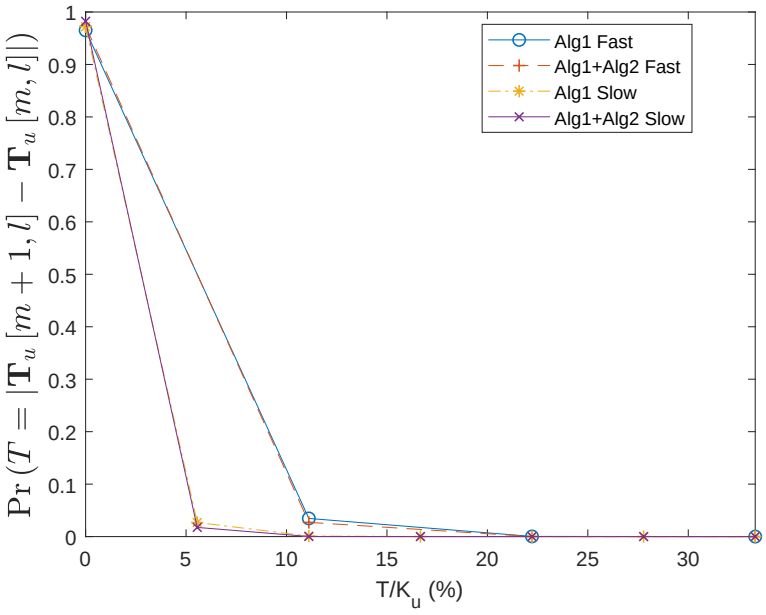

Figure 3.8: Probability that transmitter window durations in adjacent subcarriers differ by the given amount.

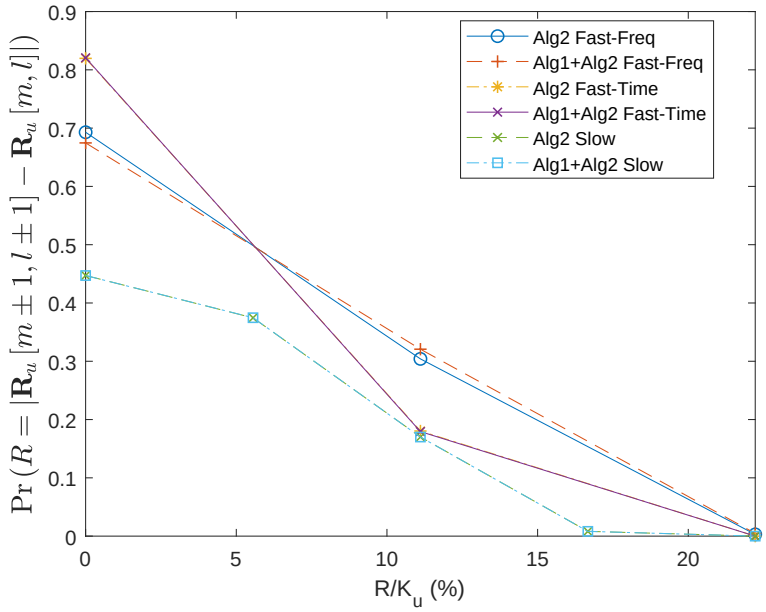

Figure 3.9: Probability that receiver window durations in adjacent REs differ by the given amount.

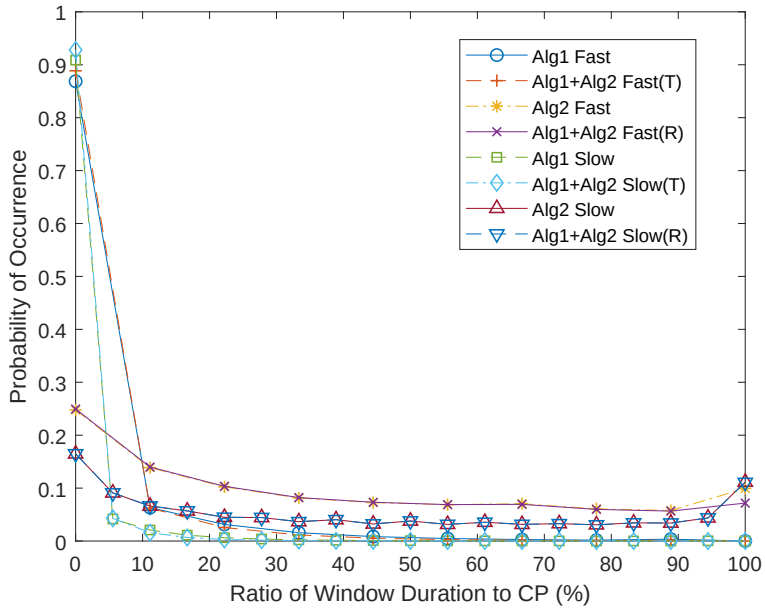

Figure 3.10: Probability of transmitter (T) and receiver (R) window durations occurring in test scenarios.

in Figure 3.10. Accordingly, the gNB and UE side computational complexities of the algorithms are presented in Table 3.3. As Algorithm 1 only runs at the gNB and Algorithm 2 only runs at the UE without any operation requirements at the counterpart, the counterpart complexities are 0 for both users. It is seen that while the gNB side complexity for Algorithm 1 is higher than that of F-OFDM, assumin that gNBs are not computationally bounded, the transparency of Algorithm 1 still makes it a possible candidate under heavy traffic. The computational complexity of Algorithm 2 is similar to that of F-OFDM if the further computational complexity reduction tricks described in the preceding paragraph are not employed, and Algorithm 2 is also transparent to the transmitter. Another interesting observation that can be made from Figure 3.10 is that for Algorithm 2, under severe ACI conditions, longer window durations may be beneficial, however since the window duration is limited by CP length, all those results manifest themselves at the upper bound, creating a high probability peak at the longest duration. Computational complexity can be further reduced if Algorithm 2 is modified to check the longest possibility before others, however these highly implementation specific details are left for future work.

Table 3.3: Computational complexities of F-OFDM and algorithms 1 and 2

Algorithm	gNB add	gNB mult	UE add	UE mult
F-OFDM	1907040	2551488	637872+ 1269168	854880+ 1696608
Alg. 1	5342353	5332295	0	0
Alg. 2	0	0	2088692+ 4166143	1054709+ 2236623

Chapter 4: Non-Redundant OFDM Receiver Windowing for 5G Frames and Beyond

The following notation is used throughout this Chapter[8]: $(\cdot)^{\mathsf{T}}$, $(\cdot)^{*}$ and $(\cdot)^{\mathsf{H}}$ denote the transpose, complex conjugate, and Hermitian operations, $\boldsymbol{e}_{i,N}$ corresponds to the ith row of the $N \times N$ identity matrix $\boldsymbol{I}_N$, $\boldsymbol{A} \odot \boldsymbol{B}$ and $\boldsymbol{A} \oslash \boldsymbol{B}$ correspond to Hadamard multiplication and division of matrices $\boldsymbol{A}$ and $\boldsymbol{B}$, and $\boldsymbol{A}$ by $\boldsymbol{B}$, $\boldsymbol{0}_{a\times b}$ and $\boldsymbol{1}_{a\times b}$ denote matrices of zeros and ones with a rows and b columns, $\mathrm{diag}\,(\boldsymbol{v})$ returns a square diagonal matrix with the elements of vector $\boldsymbol{v}$ on the main diagonal, $\mathrm{diag}\,(\boldsymbol{M})$ returns the elements on the main diagonal of matrix $\boldsymbol{M}$ in a vector, $\mathcal{CN}\left(\mu, \sigma^2\right)$ represents complex Gaussian random vectors with mean μ and variance σ^2, $\mathrm{T}(\boldsymbol{c}, \boldsymbol{r})$ yields the Toeplitz matrix where the first column is $\boldsymbol{c}$ and the first row is $\boldsymbol{r}$, $\boldsymbol{A} \otimes \boldsymbol{B}$ is the Kronecker tensor product of $\boldsymbol{A}$ and $\boldsymbol{B}$ matrices.

4.1 System Model

We aim to receive the information transmitted by a user, hereinafter referred to as the desired user, of which corresponding elements are distinguished with subscript 0 in the multi-user context. The desired user is transmitting data over D contiguous subcarriers in an N subcarrier CP-OFDM system. To prevent ISI across consecutive OFDM symbols and to transform the linear convolution of the multipath channel to a circular convolution, a CP of length L samples is prepended to each transmitted OFDM symbol. The samples corresponding to a CP-OFDM symbol of the desired user are denoted by $\boldsymbol{x}_0 \in \mathbb{C}^{(N+L)\times 1}$, and are obtained as $\boldsymbol{x}_0 = \boldsymbol{A}\boldsymbol{F}_N{}^{\mathsf{H}}\boldsymbol{M}\boldsymbol{d}$, where $\boldsymbol{F}_N \in \mathbb{C}^{N\times N}$ is the N-point FFT matrix, $\boldsymbol{M} \in \mathbb{Z}^{N\times D}$ is the subcarrier mapping matrix, $\boldsymbol{d} \in \mathbb{C}^{D\times 1}$ is the SC

[8]Part of this chapter was published in [91] and patented [92]. Permission is included in Appendix A.

modulated data vector to be transmitted and $\boldsymbol{A} \in \mathbb{R}^{(N+L)\times N}$ is the CP addition matrix defined as

$$\boldsymbol{A} = \begin{bmatrix} \mathbf{0}_{L\times(N-L)} & \boldsymbol{I}_L \\ & \boldsymbol{I}_N \end{bmatrix}. \tag{4.1}$$

During the transmission of the desired user, the adjacent bands are employed for communication by other users, hereinafter referred to as interfering users, of which signaling is neither synchronous nor orthogonal to that of the desired user. The signals transmitted from all users propagate through a time varying multipath channel before reaching the receiver. Assuming perfect synchronization to the desired user's signal, let the channel gain of the kth sample of the desired and jth interfering user's signals, for $j \neq 0$, during the reception of the nth sample be denoted by $h_{0,n,k}$ and $h_{j,n,k}$, respectively. For clarity, we assume that $\sum_{k=1}^{N+L} |h_{j,n,k}|^2 = 1, \forall j$. If the channel convolution matrix of the jth user for the scope of the desired user's symbol of interest is shown with $\boldsymbol{H}_j \in \mathbb{C}^{(N+L)\times(N+L)}$, respectively; the element in the kth column of nth row of any $\boldsymbol{H}_j$ is $h_{j,n,k}$, respectively. It should be noted that, if jth user's channel was time-invariant, $\boldsymbol{H}_j$ would be a Toeplitz matrix, whereas in this model, the elements are varying for all j and the autocorrelation functions and the power spectral densities of any diagonal of any channel convolution matrix fit those defined in [83]. The first $N + L$ samples received over the wireless medium under perfect synchronization to the desired user's signal normalized to the noise power are stored in $\boldsymbol{y} \in \mathbb{C}^{(N+L)\times 1}$, which is given as

$$\boldsymbol{y} = z + \sum_j \left(\sqrt{\gamma_j} \boldsymbol{H}_j \boldsymbol{x}_j \right), \tag{4.2}$$

where $z \sim \mathcal{CN}(0, 1)$ is the background AWGN, γ_0 and γ_j are the SNRs of the desired and jth interfering user, respectively, and $\boldsymbol{x}_j$ is the sample sequence transmitted by jth interfering user in the reference duration of the desired symbol for $j \neq 0$.

4.1.1 Reception in Self-Orthogonal RW-OFDM Systems

A brief review of channel estimation, equalization and ICI in self-orthogonal conventional RW-OFDM systems may help understand the derivation of the aforementioned for Hann RW-OFDM.

For the sake of brevity, assume the receiver utilizes an extensionless receiver windowing function of tail length $K \in \mathbb{N}_{\leq L}$ for all subcarriers to receive the data transmitted by the desired user, and the window function coefficients scaling the CP are shown as $\breve{\boldsymbol{w}}_K \in \mathbb{R}^{K\times 1}$ [64]. Then, the windowed CP removal matrix $\boldsymbol{B}_K \in \mathbb{R}^{N\times(N+L)}$ is obtained as

$$\boldsymbol{B}_K = \begin{bmatrix} \boldsymbol{0}_{(N-K)\times(L-K)} & \boldsymbol{0}_{(N-K)\times K} & \boldsymbol{I}_{(N-K)\times(N-K)} & \boldsymbol{0}_{(N-K)\times K} \\ \boldsymbol{0}_{K\times(L-K)} & \operatorname{diag}(\breve{\boldsymbol{w}}_K) & \boldsymbol{0}_{K\times(N-K)} & \boldsymbol{I}_K - \operatorname{diag}(\breve{\boldsymbol{w}}_K) \end{bmatrix}. \tag{4.3}$$

Note that for $K = 0$, eq. (4.3) reduces to the rectangular windowing CP removal matrix $\boldsymbol{B}_0 = \begin{bmatrix} \boldsymbol{0}_{N\times L} & \boldsymbol{I}_N \end{bmatrix}$. The received symbols in a RW-OFDM system are then given as

$$\boldsymbol{r} = \boldsymbol{M}^{\mathsf{T}}\boldsymbol{F}_N\boldsymbol{B}_K\boldsymbol{y} \tag{4.4}$$

$$= \boldsymbol{M}^{\mathsf{T}}\boldsymbol{\Theta}\boldsymbol{d} + \boldsymbol{M}^{\mathsf{T}}\tilde{\boldsymbol{z}}, \tag{4.5}$$

where the channel disturbance vector $\tilde{\boldsymbol{z}} \in \mathbb{C}^{N\times 1}$ is

$$\tilde{\boldsymbol{z}} = \boldsymbol{F}_N\boldsymbol{B}_K\left(z + \sum_{j\in\mathbb{Z}, j\neq 0}\left(\sqrt{\gamma_j}\boldsymbol{H}_j\boldsymbol{\chi}_j\right)\right) \tag{4.6}$$

$$\equiv \begin{bmatrix} z_1 & z_2 & \dots & z_N \end{bmatrix}^{\mathsf{T}}, \tag{4.7}$$

of which components are assumed to be z_i $\mathcal{CN}\left(0, \sigma^2_{\tilde{z}_i}\right)$, $\forall i \in \mathbb{N}_{\leq N}$ where $\sigma^2_{\tilde{z}_i}$ is the noise and ACI power[9] affecting ith subcarrier that can be calculated per [7, 64];

$$\sigma^2_{\tilde{z}} \in \mathbb{R}^{+}_{N\times 1} = \begin{bmatrix} \sigma^2_{\tilde{z}_1} & \sigma^2_{\tilde{z}_2} & \dots & \sigma^2_{\tilde{z}_N} \end{bmatrix}^{\mathsf{T}} \tag{4.8}$$

is the disturbance variance vector, and $\boldsymbol{\Theta} \in \mathbb{C}^{N\times N}$ is the complete CFR matrix of the desired user's channel obtained as

$$\boldsymbol{\Theta} = \boldsymbol{F}_N \boldsymbol{B}_K \boldsymbol{H}_0 \boldsymbol{A} \boldsymbol{F}_N{}^{\mathsf{H}}. \tag{4.9}$$

The diagonal components of eq. (4.9) are the channel coefficients scaling the subcarrier in interest, and is referred to as the CFR in the literature, hereinafter shown with $\boldsymbol{\theta} \in \mathbb{C}^{N\times 1}$ where

$$\boldsymbol{\theta} = \operatorname{diag}\left(\boldsymbol{\Theta}\right), \tag{4.10}$$

whereas the off-diagonal component on the kth column of $n \neq k$th row, would be the coefficient scaling the interference from the kth subcarrier to the nth subcarrier. Had there been no time variation in the channel and the MED of the channel was shorter than the discarded CP duration at all times, that is,

$$h_{0,n_1,n_1-\Delta k} = h_{0,n_2,n_2-\Delta k}, \qquad \forall n_1, n_2, \Delta k, \tag{4.11}$$

$$h_{0,n,k} = 0, \qquad \forall k < n - (L-K), \forall n, \tag{4.12}$$

$\boldsymbol{B}_K \boldsymbol{H}_0 \boldsymbol{A}$ would have resulted in a Toeplitz matrix, meaning $\boldsymbol{\Theta}$ would be a diagonal matrix, and the system would be ICI and ISI-free. Most modern receivers assume these conditions are valid and ignore ICI and ISI, which can only be estimated using advanced time-domain channel estimation algorithms such as [93]. Although results are numerically verified using signals received over time-varying vehicular channels, all algorithms, proposed or presented for comparison in this work,

[9] ISI due to the previous OFDM symbol transmitted by the desired user may also exist, however it is omitted as the system is modeled for a single OFDM symbol for the sake of clarity. Interested readers may see the detailed multi-symbol system models provided in [7, 64].

estimate the channel assuming eq. (4.11) and eq. (4.12) are valid. Equation eq. (4.10) can also be written as

$$\boldsymbol{\theta} = \boldsymbol{F}_N \boldsymbol{h}, \forall n \in \mathbb{N}^*_{\leq N}, \tag{4.13}$$

where the vector $\boldsymbol{h} \in \mathbb{C}^{N\times 1} \triangleq \begin{bmatrix} \hat{h}_0 & \hat{h}_1 & \dots & \hat{h}_{N-1} \end{bmatrix}^{\mathsf{T}}$ is the static CIR estimate of the desired user's channel during that OFDM symbol, of which elements in fact correspond to

$$\hat{h}_k = \frac{1}{N} \sum_{n=1}^{N} \boldsymbol{e}_{n,N} \boldsymbol{B}_K \boldsymbol{H}_0 \boldsymbol{A} \boldsymbol{e}_{\alpha,N}{}^{\mathsf{T}}, \tag{4.14}$$

where $\alpha = ((n-k-1) \bmod N) + 1$. Thus, ignoring the noise and ACI for the time being, if a known SC symbol sequence denoted by $\tilde{\boldsymbol{d}}$, commonly referred to as the pilot sequence, is transmitted, the following symbols are expected to be received under aforementioned assumptions:

$$\begin{aligned} \boldsymbol{r} &= \sqrt{\gamma_0} \boldsymbol{M}^{\mathsf{T}} \boldsymbol{F}_N \boldsymbol{B}_K \boldsymbol{H}_0 \boldsymbol{A} \boldsymbol{F}_N{}^{\mathsf{H}} \boldsymbol{M} \tilde{\boldsymbol{d}} && (4.15)\\ &= \sqrt{\gamma_0}\, \mathrm{diag}\left(\boldsymbol{M}^{\mathsf{T}} \boldsymbol{F}_N \boldsymbol{h}\right) \tilde{\boldsymbol{d}} && (4.16)\\ &= \sqrt{\gamma_0}\, \mathrm{diag}\left(\tilde{\boldsymbol{d}}\right) \boldsymbol{M}^{\mathsf{T}} \boldsymbol{F}_N \boldsymbol{h}. && (4.17) \end{aligned}$$

Equation eq. (4.17) is an algebraic manipulation of eq. (4.16) in an effort to take the CIR outside the diagonalization for estimation in the next step. Assuming the receiver does not assume apriori knowledge of the SNR component and it is inherited within the CIR, the CIR estimate is obtained as

$$\boldsymbol{h} = \left(\mathrm{diag}\left(\tilde{\boldsymbol{d}}\right) \boldsymbol{M}^{\mathsf{T}} \boldsymbol{F}_N\right)^{-1} \boldsymbol{r}, \tag{4.18}$$

wherein the inversion refers to the Moore-Penrose pseudoinverse. The CIRs of data carrying OFDM symbols between pilot carrying OFDM symbols are interpolated and according CFR responses are calculated. Finally, equalized data symbol estimates are obtained as [68]

$$\hat{\boldsymbol{d}} = \boldsymbol{M}^{\mathsf{T}} \left(\left(\mathrm{diag}\left(\boldsymbol{\theta} \odot \boldsymbol{\theta}^* + \sigma_{\tilde{z}}^2 \right) \right)^{-1} \mathrm{diag}\left(\boldsymbol{\theta}\right)^* \boldsymbol{F}_N \boldsymbol{B}_K \boldsymbol{y} \right). \tag{4.19}$$

4.2 Proposed Method

The Hann window must consist exactly of N samples so that the spectrum is sampled at the right points as seen in Figures 1.5 and 1.6. Furthermore, discarding the L CP samples at the beginning helps prevent ISI across consecutive desired OFDM symbols transmitted by the desired user. The sample indices for the remaining samples can be written as $\boldsymbol{n} = \begin{bmatrix} 0 & 1 & \dots & N-1 \end{bmatrix}$. The Hann window function normalized to window this interval without changing it's energy is obtained as

$$\boldsymbol{w} = \frac{4N}{2N + \sin\left(\frac{\pi - 2\pi N}{N-1}\right)\csc\left(\frac{\pi}{N-1}\right) - 1} \sin^2 \frac{\pi \boldsymbol{n}}{N-1}. \tag{4.20}$$

The Hann windowing matrix $\boldsymbol{W} \in \mathbb{R}^{N \times (N+L)}$, that removes the CP and windows the remaining received samples with the Hann function is formed as

$$\boldsymbol{W} = \begin{bmatrix} \boldsymbol{0}_{N \times L} & \operatorname{diag}(\boldsymbol{w}) \end{bmatrix}. \tag{4.21}$$

The received subcarrier vector $\tilde{\boldsymbol{r}} \in \mathbb{C}^{N \times 1}$ that contains all Hann windowed subcarriers is obtained as

$$\tilde{\boldsymbol{r}} = \boldsymbol{F}_N \boldsymbol{W} \boldsymbol{y}. \tag{4.22}$$

4.2.1 ICI and Channel Estimation in Hann RW-OFDM

A quick investigation of eq. (4.20) and eq. (4.21) show that the orthogonality conditions presented in [44] are not satisfied. In this subsection, we calculate the consequent ICI induced by the Hann window function, and accordingly engineer a method to estimate the CFR and the disturbance variances using any pilot structure, including those of 4G & 5G mobile communication.

Straightforward calculation reveals that

$$\boldsymbol{F}_N \operatorname{diag}(\boldsymbol{w}) \boldsymbol{F}_N{}^{\mathsf{H}} = \mathrm{T}\left(\boldsymbol{v}^{\mathsf{T}}, \boldsymbol{v}\right), \tag{4.23}$$

where $\boldsymbol{\nu} = \begin{bmatrix} 1 & -1/2 & \mathbf{0}_{1\times(N-2)} \end{bmatrix}$. Hence, assuming that eq. (4.11) and eq. (4.12) are valid, the CFR of the desired user's channel, if the Hann window is used, is given as

$$\tilde{\boldsymbol{\Theta}} = \boldsymbol{F}_N \boldsymbol{W} \boldsymbol{H}_0 \boldsymbol{A} \boldsymbol{F}_N{}^{\mathsf{H}} \tag{4.24}$$

$$= \mathfrak{T}\left(\boldsymbol{\nu}^{\mathsf{T}}, \boldsymbol{\nu}\right) \boldsymbol{\Theta}. \tag{4.25}$$

Before the relevant subcarriers are demapped, note that Hann windowing causes received subcarriers that are adjacent to the edgemost pilot-transmitted subcarriers to carry copies of the pilots transmitted at these subcarriers. In an attempt to utilize this energy, this receiver demaps these subcarriers as well using an extended demapping matrix $\check{\boldsymbol{M}}^{\mathsf{T}} \in \mathbb{Z}^{(D+2)\times N}$. Thus, ignoring channel disruption for the time being, if pilot symbols were transmitted, the received pilot symbols are obtained as

$$\boldsymbol{\Delta} = \check{\boldsymbol{M}}^{\mathsf{T}} \tilde{\boldsymbol{\Theta}} \boldsymbol{M} \tilde{\boldsymbol{d}} \tag{4.26}$$

$$= \check{\boldsymbol{M}}^{\mathsf{T}} \mathfrak{T}\left(\boldsymbol{\nu}^{\mathsf{T}}, \boldsymbol{\nu}\right) \boldsymbol{\Theta} \boldsymbol{M} \tilde{\boldsymbol{d}} \tag{4.27}$$

$$= \check{\boldsymbol{M}}^{\mathsf{T}} \mathfrak{T}\left(\boldsymbol{\nu}^{\mathsf{T}}, \boldsymbol{\nu}\right) \operatorname{diag}\left(\boldsymbol{F}_N \boldsymbol{h}\right) \boldsymbol{M} \tilde{\boldsymbol{d}} \tag{4.28}$$

$$= \check{\boldsymbol{M}}^{\mathsf{T}} \mathfrak{T}\left(\boldsymbol{\nu}^{\mathsf{T}}, \boldsymbol{\nu}\right) \operatorname{diag}\left(\boldsymbol{M} \tilde{\boldsymbol{d}}\right) \boldsymbol{F}_N \boldsymbol{h}. \tag{4.29}$$

The result of $\mathfrak{T}\left(\boldsymbol{\nu}^{\mathsf{T}}, \boldsymbol{\nu}\right) \operatorname{diag}\left(\boldsymbol{M} \tilde{\boldsymbol{d}}\right)$, which can be thought as a filtering operation as it involves multiplication of pilot vector with a Toeplitz matrix as denoted in Figure 1.8, may include nulled pilots in some subcarriers due to induced ICI in case QPSK modulated Gold sequences are utilized as pilot signals [6]. However, the ACI rejection allows estimating the CIR better, namely, the disturbance level in

$$\boldsymbol{h} = \left(\check{\boldsymbol{M}}^{\mathsf{T}} \mathfrak{T}\left(\boldsymbol{\nu}^{\mathsf{T}}, \boldsymbol{\nu}\right) \operatorname{diag}\left(\boldsymbol{M} \tilde{\boldsymbol{d}}\right) \boldsymbol{F}_N\right)^{-1} \boldsymbol{\Delta} \tag{4.30}$$

is less than that of eq. (4.18) if the ACI significantly outpowers AWGN. It is noteworthy that although eq. (4.30) still does not have a full-rank solution, exploiting the low density of $\boldsymbol{h}$ as pointed out

in [94] allows implementation of an approximate linear minimum mean square error (LMMSE) estimator relating the two sides as presented in [95]. Any other variation of [94] may be used, but [95] is chosen in the numerical verification of this work since the computational complexity, error bounds and introduced delays of this approach remain within vehicular communication requirements as accepted by the community. Furthermore, depending on the ratio of nonzero pilot products to the delay spread, the estimation error can be shown to converge to zero [96]. The solution was later modified to be stable regardless of the condition of the pilot product matrix [97] and also computationally highly efficient [98]. Furthermore, the DFT of the disruption-only taps described in [95] is used to estimate $\boldsymbol{\sigma}_{\tilde{z}}^2 \in \mathbb{C}^{N\times 1}$, which is then interpolated throughout the data carriers similar to CIR estimates. After the CIR estimates are interpolated, they are transformed to frequency domain to obtain the CFR estimates $\hat{\boldsymbol{\theta}} \in \mathbb{C}^{D\times 1}$.

4.2.2 Design of an MRC-SIC Receiver

Similar to the described channel estimation, this receiver also attempts to utilize the energy in the subcarriers adjacent to the edgemost data carriers. In this case, the received symbols $\check{\boldsymbol{d}} \in \mathbb{C}^{(D+2)\times 1}$ are written as

$$\check{\boldsymbol{d}} = \check{\boldsymbol{M}}^{\mathsf{T}} \boldsymbol{r} \tag{4.31}$$

$$= \tilde{\boldsymbol{H}} \boldsymbol{d} + \check{\boldsymbol{M}}^{\mathsf{T}} \boldsymbol{F}_N \boldsymbol{W} \boldsymbol{z}, \tag{4.32}$$

where, the extended effective channel matrix $\tilde{\boldsymbol{H}} \in \mathbb{C}^{(D+2)\times D}$ is obtained as

$$\tilde{\boldsymbol{H}} = \mathrm{T}\left(\begin{bmatrix} -1/2 & \tilde{\boldsymbol{v}} \end{bmatrix}^{\mathsf{T}}, \begin{bmatrix} -1/2 & \boldsymbol{0}_{1\times(D-1)} \end{bmatrix} \right) \mathrm{diag}\left(\hat{\boldsymbol{\theta}}\right), \tag{4.33}$$

where $\tilde{\boldsymbol{v}} = \begin{bmatrix} 1 & -1/2 & \boldsymbol{0}_{1\times(D-1)} \end{bmatrix}$. The energy due to the signal modulated to the mth transmitted subcarrier on the kth observed subcarrier is in the kth row and mth column of $\boldsymbol{\Sigma} \in \mathbb{R}^{(D+2)\times D}$ where

$$\boldsymbol{\Sigma} = \tilde{\boldsymbol{H}} \odot \tilde{\boldsymbol{H}}^{*}. \tag{4.34}$$

The signal-plus-ICI power on the kth observed subcarrier is given in the kth column of $\boldsymbol{\sigma} \in \mathbb{R}^{1\times(D+2)}$, where

$$\boldsymbol{\sigma} = \mathbf{1}^{1\times D}(\boldsymbol{\Sigma})^{\mathsf{T}}. \tag{4.35}$$

If the mth transmitted subcarrier is in interest, the disruption-plus-ICI power contribution that would come from combining the kth observed subcarrier with unit gain is given on the mth row and kth column of

$$\hat{\boldsymbol{\Sigma}} = \left(\mathbf{1}^{D\times 1} \otimes \left(\boldsymbol{\sigma}_{\check{\boldsymbol{z}}}^{2\mathsf{T}} + \boldsymbol{\sigma}\right)\right) - (\boldsymbol{\Sigma})^{\mathsf{T}}, \tag{4.36}$$

where $\hat{\boldsymbol{\Sigma}} \in \mathbb{R}^{D\times(D+2)}$ and $\boldsymbol{\sigma}_{\check{\boldsymbol{z}}}^{2} \in \mathbb{R}^{D+2\times 1}$ is the disruption variance vector at the output of the extended demapper. The MRC matrix is then [79]

$$\tilde{\boldsymbol{C}} = \tilde{\boldsymbol{H}}^{\mathsf{H}} \odot \left(\boldsymbol{\Sigma}^{\mathsf{T}} \oslash \hat{\boldsymbol{\Sigma}}\right), \tag{4.37}$$

where $\tilde{\boldsymbol{C}} \in \mathbb{C}^{D\times(D+2)}$. Although $\tilde{\boldsymbol{C}}$ maximizes the SINR, the resulting data estimates $\tilde{\boldsymbol{C}}\check{\boldsymbol{d}}$ would be scaled with non-unity coefficients. The "equalized" MRC matrix $\boldsymbol{C} \in \mathbb{C}^{D\times(D+2)}$ is obtained as

$$\boldsymbol{C} = \tilde{\boldsymbol{C}} \oslash \left(\mathbf{1}^{1\times(D+2)} \otimes \operatorname{diag}\left(\tilde{\boldsymbol{C}}\tilde{\boldsymbol{H}}\right)\right). \tag{4.38}$$

The symbol estimates at the MRC output $\check{\boldsymbol{d}} \in \mathbb{C}^{D\times 1}$ is

$$\check{\boldsymbol{d}} = \boldsymbol{C}\check{\boldsymbol{d}}. \tag{4.39}$$

The post-MRC gain of the ICI component present on the mth subcarrier due to the kth subcarrier is given on the mth row and kth column of $\boldsymbol{G} \in \mathbb{C}^{D\times D}$ where

$$\boldsymbol{G} = \boldsymbol{C}\tilde{\boldsymbol{H}} - \boldsymbol{I}^{D}. \tag{4.40}$$

The disruption power accumulated on the mth subcarrier after MRC is given on the mth column of

$$\boldsymbol{\rho} = |\boldsymbol{C}|^2 \sigma_{\check{\boldsymbol{z}}}^2, \tag{4.41}$$

where $\boldsymbol{\rho} \in \mathbb{R}^{1\times D}$. $\check{\boldsymbol{d}}$, $\boldsymbol{G}$ & $\boldsymbol{\rho}$ are fed to the SISO decoder in [99, Sec V], and the soft decision turbo SIC equalizer described thereon is used to obtain symbol estimates $\hat{\boldsymbol{d}}$.

4.2.2.1 Computational Complexity

The derivation of the MRC operation may create an impression that it requires series of sequential operations. Although these steps are detailed for the derivation, the implementation complexity is limited as a result of the limited number of interference terms. For example, if the index of the extended demapped subcarriers are considered to be 0 and $D+1$ for the sake of brevity in this context, the $d \in \mathbb{Z}_{1<d<D}$th term of eq. (4.39) is explicitly stated as

$$\check{\boldsymbol{d}}_d = \frac{\sum_{\kappa=d-1}^{d+1} \tilde{\gamma}_{d,\kappa} \tilde{\boldsymbol{H}}_{d,\kappa}^{*} \check{\boldsymbol{d}}_\kappa}{\sum_{\kappa=d-1}^{d+1} \tilde{\gamma}_{d,\kappa} |\tilde{\boldsymbol{H}}_{d,\kappa}|^2}, \tag{4.42}$$

where

$$\tilde{\gamma}_{d,\kappa} = \frac{|\tilde{\boldsymbol{H}}_{d,\kappa}|^2}{\sigma_{\check{z}_\kappa}^2 + \sum_{\substack{\tau\in\{\kappa-1,\kappa,\kappa+1\} \\ \tau\neq d}} |\tilde{\boldsymbol{H}}_{\tau,\kappa}|^2} \tag{4.43}$$

is the SINR of the symbol transmitted in the dth subcarrier at the κth received subcarrier. Noting that the off-diagonal components of $\tilde{\boldsymbol{H}}$ can be obtained from $\boldsymbol{\theta}$ using simple bit operations, calculation of $|\tilde{\boldsymbol{H}}|^2$ is ignored as well as the channel estimation using [95, 98] and Fourier transform in eq. (4.22) since they are included in all algorithms. The complexity of the rest of the steps are provided in Table 4.1, where M is the cardinality of the used constellation and the approximations refer to the cases where constant magnitude (phase shift keying (PSK)) constellations are used.

Note that the proposed method does not include any non-linear or sequential operation, hence it is possible to obtain the extrinsic probabilities at the end of any number of SIC iterations in a single clock cycle if the memory and hardware architecture allows [99, Sec. V].

Table 4.1: Computational complexity of algorithm steps

Step	Real Multiplications	Real Additions
eq. (4.22)	$2N$	0
eq. (4.43)	$3D$	$6D$
eq. (4.39)	$22D$	$12D$
eq. (4.40)	$24D$	$16D$
eq. (4.41)	$9D$	$5D$
A priori probabilities	$4MD$	$3MD$
Equalized MRC Total	$2N + (58 + 4M)D$	$(39 + 3M)D$
[99, Sec. V, μ]	$3MD$	$2(M-1)D$
[99, Sec. V, σ^2]	$(M+2)D \approx 2D$	$(M+1)D$
[99, Sec. V, $\tilde{y}$]	$16D$	$16D$
[99, Sec. V, Σ]	$4D$	$4D$
Extrinsic probabilities	$4MD$	$3MD$
Each SIC Iteration	$(22 + 4M)D$ $\approx (22 + 3M)D$	$(19 + 3M)D$

4.3 Numerical Verification

The gains of Hann windowing OFDM receivers are shown using numerical simulations and compared to other methods. The assumptions advised in [82] for the 3GPP NR band "n41" [100] and a system bandwidth of 50 MHz were used. There are two identical interfering users each utilizing the bands on either side of the band occupied by the desired user. Both interfering users' experience channels with 20 dB SNR having TDL-C PDP with 300 ns RMS delay spread and mobility 3 km/h. The desired user's channel has the TDL-A PDP with 10 ns and 30 ns RMS delay spread [80], mobility 120 km/h and was evaluated for 10 dB to 30 dB SNR. The guard bands between users also vary from 30 kHz to 105 kHz. The desired user has a subcarrier spacing of 60 kHz corresponding to $N = 1024$, whereas both interfering users have subcarrier spacings of 15 kHz corresponding to 4096-FFT. Starting from the fourth symbol, all subcarriers of every seventh OFDM symbol of the desired user is loaded with PUSCH DMRS symbols defined in [6]. The desired user utilizes $D = 12$ subcarriers in the remaining symbols to convey data using the same MCS for all SNR values which consists of QPSK modulation and $(51/63) \times (7/16)$ standard [86, 87] and extended [88] BCH Turbo product code (TPC) [89]. The interfering users

utilize 1632 subcarriers each throughout the whole communication duration. There is also 128 samples time offset between the the desired user and both interfering users. The bit probabilities are calculated using approximate log-likelihood ratios (LLRs) for all receivers.

Both interfering users transmit 2-continuous OFDM for the results labeled with NC-OFDM, while the desired user transmits 1-continuous OFDM and the receiver performs 6 iterations to estimate the transmitted correction vector [50] and cancel it. Both interfering users perform transmit filtering in results labeled with F-OFDM as described in [85] while the samples of desired user are match filtered, where tone offset values are set to the respective guard band of that simulation for all users. For all other results, both interfering users utilize normal CP overhead and window the ISI-free CP samples at the transmitter using SSW functions optimized to maximize their frequency localization [46]. The desired user employs normal CP overhead for all cases and the ISI-free samples are utilized for SSW maximizing ACI rejection [46] in the results labeled as RW-OFDM. For the results labeled as adaptive RW-OFDM (ARW-OFDM), the window duration of each subcarrier is determined per [64]. A total of 6 SIC iterations are performed for the Hann windowing receivers and the BER values at the output of each iteration are obtained and presented in the BER results. The number of iterations are denoted accordingly, and not all iterations were presented in all BER results for the sake of clarity. Furthermore, the theoretical BER bound achievable by an Hann windowing receiver if ICI is cancelled perfectly is obtained from the Hann-windowed channel disruption and presented with the label Hann-Theory. It should be noted that the receiver design featured in this work is suboptimal in most cases, and is only presented to demonstrate the concept using a receiver that is suitable for the low-latency requirements of uRLLC. Non-linear or decision directed receivers that consistently achieve theoretical BER bound are left as future work.

Figure 4.1 demonstrates that for little guard band and short delay spread, orthogonal windowing algorithms outperform Hanning receivers for the low SNR regions, as low SINR prevents successful ICI estimation and cancellation. However, Hanning receivers with as little as 3 iterations achieve the target 10^{-3} BER earlier than orthogonal windowing algorithms and experience

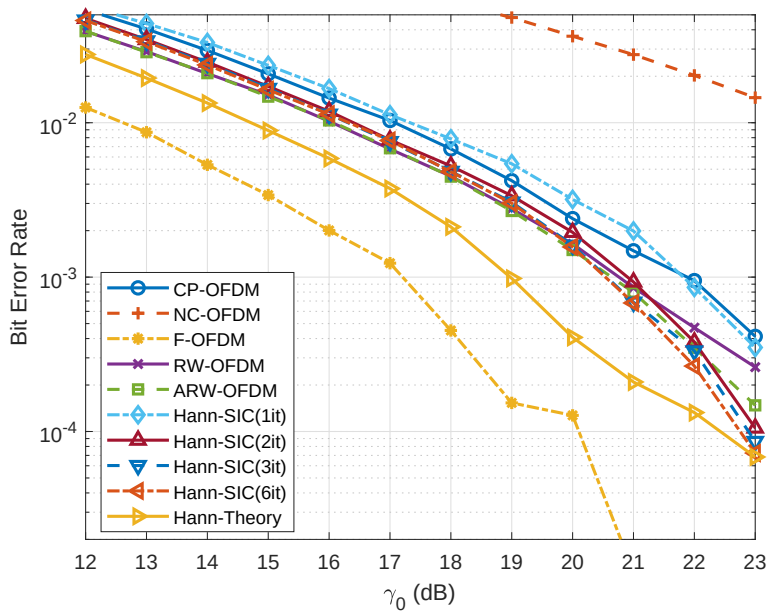

Figure 4.1: BERs of various transceivers for guard bands of 30 kHz between each user and 10 ns RMS delay spread.

the so-called BER waterfall at a lower SNR threshold than compared to orthogonal windowing algorithms. As SNR increases further, even 2 iterations are sufficient to outperform orthogonal windowing algorithms while as little as 6 iterations allow rates very close to the theoretical limit. The motivation behind Hanning receivers become clearer in Figure 4.2 as delay spread elongates. As orthogonal windowing algorithms lose the advantage of longer windowing durations, their rates shift closer to the baseline rectangular receiver, while the effect on Hanning receivers remain limited to increased fading. Hanning receiver with only 1 iteration show the same performance as orthogonal windowing receivers performance for the high SNR region, while as little as 2 iterations outperform the orthogonal windowing receivers at all SNR values. The only observable effect on Hanning receivers is the shift of the waterfall threshold to higher SNRs. Increasing the guard band drastically reduces the ACI present on the desired user's band and narrows the gap between all algorithm as seen in Figures 4.3 and 4.4. In Figure 4.3, compared to Figure 4.1, the increase in the guard band extended the orthogonal windowing algorithm's lead against Hanning receivers beyond the target BER. However, it is seen that Hanning receivers, although requiring one more

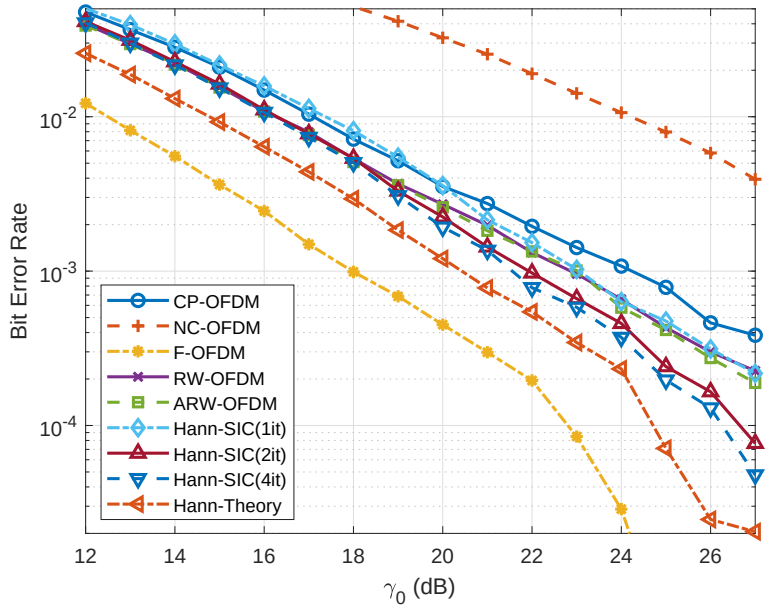

Figure 4.2: BERs of various transceivers for guard bands of 30 kHz between each user and 30 ns RMS delay spread

.

iteration, still outperform orthogonal windowing algorithms. Similarly as delay spreads elongate in Figure 4.4, the Hanning receiver's advantage becomes more obvious with waterfall threshold moving further to lower SNRs compared to orthogonal windowing algorithms.

Noting that the ACI sources utilize either transmitter W-OFDM or F-OFDM in other scenarios, both having superior OOB emission suppression compared to NC-OFDM, the need to properly estimate and cancel the correction vector limits the BER performance of NC-OFDM. While F-OFDM has better BER performance beyond that theoretically achievable by Hanning receivers, Hanning receivers are used to resolve conventional CP-OFDM signals whereas F-OFDM can only be used to receive signals transmitted using a F-OFDM transmitter. Particularly, the filter lengths are $N/2+1$ per [85], the computational complexity of F-OFDM is $(N+L)(2N+4)$ real multiplications and $(N+L)(3N/2+2)$ real additions at both transmitter and receiver accordingly as filters consist of complex values. Similarly, the SSW RW-OFDM scheme described in [46] requires $6KD$ real multiplications and $4KD$ real additions to estimate received symbols. It is noteworthy that the complexity of F-OFDM scales on the order of FFT-size squared, whereas the

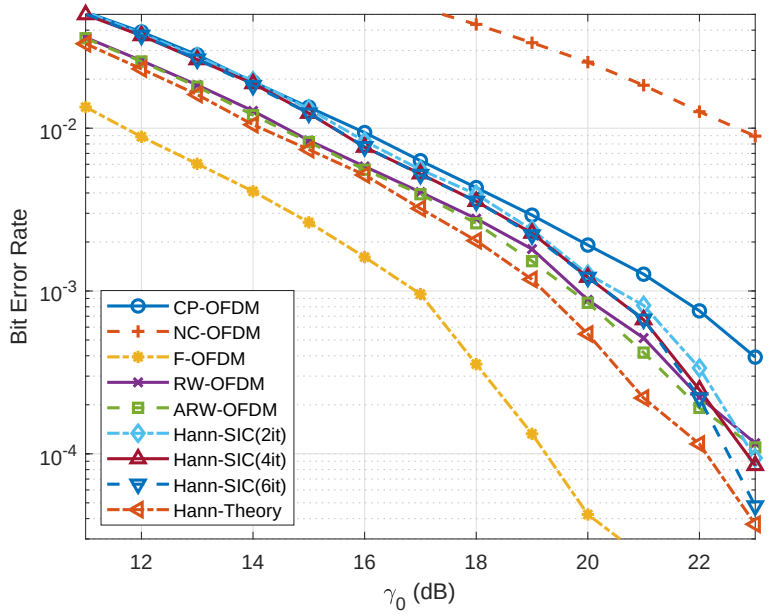

Figure 4.3: BERs of various transceivers for guard bands of 105 kHz between each user and 10 ns RMS delay spread.

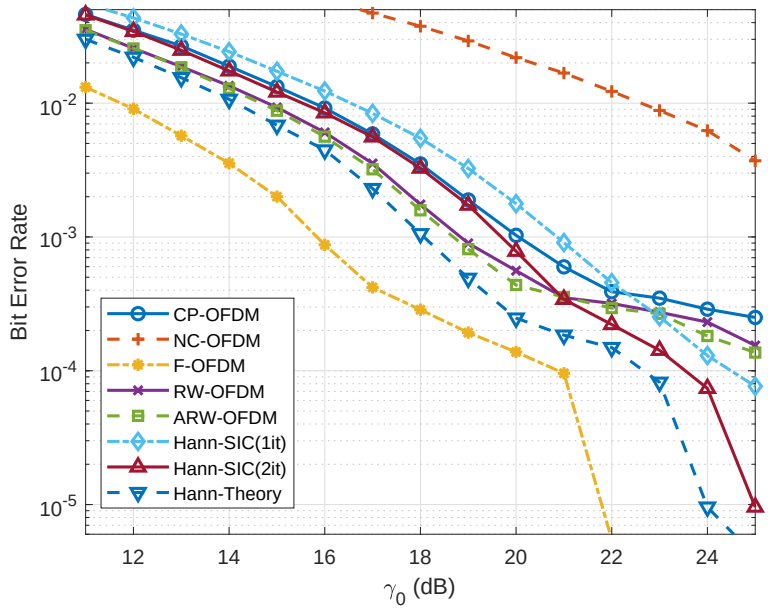

Figure 4.4: BERs of various transceivers for guard bands of 105 kHz between each user and (a) 10 ns and (b) 30 ns RMS delay spread.

Table 4.2: Computational complexity comparison

Algorithm	**Real Mult.**	**Real Add.**
F-OFDM	2,248,992	1,685,648
RW-OFDM	3,672	2,448
Hann-SIC(1it)	3,224	984
Hann-SIC(2it)	3,632	1,356
Hann-SIC(3it)	4,040	1,728
Hann-SIC(4it)	4,448	2,100
Hann-SIC(6it)	5,264	2,844

complexity of windowing receivers scale linearly with the number of data-carrying subcarriers. Therefore, windowing receivers are particularly important for narrowband communications. The receiver computational complexity of Hanning receivers are accordingly compared with F-OFDM and RW-OFDM in Table 4.2. Note that F-OFDM has symmetric computational complexity between the transmitting and receiving devices, whereas windowing receivers do not change the transmitter structure and do not cause any computational burden at the transmitting device. The window duration for RW-OFDM in short delay spread is considered as it makes more sense to apply RW-OFDM in that case.

Chapter 5: Future Work: Enhancing Other Layers by Extending Discussed Flexibilities

The aim of the methods discussed in the previous sections was to address the increasing variety of user requirements by utilizing the flexible aspects of the RAT. However, RAT is not the only flexible component of the communication systems. This chapter[10] discusses how the aforementioned concepts can be extended to other layers of communication systems.

5.1 Cellular Structure and Flexible Signaling

For instance, deploying cells with several sizes by using BSs with different transmit powers could be considered as a flexibility at the system level. Heterogeneous networks (HetNets) utilize this flexibility and aim to increase the system capacity along with addressing various mobile station (MS) densities and regions with higher data demands [101]. In this section, we question whether the aspects we have previously discussed are relevant to the different challenges experienced in HetNets and how these problems can be handled by utilizing different aspects of RAT flexibility.

In HetNets, there are several advantages and challenges of associating with smaller and larger cells. The mobile network operators (MNOs) desire to offload users to smaller cells for reducing the traffic congestion at the macro BS and increase overall system capacity [102]. Most users desire to connect to smaller cells as well since there are less number of users sharing the resources. Also, smaller link distances decrease the power consumption drastically [103]. However, users connected to smaller cells experience elevated inter-cell interference due to increasing frequency reuse and decreasing re-use distances [104].

Since local small cell networks are not available everywhere, users may have to associate with larger cells regardless of their applications. Furthermore, there are exceptional user groups that require association with larger cells, such as high mobility users. As associating with smaller

[10]Part of this chapter was published in [5]. Permission is included in Appendix A.

cells would cause an infeasible rate of hand-offs, high mobility users prefer association with larger cells [105]. Nevertheless, the variation of the delay spread experienced by a cell increases proportionally to cell size [106]. Combining this variation with the coexistence of low and high mobility users, it can be seen that the variation in the Doppler spread is also proportional to the cell size [107].

Based on the given observations, we conclude that MSs associated with larger cells experience a wider variety of channel conditions and require support of a comprehensive range of applications. The methods described in the previous sections effectively address these problems and lay guidelines to support such challenging medley of requirements.

Quite the reverse, coexistence issues become irrelevant for MSs associated with smaller cells as they experience similar channels and request support for less variety of applications. The inter-cell interference problem, on the other hand, gains importance as cell sizes get smaller. Until now, most researchers who attempted to reduce the interference on small cells either from larger cells [108] or from other small cells [109] have based their work on coordination in the network layer. On this basis, one may erroneously conclude that the flexibility aspects of the RAT components can only increase the performance within larger cells and remain useless for this problem. However, the flexibility aspects of radio access technologies are not limited to the examples discussed above.

Flexible radio access technologies can be developed to address this problem, such as the concept of partially overlapping tones (POT) in [110]. It is a flexible waveform design framework that allows networks to interchange between other user interference and self-interference flexibly by creating an intentional frequency offset and adjusting the pulse shaping filter accordingly. Let us clarify the process with a brief example by considering small cells that use filter bank multicarrier (FBMC) waveform and utilize Gaussian filters in their numerologies. In any case, BSs first determine unique frequency offset values using the sensed spectrum with the intention to align the center of their pulses to the nulls of other BSs' pulses. In case of low inter-cell interference power, BSs utilize wideband pulse shapes so that the desired high power signals overlap little and the interfering signals are allowed to overlap more with the desired signals as they have low power,

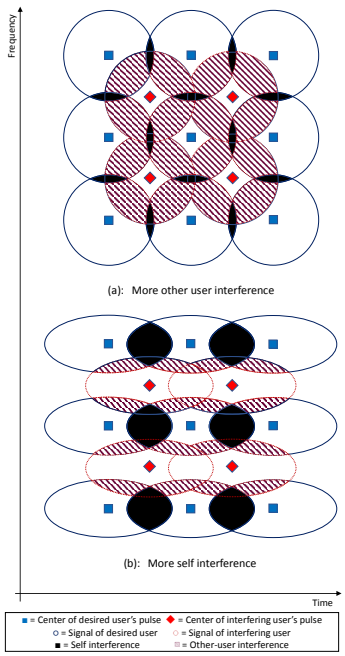

Figure 5.1: Figure showing how self-interference and other-user-interference from adjacent cells can be interchanged using POT.

as demonstrated in Figure 5.1 (a). However, as inter-cell interference power increases, because self-interference is easier to mitigate than other-user-interference using equalizers, the desired signals are allowed to overlap in time by utilizing narrow band pulse shapes as doing so decreases the interference power received from other users, as demonstrated in Figure 5.1 (b). In addition to provide such a smooth solution to inter-cell interference, this concept is more practical than the network layer solutions, as it can be used even in uncoordinated networks frequently encountered in dense and unplanned deployments.

In conclusion, we have demonstrated that the inter-cell interference can be overcome using the flexibility of the radio access technologies. This proves that challenges faced in other domains can also be dealt with adaptations in the RAT. Furthermore, the solutions presented in this paper provide an overview of the literature; however, flexibility aspect of the RAT is open to further investigation.

5.2 Enhancing Multiple Accessing Schemes with RAT Flexibility

We have shown that several numerologies using different signaling schemes can be freely utilized in the same frame as long as the guard time and band requirements are met, and windowing can be utilized to minimize both. In this section, we investigate how to use this flexibility in order to improve current MA schemes and address the different user requirements conveniently. We first briefly go over the advantages and disadvantages of various MA schemes for the future radio access and show how they affect the system performance under different cellular scenarios and user requirements. It will be clear that none of the available MA candidates can meet all the expectations for the use cases pointed out, therefore, similar to proposed numerologies and waveforms, several MA schemes should coexist in the future radio-access network (RAN) to achieve further efficiency and reliability. We aim to show how these schemes can be further improved by extending the flexibility aspects of the radio access technologies as explained in the rest of this study.

5.2.1 OMA

In orthogonal multiple accessing (OMA) schemes, each user receives their own symbols in a resource block orthogonal to the other users', in either time, frequency or code domains [111]. OMA schemes must always be part of the RAN as they;

- work best to provide high data rates to a relatively low number of users when overloading is not necessary, as can be exampled in a scenario where few eMBB MSs connected to smaller cells [102] (Figure 5.2 (a)),
- are required by very low power massive machine type communications (mMTC) devices due to their low computational complexity (Figure 5.2 (a)),
- are required by applications that rely on time critical information such as uRLLC services due to their low computational delay [112] (Figure 5.2 (b)).

However, for massive number of mMTC devices that sporadically access the network for small packets, OMA schemes;

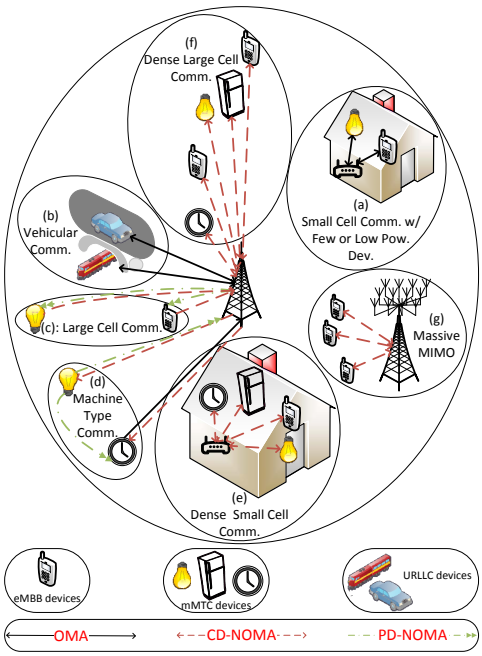

Figure 5.2: Comprehensive visualization of several MA and cellular scenarios.

- limit the maximum number of connections [113],
- cannot achieve the sum rate capacity in the downlink if knowledge of the channel is unavailable at the BS [114],
- require dynamic scheduling (request and grant) especially in the UL which increases the latency and overhead significantly for small packets [115].

NOMA schemes outperform OMA schemes for the aforementioned use cases by assigning multiple users on the same resource element. If compressive (sensing) random access is used, grant-free UL is possible which significantly decreases the scheduling overhead for massive number of connections [116].

The techniques aforementioned in this study are already addressing how OMA schemes can be flexibly utilized. Let us review the strengths and weaknesses of major NOMA schemes and explore how they can be improved using RAT flexibilities.

5.2.2 PD-NOMA

Introduction of multiuser superposition transmission (MUST) to improve the system capacity [117] in Long Term Evolution-Advanced (LTE-A) Pro was a milestone since commercial cellular systems implemented a NOMA scheme for the first time. power domain non-orthogonal multiple accessing (PD-NOMA) schemes exploit the power variation between cell center and cell edge users, and consist of superposed signals of these users inversely proportional to their received powers. The receiver at the cell center, referred to as near receiver in this context, experiences a high SNR. Therefore, it can extract their own low power signal by detecting the far users high power signal first and subtracting it from the received signal. When the signals reach the cell edge user, referred to as the far receiver, the low power signal of the near receiver fades heavily, therefore the far receiver proceeds detection of their signal without further processing [118]. Two main reasons got PD-NOMA adoption ahead of code domain non-orthogonal multiple accessing (CD-NOMA). Firstly, the SIC detector is only required at the near receiver, reducing the computational complexity. Secondly, because the far receiver is able to use classical receiver algorithms, the scheme is backward compatible to some extent as the process itself is almost invisible to the far user.

Unfortunately, because this scheme exploits solely the variation of channel conditions of different users, it is considered to be useful only for the DL of larger cells [119], as shown in Figure 5.2 (c).

A future direction of research for PD-NOMA would be an attempt to couple UL transmissions with sidelink (SL)[11] transmissions to close proximity fellow receivers, as demonstrated in Figure 5.2 (d). An example to how such a scheme would be useful is the combination of vehicle-to-vehicle (V2V) signaling with the vehicle-to-infrastructure (V2X) signaling.

Furthermore, the current schemes use the same numerology for both the near and the far receivers. Forcing the same numerology to be used by receivers experiencing different delay spreads reduces the efficiency as we have concluded throughout the dissertation. The theoretical proof in [120] suggests that PD-NOMA concept could be made flexible in terms of waveform and

[11] SL refers to device-to-device (D2D) links in the 3GPP terminology.

numerology with different numerologies used for the near and far receiver. The solutions presented in [120] can be generalized to partial overlapping of different waveforms. Further theoretical investigation of this approach along with case studies for different waveforms is needed.

5.2.3 CD-NOMA

CD-NOMA schemes achieve high overloading in any link type regardless of the cell size as shown in Figure 5.2 (e) and user density as demonstrated in Figure 5.2 (f) by using codebooks with different overloading factors [121]. The cost of using CD-NOMA schemes is the advanced transmitter design, but more importantly, the complexity of the message passing algorithm (MPA) decoder at the receiver [122]. However, receiver complexity is not an issue in the UL, making this scheme attractive for UL connections, as shown in Figure 5.2 (c) [123]. If the channel state information (CSI) is unavailable at the transmitter, CD-NOMA schemes benefit from spreading gain which increases the reliability under bad channel conditions, providing a viable solution to the pilot contamination problem experienced by massive MIMO networks, as shown in Figure 5.2 (g). Also they can further benefit from shaping gain if bandwidth can be sacrificed [124]. Well studied CD-NOMA schemes are thoroughly worked;

- for code division multiple accessing (CDMA) ([125] and references therein),
- by replacing the chips with subcarriers, using OFDMA [126],
- by utilizing the sparse CDMA codes at the mapping and spreading to combine these codebooks with OFDMA, [127].

It is easy to predict that the same concept can be applied to the many flexibility aspects of millimeter wave (mmWave) frequencies, such as beam switching and polarization, which can be utilized in the implementation of the same concepts [128]. Numerous other future research directions may be proposed for CD-NOMA, however to make this concept feasible for use in real life implementations, the decoding complexity under doubly dispersive channels need to be reduced for various channel conditions, which can be made possible through careful real-time adaptation of

the more flexible radio access technologies. For the development of this direction, one can observe that the further degrees of freedom could be obtained for other, more parameterized waveforms. For example, the filter type and parameter selection flexibility of the FBMC numerologies can be utilized to shape the future of CD-NOMA [129], and can be used as a distinguishing feature reducing the interference between users in the physical layer under doubly dispersive channels.

5.3 Enhancing Secrecy and Throughput of Practical MIMO Systems Using ASs

Throughout this section[12], vectors are represented using lowercase bold-face letters, matrices are uppercase bold-face letters, and non-bold letters are used for scalars. The superscripts $(\cdot)^{\mathsf{H}}$, $(.)^{-1}$ stand for the conjugate-transpose, and inverse operations, respectively. $\mathbb{C}$ represents the complex numbers domain, and $\sim \mathcal{CN}\left(\mu, \sigma^2\right)$ corresponds to complex Gaussian distributed random variable with mean μ and variance σ^2. $\|\cdot\|$ corresponds to the Euclidean norm.

5.3.1 System Model

A transmitting device, hereinafter referred to as Alice, wishes to convey information to another device, hereinafter referred to as Bob. Alice transmits the information over N antennae while Bob receives the information over M antennae, where $M \leq N$. The communication channel between each antenna of Alice and Bob is representable in the form of one tap over the utilized bandwidth, and is time-invariant over the transmission interval. The channel coefficient between Alice's nth antenna and Bob's mth antenna is represented in the mth row and nth column of the matrix $\boldsymbol{H} \in \mathbb{C}^{M \times N}$, and all elements are assumed to be known perfectly by Alice. The information symbols that are desired to be conveyed over a transmission interval are denoted by the vector $\boldsymbol{s} \in \mathbb{C}^{M \times 1}$.

Ideally, the mutual information (MI) between the information symbols and their received counterparts is maximized if Alice precodes the symbols with $\boldsymbol{V} \in \mathbb{C}^{N \times M}$, comprising the first M columns of the unitary matrix $\check{\boldsymbol{V}} \in \mathbb{C}^{N \times N}$ and Bob combines the channel outputs with the unitary

[12]Part of this section was published in [130] and patented [131].Permission is included in Appendix A.

matrix $\boldsymbol{U}^{\mathsf{H}} \in \mathbb{C}^{M\times M}$, where [132]

$$\boldsymbol{H} = \boldsymbol{U}\boldsymbol{D}\check{\boldsymbol{V}}^{\mathsf{H}} \tag{5.1}$$

is the SVD of the channel coefficient matrix $\boldsymbol{H}$ [133, Sec. 3]. The received symbol estimates $\hat{\boldsymbol{s}} \in \mathbb{C}^{M\times 1}$ in the ideal case are modeled as

$$\hat{\boldsymbol{s}} = \boldsymbol{D}^{-1}\boldsymbol{U}^{\mathsf{H}}\left(\boldsymbol{H}\boldsymbol{V}\boldsymbol{s} + \boldsymbol{n}\right), \tag{5.2}$$

where the parenthesized content is the signal received at Bob's antennae, where elements of $\boldsymbol{n} \in \mathbb{C}^{M\times 1}$ are independent and identically distributed with $\sim \mathcal{CN}\left(0, {}^{1}/_{\gamma}\right)$ where γ is the overall SNR of Bob for mean channel gain.

While the scheme described in eq. (5.2) maximizes capacity and is secure, in practice, precoder-combiner matrix pair $\tilde{\boldsymbol{V}}$ and $\tilde{\boldsymbol{U}}^{\mathsf{H}}$ that are imperfect approximations of the similarly denoted counterparts in eq. (5.1) may be used due to reasons made clear in Chapter 1. Let

$$\tilde{\boldsymbol{H}} = \sqrt{\phi}\boldsymbol{H} + \left(1 - \sqrt{\phi}\right)\boldsymbol{W} \tag{5.3}$$

denote the precoder-combiner induced channel $\tilde{\boldsymbol{H}} \in \mathbb{C}^{M\times N}$ where $0 \leq \phi \leq 1$ denotes the correlation between $\boldsymbol{H}$ and $\tilde{\boldsymbol{H}}$; and $\boldsymbol{W} \in \mathbb{C}^{M\times N}$ is the mismatch between them. Accordingly, eq. (5.2) will hereinafter be considered as

$$\hat{\boldsymbol{s}} = \boldsymbol{D}^{-1}\tilde{\boldsymbol{U}}^{\mathsf{H}}\left(\boldsymbol{H}\tilde{\boldsymbol{V}}\boldsymbol{s} + \boldsymbol{n}\right). \tag{5.4}$$

The $\tilde{\boldsymbol{V}}$ and $\tilde{\boldsymbol{U}}^{\mathsf{H}}$ matrix pairs are public knowledge, and are known by a third device with $L > N$ antennae, hereinafter referred to as Eve, that does not respect the confidentiality principle and wishes to unlawfully eavesdrop the information Alice conveys to Bob. Let $\check{\boldsymbol{H}} \in \mathbb{C}^{L\times N}$ similarly refer to the communication channel between Alice and Eve, known perfectly by Eve, and similarly denoted and sized counterparts of elements in eq. (5.4) to other modeled properties. Eve estimates

the information signals as

$$\breve{\boldsymbol{s}} = \tilde{\boldsymbol{V}}^{\mathsf{H}} \breve{\boldsymbol{H}}^{\dagger} \left(\breve{\boldsymbol{H}} \tilde{\boldsymbol{V}} \boldsymbol{s} + \breve{\boldsymbol{n}} \right), \tag{5.5}$$

wherein $\breve{\boldsymbol{H}}^{\dagger} = \breve{\boldsymbol{H}}^{\mathsf{T}} \left(\breve{\boldsymbol{H}} \breve{\boldsymbol{H}}^{\mathsf{T}} \right)^{-1}$ is the Moore-Penrose pseudo-inverse of $\breve{\boldsymbol{H}}$.

5.3.2 Artificial Signal Construction

Instead of transmitting the information symbols directly or precoding them with the nonideal precoder, an artificial signal (AS) that maximizes the mutual information between $\boldsymbol{s}$ and $\hat{\boldsymbol{s}}$ can be designed. ZF the AS such that the least squares (LS) estimates match the information symbols perfectly results in a power-unbounded AS of which power has to be downscaled to meet the transmit power requirements, hence is not an efficient way to approach the problem. The AS minimizing the instantaneous error while efficiently utilizing the transmit power can be formulated as

$$\tilde{\boldsymbol{x}} = \arg\min_{\boldsymbol{\xi}} \| \boldsymbol{D}^{-1} \tilde{\boldsymbol{U}}^{\mathsf{H}} \boldsymbol{H} \tilde{\boldsymbol{V}} \boldsymbol{\xi} - \boldsymbol{s} \| \tag{5.6a}$$

$$\text{subject to} \quad \| \boldsymbol{\xi} \| \leq \sqrt{N}, \tag{5.6b}$$

which is a convex optimization problem that can be solved computationally efficiently without introducing long processing delays [134].

Note that $\tilde{\boldsymbol{x}} \in \mathbb{C}^{M \times 1}$ designed in (5.6) takes the precoder into account. This is particularly useful if the precoding operation is performed in the hardware level, such as hybrid beamformers [135] or other mechanical beamformers [136] such as lens array beamformers [137], and these beamformers are not to be removed from the system. Hardware limitations such as the resolutions of the phase shifters, digital to analog converters (DACs) and the analog to digital converters (ADCs) at the receiver (if known) are also reflected in the precoder and combiner matrices [138]. On the other hand, if the transmitter is capable of digital beamforming, a signal design allowing the

removal of the precoder from the system is possible. Accordingly, (5.6) can be further simplified to

$$\boldsymbol{x} = \arg\min_{\boldsymbol{\xi}} \|\boldsymbol{D}^{-1}\tilde{\boldsymbol{U}}^{\mathsf{H}}\boldsymbol{H}\boldsymbol{\xi} - \boldsymbol{s}\| \tag{5.7a}$$

$$\text{subject to} \quad \|\boldsymbol{\xi}\| \leq \sqrt{N}, \tag{5.7b}$$

which also provides more freedom as $\boldsymbol{x} \in \mathbb{C}^{N\times 1}$.

The complexity of the algorithms are not derived, but compared to the prior art, the equations involve lesser number of variables, therefore the complexity is logically expected to be lower than those already found acceptable.

5.3.3 Results

The gains of the proposed technique are numerically verified by comparing the EVMs and uncoded BERs at Bob and Eve as well as the secrecy capacity for conventional codebook transmission, precoded AS (PAS) transmission per (5.6) and direct AS transmission per (5.7) as a function of ϕ and γ. $M = 4$, $N \in \{8, 16\}$, $L = 32$, $\boldsymbol{W} \sim \mathcal{CN}(0, 1)$ in accord with [139] and information symbols comprising $\boldsymbol{s}$ are QPSK modulated regardless of SNR, which ranges from 0 dB to 10 dB. Both (5.6) and (5.7) were solved using CVX, a package for specifying and solving convex programs [134, 140]. In the following figures, the curve is observed at Bob if only N is provided, whereas it is observed at Eve if L is also provided. In Figures 5.3 and 5.4, $\phi = 1$ (precoder perfectly aligned to the channel) results are not shown as all schemes abruptly converge as expected, which occurs at a value very different than the rest of the figure.

Figure 5.3 demonstrates the change in the precoding-combining quality provided by the proposed technique by comparing the EVM at various receivers in the absence of noise as a function of ϕ. It is seen that the conventional scheme does not yield a waterfall gain unless $\phi \to 1$, and doubling the number of transmitter antennae reduces EVM by about 1 dB. The proposed algorithms, however, present waterfalling EVM schemes at the legitimate receiver for any channel correlation and greatly outperform the conventional scheme for any nonunitary ϕ. While the number

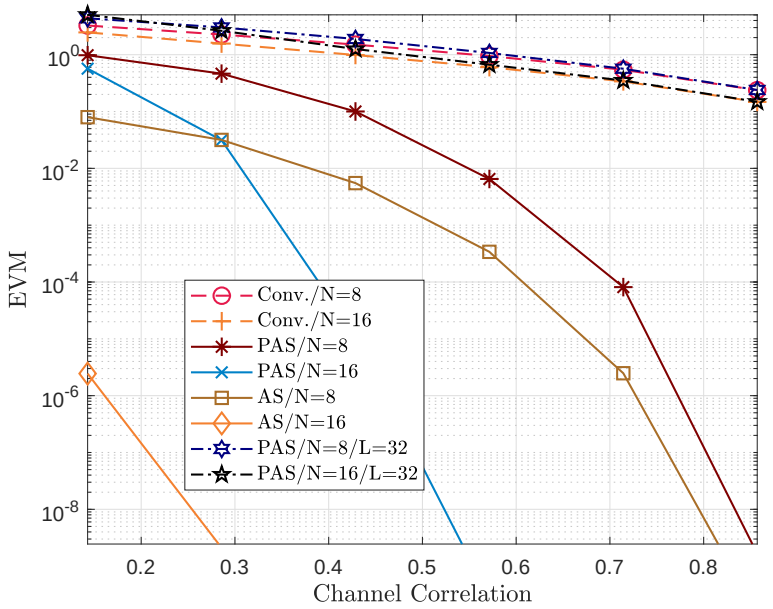

Figure 5.3: EVM at various receivers in the absence of noise.

of transmitter antennae is the most significant factor in reducing EVM for both proposed algorithms, AS significantly outperforms PAS due to the increased level of flexibility for lower ϕ values while the difference narrows as ϕ increases. In the meantime, both proposed algorithms (AS not drawn due to overlapping) limit the EVM performance at Eve to that provided by the conventional schemes at the legitimate receiver for $\phi \neq 1$. The EVM at Eve for conventional transmission is mathematically insignificant for all investigated valid number of antennae combinations, hence is not shown.

Figure 5.4 shows the secrecy capacity comprising the difference of capacities between Bob and Eve as a function of ϕ in the absence of noise. The findings of Figure 5.3 are confirmed, AS is more secure than PAS at lower ϕ as a result of the additional flexibility, which is later dominated by N as ϕ increases due to additional diversity. The secrecy capacity increases up to $\phi \rightarrow 85\%$ and diminishes to zero beyond higher correlations as Eve's capacity increases. The secrecy capacity of conventional transmission is zero hence is not shown.

Figure 5.5 shows the BER as a function of ϕ for 3 dB SNR. Under noisy reception, the performance of AS becomes independent of ϕ as the introduced flexibility allows matching the exact channel at any ϕ and is dominated by the diversity provided by the number of antennas. The

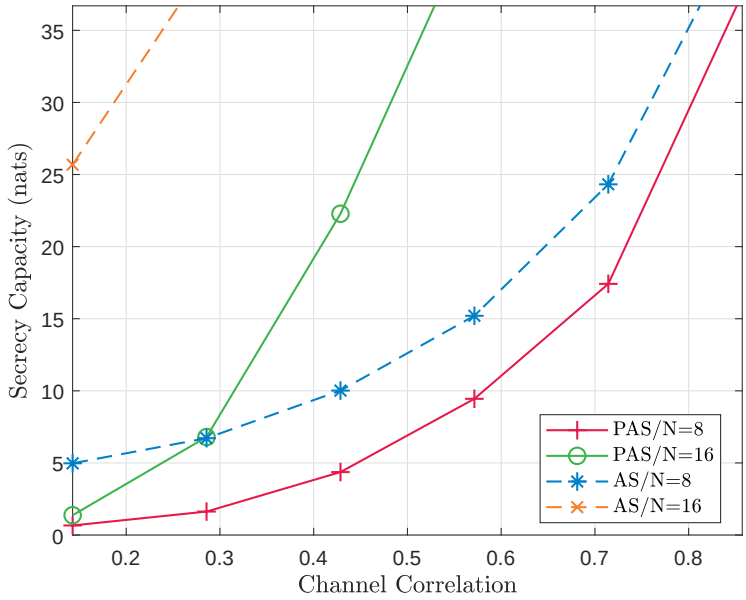

Figure 5.4: Secrecy capacity between Bob and Eve.

performance of PAS converges to that of AS, and the convergence ϕ value decreases with increasing the number of antennas as the increased diversity allows easier matching. The performance of conventional transmission converges to that of proposed schemes as $\phi \to 1$, and the proposed schemes have significant advantage otherwise. The performance at Eve waterfalls with ϕ, confirming that ϕ is the dominating factor in noisy reception as the high diversity greatly improves SNR.

Figures 5.6 and 5.7 show the BER as a function of SNR for $\phi = 30\%$ and $\phi = 70\%$, respectively. The theoretical limits derived in [133] for an optimally precoded and combined ($\phi = 1$) transmission are also presented for comparison. The performance of the conventional scheme is bottlenecked by ϕ independent of SNR for low ϕ, whereas the performance of PAS increases before being bottlenecked by ϕ for low ϕ values. On the other hand, the performance of AS converges to the theoretical limit with increasing SNR regardless of ϕ, a phenomenon commonly observed in fading channels with suboptimum equalization, of which optimization falls beyond the scope of this article. The gap between theoretical limit and AS performance is independent of ϕ for $\phi > 30\%$ in accord with Figure 5.5. Furthermore, the gap between PAS and AS closes as ϕ increases in accord with Figure 5.5. The BER at Eve, which has 8 times the diversity of Bob,

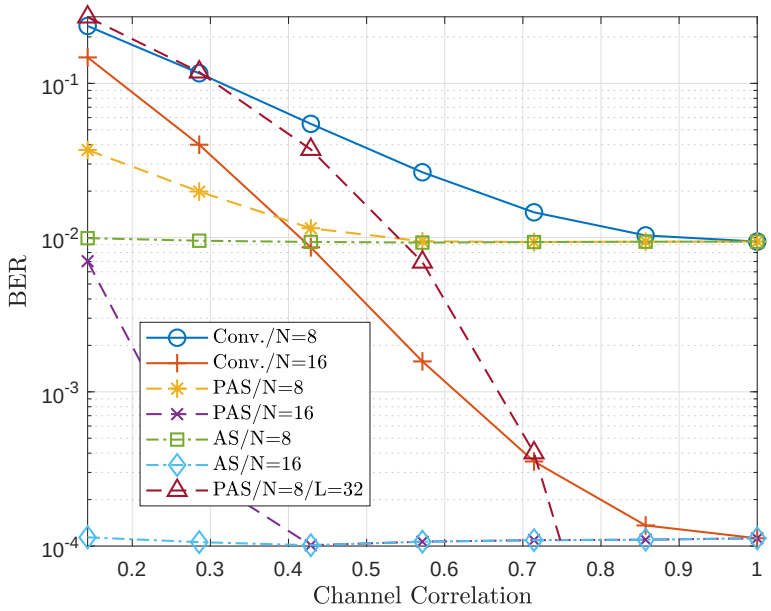

Figure 5.5: BER at various receivers for SNR=3 dB.

remains bottlenecked by ϕ and does not depend much on SNR for both proposed schemes at both ϕ values, showing that the security gap between the two proposed signal designs is insignificant in practical SNR values.

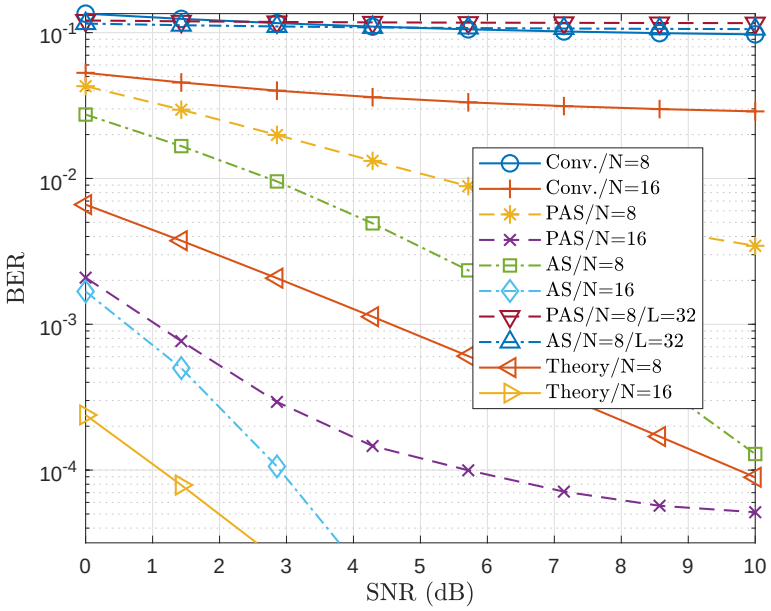

Figure 5.6: BER at various receivers for $\phi = 30\%$.

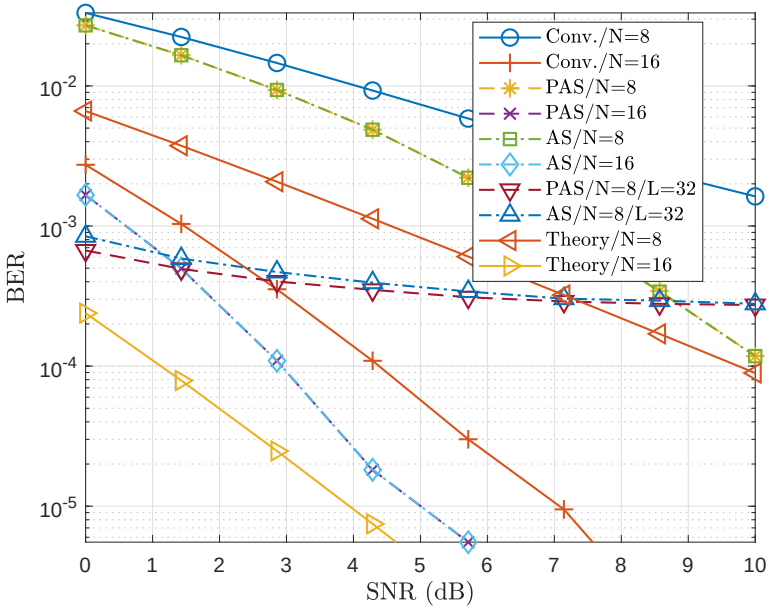

Figure 5.7: BER at various receivers for $\phi = 70\%$.

Chapter 6: Concluding Remarks

In the second chapter, we have determined expected and instantaneous interference powers. Interference power is used to determine subcarrier specific window lengths minimizing the interference. We laid down numerous guidelines with various computational complexities to determine optimal window lengths under insufficient CP. The proposed subcarrier specific windowing scheme improves SIR even when CP is insufficient. Average optimal window lengths depend only on PDPs, and although instantaneous optimal window lengths depend on users' CIRs, fluctuation is little. Therefore, subcarrier specific windowing outperforms fixed windowing even with outdated window lengths in case of powerful interferers.

In the third chapter, we have demonstrated the concept of frame structure compliant computationally efficient adaptive per-RE extensionless transmitter windowing to maximize fair proportional beyond 5G network capacity in the DL, and universal per-RE receiver windowing that requires no additional knowledge. Results demonstrate that gains are possible from windowing without introducing extra extensions that defy the frame structure if the side, RE and duration to apply windowing is calculated carefully. The user with higher excess SNR must apply longer transmitter windowing as they can resist the SNR reduction, whereas the user with lower excess SNR must apply longer receiver windowing. Users with higher subcarrier spacing and higher mobility cause more interference in the system hence should apply more transmitter windowing, whereas users with lower subcarrier spacing must focus on receiver windowing. Optimum transmitter window durations are longer at the edges whereas optimum receiver window durations are longer at band centers. Emulating the multipath multiple access channel allows the gNB to estimate optimum transmitter windowing durations prior to transmission with 95% confidence. Using the variance of received symbols allows the UEs to calculate optimal receiver windowing durations without

calculations requiring further knowledge about the network and channel. While both algorithms are presented for per-RE calculations, spectrotemporal correlation of window durations allow reduced computational complexity implementations than those described. Extensionless windowing at either side does not require action and information transfer to the communication counterpart and is fully compatible with previous and current generations, however the knowledge of adaptive windowing applied at the counterpart allows joint optimization that reveals higher gains.

Chapters 2 and 3 demonstrate that ACI is a critical problem in 5G and beyond scenarios due to the coexistence of OFDM based non-orthogonal signals. To tackle the ACI problem, we propose a novel Hann window function based low complexity receiver windowing method that is fully compatible with the frame structure of existing standards and needs no redundancy in the signal and no modifications on the transmitting devices in the fourth chapter. The proposed method improves the achievable capacity in the presence of high power non-orthogonal signals on adjacent channels when it is coupled with simple interference mitigation techniques. The proposed method allows superior ACI rejection and reducing guard bands without requiring extensions, and on the contrary, allows shortening the currently used extension for future higher mobility applications. Although the gap between prior art and the proposed methods widens with increasing delay spread and decreasing guard bands, the proposed methods outperform prior art in short delay spreads and large guard bands as well. This study paves the way towards future standard compliant ACI rejection research by showing gains of a simple receiver, inspiring sophisticated algorithms that outperform the presented by achieving performance bounds with less receiver complexity.

In chapter 5, we proposed two different approaches to construct an artificial signal, which can mitigate the mismatch between the channel and the codebook-based precoders. The constructed signal is able to reduce the BER experienced by legitimate user, while keeping eavesdropper's BER at a high level. The secrecy performance of PAS and AS are theoretically different at infinite SNR, but for practical SNR values the approaches are indifferent. If the hardware allows full digital beamforming this increases the capacity at the intended receiver, whereas the eavesdropper will keep believing a precoder is used, creating additional confusion. The performance of precoded

method converges to that of nonprecoded beyond a certain correlation, of which value decreases as diversity rank increases. Even though the proposed algorithms still enhances the performance in case of low or no correlation, we suggest that it would be more beneficial to keep the operating point around 0.6 to 0.9. At that operating range, both the performance of legitimate user and the secrecy gap experience a satisfying enhancement.

References

[1] D. Astely, E. Dahlman, A. Furuskär, Y. Jading, M. Lindström, and S. Parkvall, "LTE: the evolution of mobile broadband," *IEEE Communications Magazine*, vol. 47, no. 4, pp. 44–51, Apr. 2009.

[2] J. Andrews, S. Buzzi, W. Choi, S. Hanly, A. Lozano, A. Soong, and J. Zhang, "What will 5G be?" *IEEE Journal on Selected Areas in Communications*, vol. 32, no. 6, pp. 1065–1082, Jun. 2014.

[3] R. W. Chang, "Synthesis of band-limited orthogonal signals for multichannel data transmission," *Bell Syst. Tech. J.*, vol. 45, no. 10, pp. 1775–1796, Dec. 1966.

[4] S. Chen and J. Zhao, "The requirements, challenges, and technologies for 5G of terrestrial mobile telecommunication," *IEEE Communications Magazine*, vol. 52, no. 5, pp. 36–43, May 2014.

[5] Z. Ankaralı, B. Peköz, and H. Arslan, "Flexible Radio Access Beyond 5G: A Future Projection on Waveform, Numerology Frame Design Principles," *IEEE Access*, vol. 5, no. 1, pp. 18 295–18 309, 2017.

[6] 3GPP, "NR; Physical channels and modulation," 3rd Generation Partnership Project (3GPP), Technical Specification (TS) 38.211, 01 2018, version 15.0.0. [Online]. Available: http://www.3gpp.org/DynaReport/38211.htm

[7] X. Zhang, L. Zhang, P. Xiao, D. Ma, J. Wei, and Y. Xin, "Mixed numerologies interference analysis and inter-numerology interference cancellation for windowed OFDM systems," *IEEE Transactions on Vehicular Technology*, vol. 67, no. 8, pp. 7047–7061, Aug. 2018.

[8] R. Lupas and S. Verdu, "Near-far resistance of multiuser detectors in asynchronous channels," *IEEE Transactions on Communications*, vol. 38, no. 4, pp. 496–508, Apr. 1990.

[9] 3GPP, "NR; Physical layer procedures for data," 3rd Generation Partnership Project (3GPP), Technical Specification (TS) 38.214, 01 2018, version 15.0.0. [Online]. Available: http://www.3gpp.org/DynaReport/38214.htm

[10] ——, "NR; Physical layer; General description," 3rd Generation Partnership Project (3GPP), Technical Specification (TS) 38.201, 01 2018, version 15.0.0. [Online]. Available: http://www.3gpp.org/DynaReport/38201.htm

[11] Z. E. Ankaralı, B. Peköz, and H. Arslan, "Enhanced OFDM for 5G RAN," *ZTE Commun.*, vol. 15, no. S1, pp. 11–20, 2017.

[12] C. Hofbauer, M. Huemer, and J. B. Huber, "Coded ofdm by unique word prefix," in *2010 IEEE International Conference on Communication Systems*, Nov 2010, pp. 426–430.

[13] M. Huemer, C. Hofbauer, and J. B. Huber, "Non-Systematic Complex Number RS Coded OFDM by Unique Word Prefix," *IEEE Transactions on Signal Processing*, vol. 60, no. 1, pp. 285–299, Jan. 2012.

[14] M. Huemer, A. Onic, and C. Hofbauer, "Classical and Bayesian Linear Data Estimators for Unique Word OFDM," *IEEE Transactions on Signal Processing*, vol. 59, no. 12, pp. 6073–6085, Dec. 2011.

[15] A. T. Harri Holma, *LTE for UMTS: Evolution to LTE-Advanced*, second edition ed., H. Holma and A. Toskala, Eds. Chichester, West Sussex, United Kingdom: Wiley John + Sons, 2011.

[16] S. Sesia, I. Toufik, and M. Baker, *LTE-the UMTS long term evolution*, S. Sesia, I. Toufik, and M. Baker, Eds. Wiley Online Library, feb 2009. [Online]. Available: http://onlinelibrary.wiley.com/doi/10.1002/9780470742891.fmatter/summary

[17] C. F. Gauss, "Nachlass: Theoria interpolationis methodo nova tractata," in *Werke*. Königliche Gesellschaft der Wissenschaften, Göttingem, 1866, vol. 3, pp. 265–330, bibtex: gauss-fft.

[18] A. Sahin, R. Yang, M. Ghosh, and R. L. Olesen, "An Improved Unique Word DFT-Spread OFDM Scheme for 5G Systems," in *2015 IEEE Globecom Workshops (GC Wkshps)*, Dec. 2015, pp. 1–6.

[19] G. Berardinelli, F. M. L. Tavares, T. B. Sorensen, P. Mogensen, and K. Pajukoski, "Zero-tail DFT-spread-OFDM signals," in *2013 IEEE Globecom Workshops (GC Wkshps)*, Dec. 2013, pp. 229–234.

[20] G. Berardinelli, F. M. L. Tavares, T. B. Sørensen, P. Mogensen, and K. Pajukoski, "On the potential of zero-tail DFT-spread-OFDM in 5G networks," in *2014 IEEE 80th Vehicular Technology Conference (VTC2014-Fall)*, Sep. 2014, pp. 1–6.

[21] G. Berardinelli, K. I. Pedersen, T. B. Sorensen, and P. Mogensen, "Generalized DFT-Spread-OFDM as 5G Waveform," *IEEE Communications Magazine*, vol. 54, no. 11, pp. 99–105, Nov. 2016. [Online]. Available: http://ieeexplore.ieee.org/document/7744817/

[22] A. Sahin, R. Yang, E. Bala, M. C. Beluri, and R. L. Olesen, "Flexible DFT-S-OFDM: Solutions and Challenges," *IEEE Communications Magazine*, vol. 54, no. 11, pp. 106–112, Nov. 2016. [Online]. Available: http://ieeexplore.ieee.org/document/7744818/

[23] O. Elijah, C. Y. Leow, T. A. Rahman, S. Nunoo, and S. Z. Iliya, "A Comprehensive Survey of Pilot Contamination in Massive MIMO–5G System," *IEEE Communications Surveys and Tutorials*, vol. 18, no. 2, pp. 905–923, 2016.

[24] P. Walk, H. Becker, and P. Jung, "OFDM channel estimation via phase retrieval," in *2015 49th Asilomar Conference on Signals, Systems and Computers*. IEEE, nov 2015, pp. 1161–1168. [Online]. Available: http://ieeexplore.ieee.org/xpls/abs_all.jsp?arnumber=7421323

[25] V. Saxena, "Pilot Contamination and Mitigation Techniques in Massive MIMO Systems," Master's thesis, Lund University, Stockholm, SE, 2014, student Paper. [Online]. Available: http://lup.lub.lu.se/student-papers/record/4730439

[26] X. Luo, X. Zhang, H. Qian, and K. Kang, "Pilot decontamination via pdp alignment," in *2016 IEEE Global Communications Conference (GLOBECOM)*, Dec 2016, pp. 1–6.

[27] R. R. Müller, L. Cottatellucci, and M. Vehkaperä, "Blind Pilot Decontamination," *IEEE Journal of Selected Topics in Signal Processing*, vol. 8, no. 5, pp. 773–786, Oct. 2014.

[28] D. Hu, L. He, and X. Wang, "Semi-Blind Pilot Decontamination for Massive MIMO Systems," *IEEE Transactions on Wireless Communications*, vol. 15, no. 1, pp. 525–536, Jan. 2016.

[29] S. Rajagopal, S. Abu-Surra, A. Gupta, S. Ramakrishna, K. Josiam, Z. Pi, and Y. Li, "Methods and apparatus for cyclic prefix reduction in mmwave mobile communication systems," U.S. Patent US20 130 315 321 A1, Nov., 2013, u.S. Classification 375/260; International Classification H04L27/26; Cooperative Classification H04L27/261, H04L1/0031, H04J13/0062, H04B7/0695, H04L27/2607. [Online]. Available: http://www.google.com/patents/US20130315321

[30] E. Zoechmann, S. Pratschner, S. Schwarz, and M. Rupp, "MIMO Transmission over High Delay Spread Channels with Reduced Cyclic Prefix Length," in *WSA 2015; 19th International ITG Workshop on Smart Antennas*, Mar. 2015, pp. 1–8.

[31] T. Pham, T. Le-Ngoc, G. Woodward, P. A. Martin, and K. T. Phan, "Equalization for MIMO-OFDM Systems with Insufficient Cyclic Prefix," in *2016 IEEE 83rd Vehicular Technology Conference (VTC Spring)*, May 2016, pp. 1–5.

[32] A. Sahin and H. Arslan, "Multi-user aware frame structure for OFDMA based system," in *Proc. 2012 IEEE 76th Veh. Technol. Conf.*, Quebec City, QC, Sep. 2012, pp. 1–5.

[33] J. Lorca, "Cyclic Prefix Overhead Reduction for Low-Latency Wireless Communications in OFDM," in *Proc. 2015 IEEE 81st Veh. Technol. Conf.*, Glasgow, SCT, May 2015, pp. 1–5.

[34] P. Szulakiewicz, R. Kotrys, M. Krasicki, P. Remlein, and A. Stelter, "OFDM interfering signal rejection from 802.11ac channel," in *Proc. 2012 IEEE 23rd Int. Symp. Personal, Indoor and Mobile Radio Commun.*, Sep. 2012, pp. 2015–2018.

[35] P. W. C. Chan, E. S. Lo, R. R. Wang, E. K. S. Au, V. K. N. Lau, R. S. Cheng, W. H. Mow, R. D. Murch, and K. B. Letaief, "The evolution path of 4G networks: FDD or TDD?" *IEEE Communications Magazine*, vol. 44, no. 12, pp. 42–50, Dec 2006.

[36] Z. You, J. Fang, and I.-T. Lu, "Out-of-band emission suppression techniques based on a generalized OFDM framework," *EURASIP Journal on Advances in Signal Processing*, vol. 2014, no. 1, p. 74, May 2014. [Online]. Available: https://doi.org/10.1186/1687-6180-2014-74

[37] J. Abdoli, M. Jia, and J. Ma, "Filtered OFDM: A new waveform for future wireless systems," in *Proc. 2015 IEEE 16th Int. Workshop Signal Process. Advances in Wireless Commun.*, Stockholm, SE, Jun. 2015, pp. 66–70.

[38] G. Turin, "An introduction to matched filters," *IRE Trans. Inform. Theory*, vol. 6, no. 3, pp. 311–329, Jun. 1960.

[39] I. P. Vaisband, R. Jakushokas, M. Popovich, A. V. Mezhiba, S. Köse, and E. G. Friedman, *On-Chip Power Delivery and Management*. Springer, Apr. 2016.

[40] J. Gozalvez, "New 3GPP standard for IoT [mobile radio]," *IEEE Vehicular Technology Magazine*, vol. 11, no. 1, pp. 14–20, March 2016.

[41] A. F. Demir, B. Peköz, S. Köse, and H. Arslan, "Innovative telecommunications training through flexible radio platforms," *IEEE Communications Magazine*, vol. 57, no. 11, pp. 27–33, Nov. 2019.

[42] M. Gudmundson and P. O. Anderson, "Adjacent channel interference in an OFDM system," in *Proc. 1996 IEEE Veh. Technol. Conf.*, vol. 2, Atlanta, GA, Apr. 1996, pp. 918–922.

[43] C. Muschallik, "Improving an OFDM reception using an adaptive Nyquist windowing," *IEEE Transactions on Consumer Electronics*, vol. 42, no. 3, pp. 259–269, Aug. 1996.

[44] E. Bala, J. Li, and R. Yang, "Shaping spectral leakage: A novel low-complexity transceiver architecture for cognitive radio," *IEEE Vehicular Technology Magazine*, vol. 8, no. 3, pp. 38–46, Sep. 2013.

[45] A. Sahin and H. Arslan, "Edge windowing for OFDM based systems," *IEEE Communications Letters*, vol. 15, no. 11, pp. 1208–1211, Nov. 2011.

[46] E. Güvenkaya, A. Şahin, E. Bala, R. Yang, and H. Arslan, "A windowing technique for optimal time-frequency concentration and ACI rejection in OFDM-based systems," *IEEE Transactions on Communications*, vol. 63, no. 12, pp. 4977–4989, Dec. 2015.

[47] 3GPP, "Study on new radio access technology," 3rd Generation Partnership Project (3GPP), Technical Report (TR) 38.912, 08 2017, version 14.1.0. [Online]. Available: http://www.3gpp.org/DynaReport/38912.htm

[48] J. Wu and P. Fan, "A Survey on High Mobility Wireless Communications: Challenges, Opportunities and Solutions," *IEEE Access*, vol. 4, pp. 450–476, 2016. [Online]. Available: http://ieeexplore.ieee.org/document/7383229/

[49] D. Slepian and H. O. Pollak, "Prolate spheroidal wave functions, fourier analysis and uncertainty - I," *Bell Syst. Tech. J.*, vol. 40, no. 1, pp. 43–63, Jan. 1961.

[50] J. v. d. Beek and F. Berggren, "N-continuous OFDM," *IEEE Communications Letters*, vol. 13, no. 1, pp. 1–3, Jan. 2009.

[51] R. B. Blackman and J. W. Tukey, "The measurement of power spectra from the point of view of communications engineering — Part I," *Bell Syst. Tech. J.*, vol. 37, no. 1, pp. 185–282, Jan. 1958.

[52] K. Murota and K. Hirade, "GMSK modulation for digital mobile radio telephony," *IEEE Transactions on Communications*, vol. 29, no. 7, pp. 1044–1050, Jul. 1981.

[53] F. J. Harris, "On the use of windows for harmonic analysis with the discrete Fourier transform," *Proceedings of the IEEE*, vol. 66, no. 1, pp. 51–83, Jan. 1978.

[54] M. L. Honig, "Overview of multiuser detection," in *Advances in Multiuser Detection*, M. L. Honig, Ed. Hoboken, N.J.: John Wiley & Sons, Inc., 2009, pp. 1–45.

[55] A. Goldsmith, S. A. Jafar, N. Jindal, and S. Vishwanath, "Capacity limits of MIMO channels," *IEEE Journal on Selected Areas in Communications*, vol. 21, no. 5, pp. 684–702, June 2003.

[56] R. W. Heath, N. González-Prelcic, S. Rangan, W. Roh, and A. M. Sayeed, "An overview of signal processing techniques for millimeter wave MIMO systems," *IEEE Journal of Selected Topics in Signal Processing*, vol. 10, no. 3, pp. 436–453, April 2016.

[57] E. Dahlman, S. Parkvall, and J. Sköld, "Multi-antenna transmission," in *5G NR: the Next Generation Wireless Access Technology*. Academic Press, 2018, pp. 225 – 240.

[58] X. Zhou, L. Song, and Y. Zhang, *Physical layer security in wireless communications*. Boca Raton, FL: CRC Press, 2013.

[59] F. Dong, W. Wang, and Z. Wei, "Low-complexity hybrid precoding for multi-user MmWave systems with low-resolution phase shifters," *IEEE Transactions on Vehicular Technology*, vol. 68, no. 10, pp. 9774–9784, Oct 2019.

[60] S. S. Thoota, P. Babu, and C. R. Murthy, "Codebook based precoding and power allocation for MU-MIMO systems for sum rate maximization," *IEEE Transactions on Communications*, pp. 1–1, 2019.

[61] X. Wang, Y. Wang, W. Ni, R. Sun, and S. Meng, "Sum rate analysis and power allocation for massive MIMO systems with mismatch channel," *IEEE Access*, vol. 6, pp. 16 997–17 009, 2018.

[62] S. Goel and R. Negi, "Guaranteeing secrecy using artificial noise," *IEEE Transactions on Wireless Communications*, vol. 7, no. 6, pp. 2180–2189, June 2008.

[63] S. Tsai and H. V. Poor, "Power allocation for artificial-noise secure MIMO precoding systems," *IEEE Transactions on Signal Processing*, vol. 62, no. 13, pp. 3479–3493, July 2014.

[64] B. Peköz, S. Köse, and H. Arslan, "Adaptive windowing of insufficient CP for joint minimization of ISI and ACI beyond 5G," in *Proc. 2017 IEEE 28th Annu. Int. Symp. Personal, Indoor, and Mobile Radio Commun.* Montreal, QC: IEEE, Oct. 2017, pp. 1–5.

[65] B. Pekoz, S. Kose, and H. Arslan, "Combined minimization of intersymbol interference (ISI) and adjacent channel interference (ACI)," U.S. patentus 10,348,530, Jul. 9, 2019.

[66] ——, "Combined minimization of intersymbol interference (ISI) and adjacent channel interference (ACI)," U.S. patentus 10,476,705, Nov. 12, 2019.

[67] D. R. Morgan, "Analysis and Realization of an Exponentially-Decaying Impulse Response Model for Frequency-Selective Fading Channels," *IEEE Signal Processing Letters*, vol. 15, pp. 441–444, 2008.

[68] R. W. Lucky, "Automatic equalization for digital communication," *Bell Syst. Tech. J.*, vol. 44, no. 4, pp. 547–588, Apr. 1965.

[69] G. Cardano, *Liber de ludo aleae*, 1564.

[70] B. Peköz, S. Köse, and H. Arslan, "Extensionless adaptive transmitter and receiver windowing of beyond 5G frames," *IEEE Transactions on Vehicular Technology*, vol. 69, no. 2, pp. 1888–1902, feb 2020.

[71] B. Pekoz, S. Kose, and H. Arslan, "Network-aware adjacent channel interference rejection and out of band emission suppression," U.S. patentus 10,511,338, Dec. 17, 2019.

[72] X. Wang, Y. Wu, J. Y. Chouinard, S. Lu, and B. Caron, "A channel characterization technique using frequency domain pilot time domain correlation method for DVB-T systems," *IEEE Transactions on Consumer Electronics*, vol. 49, no. 4, pp. 949–957, Nov. 2003.

[73] M. K. Ozdemir and H. Arslan, "Channel estimation for wireless OFDM systems," *IEEE Communications Surveys and Tutorials*, vol. 9, no. 2, pp. 18–48, 2007.

[74] G. E. Oien, H. Holm, and K. J. Hole, "Impact of channel prediction on adaptive coded modulation performance in Rayleigh fading," *IEEE Transactions on Vehicular Technology*, vol. 53, no. 3, pp. 758–769, May 2004.

[75] D. M. Brady, "Adaptive coherent diversity receiver for data transmission through dispersive media," in *Proc. IEEE Int. Conf. Commun*, San Fransisco, CA, Jun. 1970.

[76] C. E. Shannon, "A mathematical theory of communication," *Bell Syst. Tech. J.*, vol. 27, no. 3, pp. 379–423, Jul. 1948.

[77] P. Bello, "Characterization of Randomly Time-Variant Linear Channels," *IEEE Trans. Commun. Syst.*, vol. 11, no. 4, pp. 360–393, Dec. 1963.

[78] R. H. Clarke, "A statistical theory of mobile-radio reception," *Bell Syst. Tech. J.*, vol. 47, no. 6, pp. 957–1000, Jul. 1968.

[79] L. R. Kahn, "Ratio Squarer," *Proc. IRE*, vol. 42, no. 11, p. 1704, Nov. 1954.

[80] 3GPP, "Study on channel model for frequencies from 0.5 to 100 GHz," 3rd Generation Partnership Project (3GPP), Technical Report (TR) 38.901, 01 2018, version 14.3.0. [Online]. Available: http://www.3gpp.org/DynaReport/38901.htm

[81] M. Andrews, K. Kumaran, K. Ramanan, A. Stolyar, P. Whiting, and R. Vijayakumar, "Providing quality of service over a shared wireless link," *IEEE Communications Magazine*, vol. 39, no. 2, pp. 150–154, Feb. 2001.

[82] 3GPP, "Study on new radio access technology Physical layer aspects," 3rd Generation Partnership Project (3GPP), Technical Report (TR) 38.802, 09 2017, version 14.2.0. [Online]. Available: http://www.3gpp.org/DynaReport/38802.htm

[83] M. J. Gans, "A power-spectral theory of propagation in the mobile-radio environment," *IEEE Transactions on Vehicular Technology*, vol. 21, no. 1, pp. 27–38, Feb. 1972.

[84] 3GPP, "NR; Physical layer procedures for control," 3rd Generation Partnership Project (3GPP), Technical Specification (TS) 38.213, 01 2018, version 15.0.0. [Online]. Available: http://www.3gpp.org/DynaReport/38213.htm

[85] *f-OFDM scheme and filter design*, 3GPP proposal R1-165 425, Huawei and HiSilicon, Nanjing, China, May 2016.

[86] R. C. Bose and D. K. Ray-Chaudhuri, "On a class of error correcting binary group codes," *Information and Control*, vol. 3, no. 1, pp. 68–79, Mar. 1960.

[87] A. Hocquenghem, "Codes correcteurs d'erreurs," *Chiffers*, vol. 2, pp. 147–156, 1959.

[88] W. W. Peterson, "On the weight structure and symmetry of BCH codes," Hawaii Univ. Honolulu Dept. Electr. Eng., Honolulu, HI, Scientific-1 AD0626730, Jul. 1965.

[89] R. M. Pyndiah, "Near-optimum decoding of product codes: block turbo codes," *IEEE Transactions on Communications*, vol. 46, no. 8, pp. 1003–1010, Aug. 1998.

[90] C.-Y. Lin and P. Hajela, "Genetic algorithms in optimization problems with discrete and integer design variables," *Eng. Optim.*, vol. 19, no. 4, pp. 309–327, Jun. 1992.

[91] B. Peköz, Z. E. Ankaralı, S. Köse, and H. Arslan, "Non-redundant OFDM receiver windowing for 5G frames & beyond," *IEEE Transactions on Vehicular Technology*, vol. 69, no. 1, pp. 676–684, jan 2020.

[92] B. Pekoz, Z. E. Ankaralı, S. Kose, and H. Arslan, "OFDM reception under high adjacent channel interference while preserving frame structure," U.S. patentus 10,547,489, 1 28, 2020.

[93] A. Kalakech, M. Berbineau, I. Dayoub, and E. P. Simon, "Time-Domain LMMSE Channel Estimator Based on Sliding Window for OFDM Systems in High-Mobility Situations," *IEEE Transactions on Vehicular Technology*, vol. 64, no. 12, pp. 5728–5740, Dec. 2015.

[94] J.-v. d. Beek, O. Edfors, M. Sandell, S. K. Wilson, and P. O. Borjesson, "On channel estimation in OFDM systems," in *Proc. 1995 IEEE 45th Veh. Technol. Conf.*, vol. 2, Jul. 1995, pp. 815–819.

[95] G. Huang, A. Nix, and S. Armour, "DFT-Based Channel Estimation and Noise Variance Estimation Techniques for Single-Carrier FDMA," in *Proc. 2010 IEEE 72nd Veh. Technol. Conf.*, Sep. 2010, pp. 1–5.

[96] G. W. Stewart, "On scaled projections and pseudoinverses," *Linear Algebra Appl*, vol. 112, pp. 189–193, Jan. 1989. [Online]. Available: http://www.sciencedirect.com/science/article/pii/0024379589905946

[97] S. Vavasis, "Stable Numerical Algorithms for Equilibrium Systems," *SIAM J. Matrix Anal. Appl.*, vol. 15, no. 4, pp. 1108–1131, Oct. 1994. [Online]. Available: https://epubs.siam.org/doi/10.1137/S0895479892230948

[98] P. Hough and S. Vavasis, "Complete Orthogonal Decomposition for Weighted Least Squares," *SIAM J. Matrix Anal. Appl.*, vol. 18, no. 2, pp. 369–392, Apr. 1997. [Online]. Available: https://epubs.siam.org/doi/10.1137/S089547989528079X

[99] A. Barbieri, D. Fertonani, and G. Colavolpe, "Time-frequency packing for linear modulations: spectral efficiency and practical detection schemes," *IEEE Transactions on Communications*, vol. 57, no. 10, pp. 2951–2959, Oct. 2009.

[100] 3GPP, "NR; User Equipment (UE) radio transmission and reception; Part 1: Range 1 Standalone," 3rd Generation Partnership Project (3GPP), Technical Specification (TS) 38.101-1, 01 2018, version 15.0.0. [Online]. Available: http://www.3gpp.org/DynaReport/-38101-1.htm

[101] "HetNet/Small Cells." [Online]. Available: http://www.3gpp.org/hetnet

[102] H. Elsawy, E. Hossain, and D. I. Kim, "HetNets with cognitive small cells: user offloading and distributed channel access techniques," *IEEE Communications Magazine*, vol. 51, no. 6, pp. 28–36, Jun. 2013.

[103] R. Q. Hu and Y. Qian, "An energy efficient and spectrum efficient wireless heterogeneous network framework for 5G systems," *IEEE Communications Magazine*, vol. 52, no. 5, pp. 94–101, May 2014.

[104] N. H. Mahmood, M. Lauridsen, G. Berardinelli, D. Catania, and P. Mogensen, "Radio resource management techniques for eMBB and mMTC services in 5G dense small cell scenarios," in *Proc. IEEE VTC-Fall, Montreal, Canada*, 2016.

[105] D. Lopez-Perez, I. Guvenc, and X. Chu, "Mobility management challenges in 3GPP heterogeneous networks," *IEEE Communications Magazine*, vol. 50, no. 12, pp. 70–78, Dec. 2012.

[106] G. L. Stüber, "Propagation Modeling," in *Principles of Mobile Communication*. Cham: Springer International Publishing, 2017, pp. 33–145. [Online]. Available: https://doi.org/10.1007/978-3-319-55615-4_2

[107] M. Ergen, "Basics of Cellular Communication," in *Mobile Broadband*. Springer US, 2009, pp. 19–65.

[108] D. Lopez-Perez, I. Guvenc, G. d. l. Roche, M. Kountouris, T. Q. S. Quek, and J. Zhang, "Enhanced intercell interference coordination challenges in heterogeneous networks," *IEEE Wireless Communications*, vol. 18, no. 3, pp. 22–30, Jun. 2011.

[109] S. Deb, P. Monogioudis, J. Miernik, and J. P. Seymour, "Algorithms for Enhanced Inter-Cell Interference Coordination (eICIC) in LTE HetNets," *IEEE/ACM Transactions on Networking*, vol. 22, no. 1, pp. 137–150, Feb. 2014. [Online]. Available: http://ieeexplore.ieee.org/document/6475212/

[110] A. Şahin, E. Bala, I. Guvenç, R. Yang, and H. Arslan, "Partially Overlapping Tones for Uncoordinated Networks," *IEEE Transactions on Communications*, vol. 62, no. 9, pp. 3363–3375, Sep. 2014.

[111] R. Rom and M. Sidi, "Conflict-Free Access Protocols," in *Multiple Access Protocols*, ser. Telecommunication Networks and Computer Systems. Springer New York, 1990, pp. 9–45.

[112] L. Dai, B. Wang, Y. Yuan, S. Han, C. lin I, and Z. Wang, "Non-orthogonal multiple access for 5G: solutions, challenges, opportunities, and future research trends," *IEEE Communications Magazine*, vol. 53, no. 9, pp. 74–81, Sep. 2015.

[113] Z. Yuan, G. Yu, W. Li, Y. Yuan, X. Wang, and J. Xu, "Multi-User Shared Access for Internet of Things," in *2016 IEEE 83rd Vehicular Technology Conference (VTC Spring)*, May 2016, pp. 1–5.

[114] D. Tse and P. Viswanath, "Capacity of Wireless Channels," in *Fundamentals of Wireless Communication*, ser. Wireless Communications. Cambridge University Press, Jul. 2005, pp. 166–227.

[115] T. A. Levanen, J. Pirskanen, T. Koskela, J. Talvitie, and M. Valkama, "Radio Interface Evolution Towards 5G and Enhanced Local Area Communications," *IEEE Access*, vol. 2, pp. 1005–1029, 2014.

[116] G. Wunder, P. Jung, and C. Wang, "Compressive random access for post-LTE systems," in *2014 IEEE International Conference on Communications Workshops (ICC)*, Jun. 2014, pp. 539–544.

[117] Y. Yuan, Z. Yuan, G. Yu, C. H. Hwang, P. k. Liao, A. Li, and K. Takeda, "Non-orthogonal transmission technology in LTE evolution," *IEEE Communications Magazine*, vol. 54, no. 7, pp. 68–74, Jul. 2016.

[118] K. Higuchi and A. Benjebbour, "Non-orthogonal Multiple Access (NOMA) with Successive Interference Cancellation for Future Radio Access," *IEICE Transactions on Communications*, vol. E98-B, no. 3, pp. 403–414, Mar. 2015.

[119] J. Zhao, T. Q. S. Quek, and Z. Lei, "Coordinated Multipoint Transmission with Limited Backhaul Data Transfer," *IEEE Transactions on Wireless Communications*, vol. 12, no. 6, pp. 2762–2775, Jun. 2013.

[120] M. B. Çelebi and H. Arslan, "Theoretical Analysis of the Co-Existence of LTE-A Signals and Design of an ML-SIC Receiver," *IEEE Transactions on Wireless Communications*, vol. 14, no. 8, pp. 4626–4639, Aug. 2015.

[121] M. Taherzadeh, H. Nikopour, A. Bayesteh, and H. Baligh, "SCMA Codebook Design," in *Proc. IEEE 80th Vehicular Technology Conf. Fall*, Vancouver, BC, Sep. 2014, pp. 1–5.

[122] B. Wang, K. Wang, Z. Lu, T. Xie, and J. Quan, "Comparison study of non-orthogonal multiple access schemes for 5G," in *2015 IEEE International Symposium on Broadband Multimedia Systems and Broadcasting*, Jun. 2015, pp. 1–5.

[123] S. Zhang, X. Xu, L. Lu, Y. Wu, G. He, and Y. Chen, "Sparse code multiple access: An energy efficient uplink approach for 5G wireless systems," in *Proc. IEEE Global Communications Conf.*, Austin, TX, Dec. 2014, pp. 4782–4787.

[124] Y. Tao, L. Liu, S. Liu, and Z. Zhang, "A survey: Several technologies of non-orthogonal transmission for 5G," *China Communications*, vol. 12, no. 10, pp. 1–15, Oct. 2015.

[125] M. C. Chang and Y. T. Su, "Overloaded multiple access systems: A generalized model and a low-complexity multiuser decoder," in *2016 9th International Symposium on Turbo Codes and Iterative Information Processing (ISTC)*, Sep. 2016, pp. 231–235.

[126] R. Razavi, M. AL-Imari, M. A. Imran, R. Hoshyar, and D. Chen, "On Receiver Design for Uplink Low Density Signature OFDM (LDS-OFDM)," *IEEE Transactions on Communications*, vol. 60, no. 11, pp. 3499–3508, Nov. 2012.

[127] H. Nikopour and H. Baligh, "Sparse code multiple access," in *Proc. IEEE 24th Annu. Int. Symp. Personal, Indoor, and Mobile Radio Communications*, London, UK, Sep. 2013, pp. 332–336.

[128] M. Elkourdi, B. Peköz, E. Güvenkaya, and H. Arslan, "Waveform design principles for 5G and beyond," in *Proc. 2016 IEEE 17th Annu. Wireless and Microwave Technol. Conf.* Clearwater, FL: IEEE, Apr. 2016, pp. 1–6.

[129] Y. Saito, Y. Kishiyama, A. Benjebbour, T. Nakamura, A. Li, and K. Higuchi, "Non-orthogonal multiple access (NOMA) for cellular future radio access," in *Proc. IEEE 77th Vehicular Technology Conf. Spring*, Dresden, DE, 2013, pp. 1–5. [Online]. Available: http://ieeexplore.ieee.org/abstract/document/6692652/

[130] B. Peköz, M. Hafez, S. Köse, and H. Arslan, "Reducing precoder/channel mismatch and enhancing secrecy in practical MIMO systems using artificial signals," *IEEE Communications Letters*, pp. 1–4, 2020.

[131] B. Pekoz, M. Hafez, S. Kose, and H. Arslan, "Using artificial signals to maximize capacity and secrecy of multiple-input multiple-output (MIMO) communication," U.S. patentus 10,516,452, Dec. 24, 2019.

[132] R. G. Gallager, "Waveform Channels," in *Information Theory and Reliable Communication*. New York: Wiley, 1968, pp. 355–441. [Online]. Available: http://catalog.hathitrust.org/api/volumes/oclc/253841.html

[133] E. Telatar, "Capacity of multi-antenna gaussian channels," *European Transactions on Telecommunications*, vol. 10, no. 6, pp. 585–595, 1999. [Online]. Available: https://onlinelibrary.wiley.com/doi/abs/10.1002/ett.4460100604

[134] M. Grant and S. Boyd, "Graph implementations for nonsmooth convex programs," in *Recent Advances in Learning and Control*, ser. Lecture Notes in Control and Information Sciences, V. Blondel, S. Boyd, and H. Kimura, Eds. Springer-Verlag Limited, 2008, pp. 95–110.

[135] X. Huang, Y. J. Guo, and J. D. Bunton, "A hybrid adaptive antenna array," *IEEE Transactions on Wireless Communications*, vol. 9, no. 5, pp. 1770–1779, May 2010.

[136] A. A. Gheethan, M. C. Jo, R. Guldiken, and G. Mumcu, "Microfluidic based Ka-band beam-scanning focal plane array," *IEEE Antennas and Wireless Propagation Letters*, vol. 12, pp. 1638–1641, 2013.

[137] G. Mumcu, M. Kacar, and J. Mendoza, "Mm-Wave beam steering antenna with reduced hardware complexity using lens antenna subarrays," *IEEE Antennas and Wireless Propagation Letters*, vol. 17, no. 9, pp. 1603–1607, Sep. 2018.

[138] R. Méndez-Rial, C. Rusu, N. González-Prelcic, and R. W. Heath, "Dictionary-free hybrid precoders and combiners for mmWave MIMO systems," in *Proc. 2015 IEEE 16th Int. Workshop Signal Process. Advances in Wirel. Commun.*, Stockholm, SE, Jun. 2015, pp. 151–155.

[139] G. Cardano, “Cap. XIV: puncta in combined,” in *Liber de ludo aleae*, 1564.

[140] M. Grant and S. Boyd, “CVX: MATLAB software for disciplined convex programming, version 2.1,” http://cvxr.com/cvx, Mar. 2014.

Appendix A: Copyright Permissions

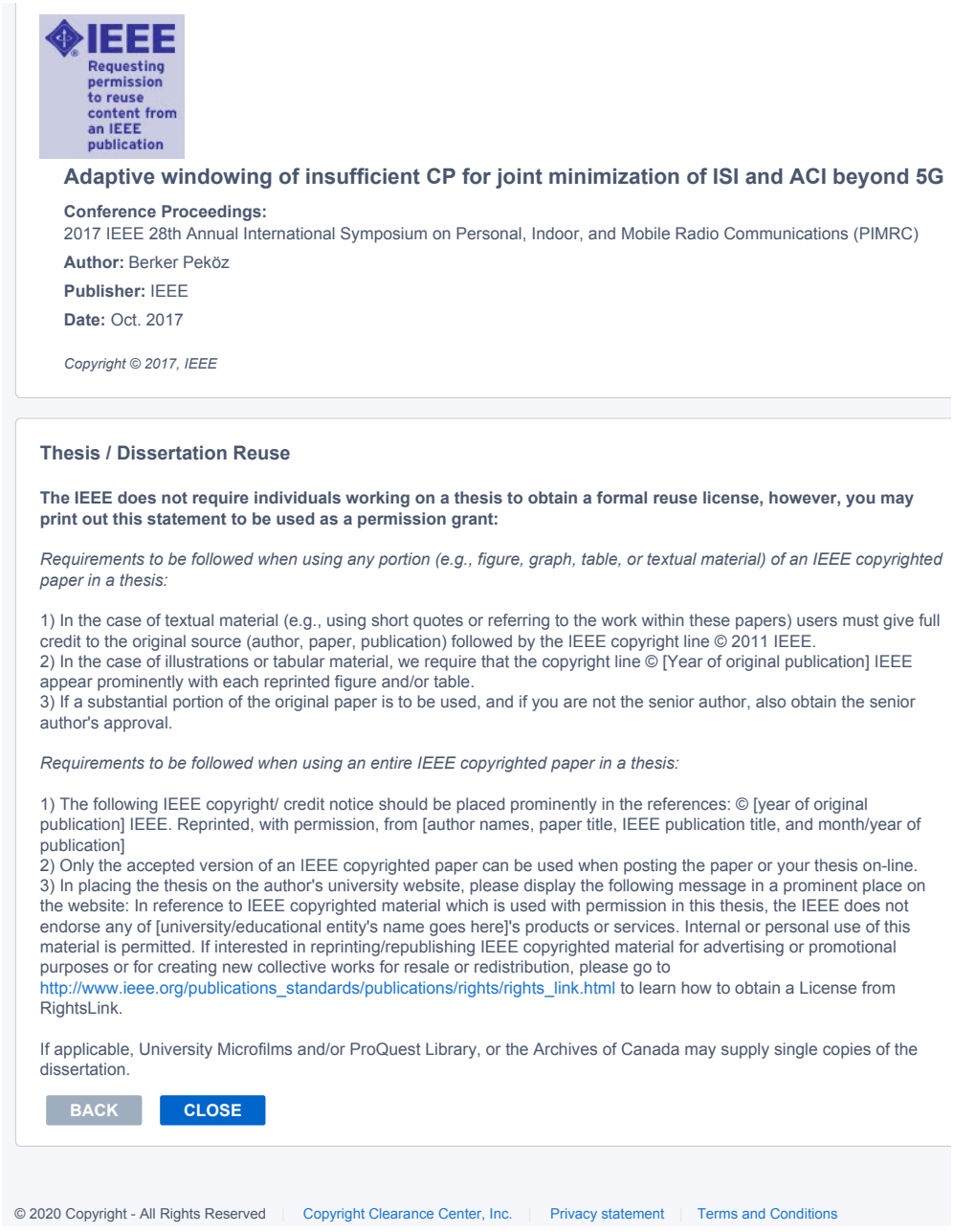

IEEE
Requesting permission to reuse content from an IEEE publication

Adaptive windowing of insufficient CP for joint minimization of ISI and ACI beyond 5G

Conference Proceedings:
2017 IEEE 28th Annual International Symposium on Personal, Indoor, and Mobile Radio Communications (PIMRC)

Author: Berker Peköz

Publisher: IEEE

Date: Oct. 2017

Copyright © 2017, IEEE

Thesis / Dissertation Reuse

The IEEE does not require individuals working on a thesis to obtain a formal reuse license, however, you may print out this statement to be used as a permission grant:

Requirements to be followed when using any portion (e.g., figure, graph, table, or textual material) of an IEEE copyrighted paper in a thesis:

1) In the case of textual material (e.g., using short quotes or referring to the work within these papers) users must give full credit to the original source (author, paper, publication) followed by the IEEE copyright line © 2011 IEEE.
2) In the case of illustrations or tabular material, we require that the copyright line © [Year of original publication] IEEE appear prominently with each reprinted figure and/or table.
3) If a substantial portion of the original paper is to be used, and if you are not the senior author, also obtain the senior author's approval.

Requirements to be followed when using an entire IEEE copyrighted paper in a thesis:

1) The following IEEE copyright/ credit notice should be placed prominently in the references: © [year of original publication] IEEE. Reprinted, with permission, from [author names, paper title, IEEE publication title, and month/year of publication]
2) Only the accepted version of an IEEE copyrighted paper can be used when posting the paper or your thesis on-line.
3) In placing the thesis on the author's university website, please display the following message in a prominent place on the website: In reference to IEEE copyrighted material which is used with permission in this thesis, the IEEE does not endorse any of [university/educational entity's name goes here]'s products or services. Internal or personal use of this material is permitted. If interested in reprinting/republishing IEEE copyrighted material for advertising or promotional purposes or for creating new collective works for resale or redistribution, please go to http://www.ieee.org/publications_standards/publications/rights/rights_link.html to learn how to obtain a License from RightsLink.

If applicable, University Microfilms and/or ProQuest Library, or the Archives of Canada may supply single copies of the dissertation.

BACK CLOSE

The permission above is for the use of materials in Chapter 2.

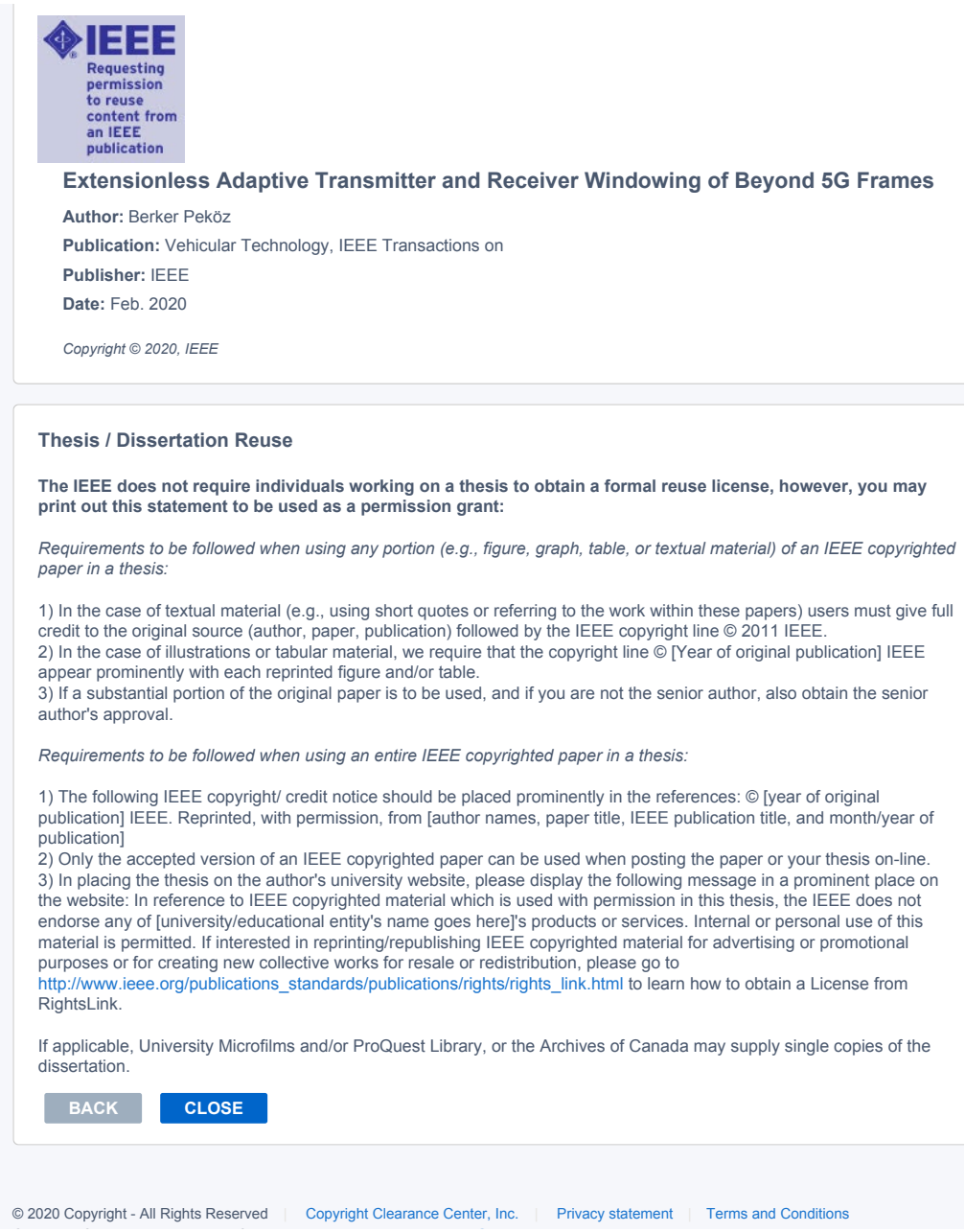

The permission above is for the use of materials in Chapter 3.

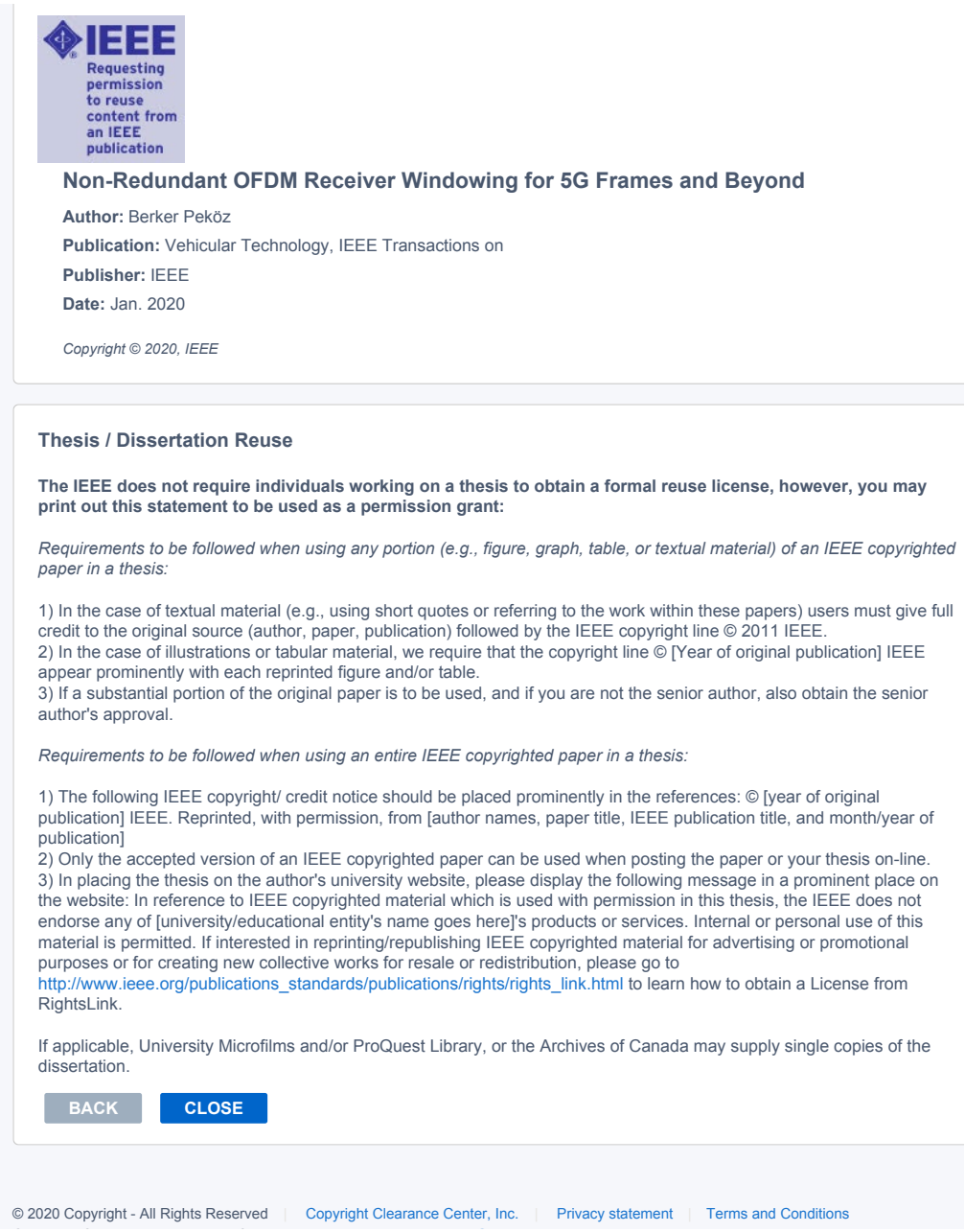

IEEE
Requesting permission to reuse content from an IEEE publication

Non-Redundant OFDM Receiver Windowing for 5G Frames and Beyond

Author: Berker Peköz

Publication: Vehicular Technology, IEEE Transactions on

Publisher: IEEE

Date: Jan. 2020

Copyright © 2020, IEEE

Thesis / Dissertation Reuse

The IEEE does not require individuals working on a thesis to obtain a formal reuse license, however, you may print out this statement to be used as a permission grant:

Requirements to be followed when using any portion (e.g., figure, graph, table, or textual material) of an IEEE copyrighted paper in a thesis:

1) In the case of textual material (e.g., using short quotes or referring to the work within these papers) users must give full credit to the original source (author, paper, publication) followed by the IEEE copyright line © 2011 IEEE.
2) In the case of illustrations or tabular material, we require that the copyright line © [Year of original publication] IEEE appear prominently with each reprinted figure and/or table.
3) If a substantial portion of the original paper is to be used, and if you are not the senior author, also obtain the senior author's approval.

Requirements to be followed when using an entire IEEE copyrighted paper in a thesis:

1) The following IEEE copyright/ credit notice should be placed prominently in the references: © [year of original publication] IEEE. Reprinted, with permission, from [author names, paper title, IEEE publication title, and month/year of publication]
2) Only the accepted version of an IEEE copyrighted paper can be used when posting the paper or your thesis on-line.
3) In placing the thesis on the author's university website, please display the following message in a prominent place on the website: In reference to IEEE copyrighted material which is used with permission in this thesis, the IEEE does not endorse any of [university/educational entity's name goes here]'s products or services. Internal or personal use of this material is permitted. If interested in reprinting/republishing IEEE copyrighted material for advertising or promotional purposes or for creating new collective works for resale or redistribution, please go to http://www.ieee.org/publications_standards/publications/rights/rights_link.html to learn how to obtain a License from RightsLink.

If applicable, University Microfilms and/or ProQuest Library, or the Archives of Canada may supply single copies of the dissertation.

BACK CLOSE

The permission above is for the use of materials in Chapter 4.

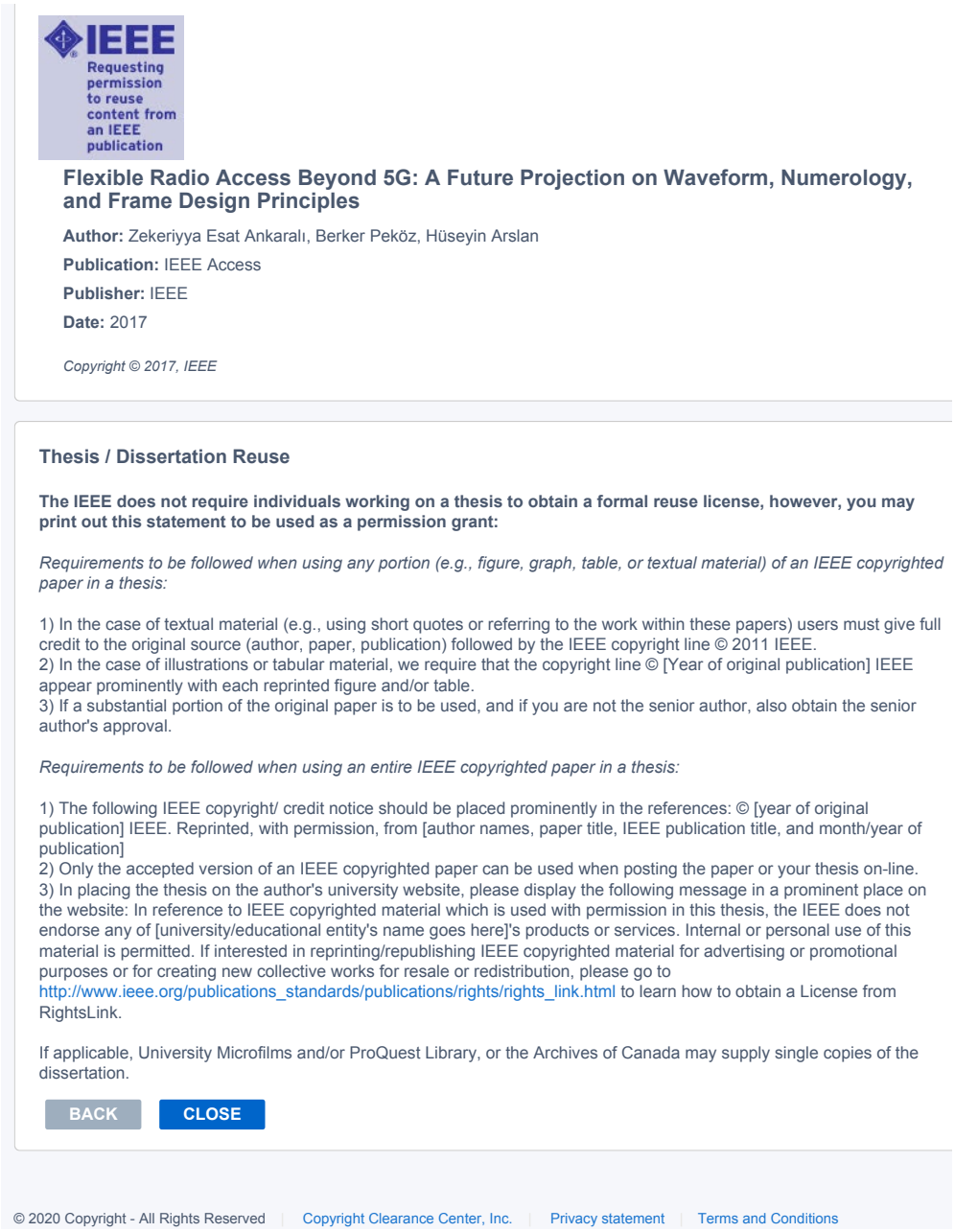

The permission above is for the use of materials in Chapter 5.

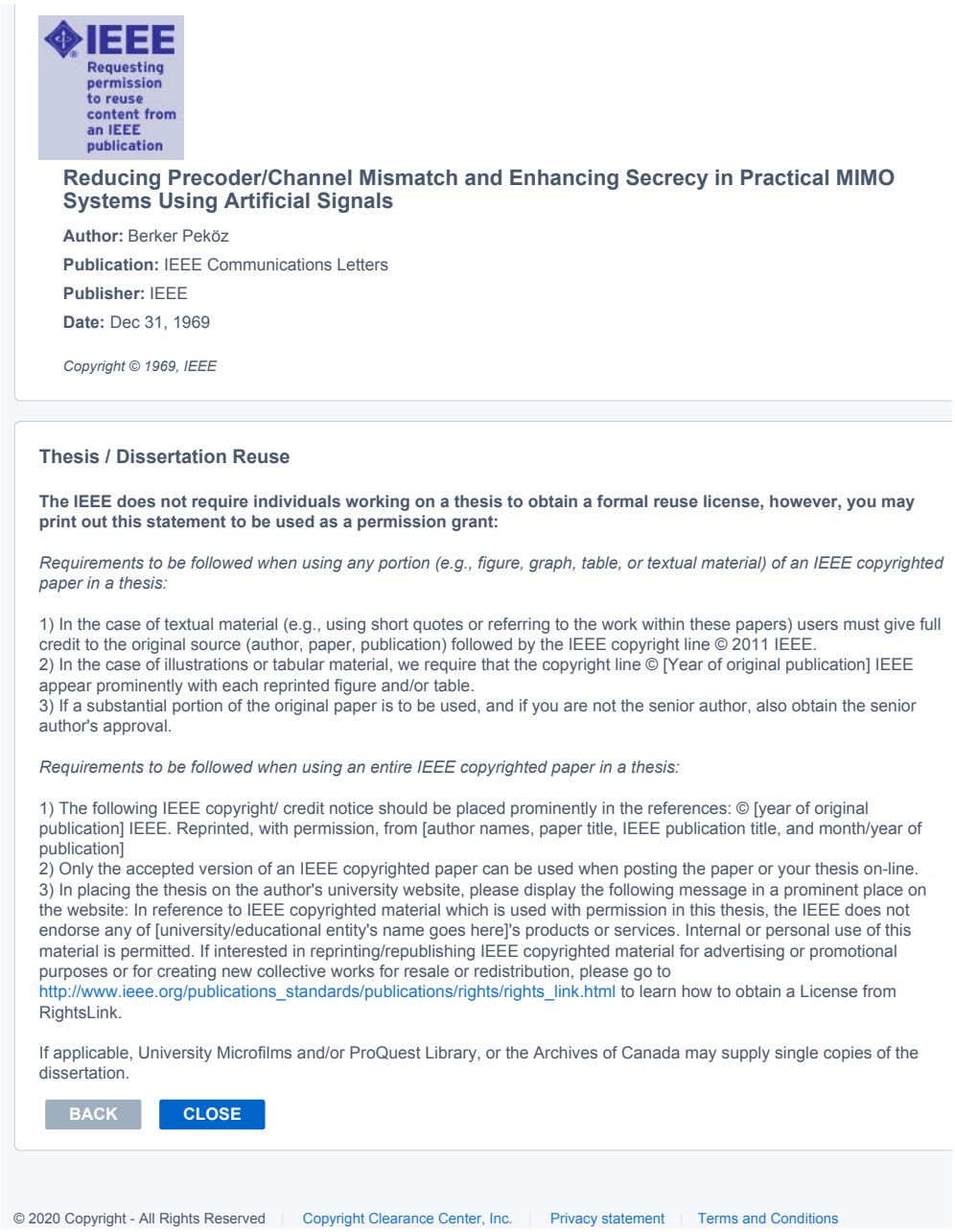

The permission above is for the use of materials in Section 5.3.

About the Author

Berker Peköz received the B.S. degree with high honours in electrical and electronics engineering from the Middle East Technical University, Ankara, Turkey in 2015, and the M.S.E.E. degree from the University of South Florida, Tampa, FL, USA, in 2017. He was a Co-op Intern with the Space Division of Turkish Aerospace Industries, Inc., Ankara, Turkey, in 2013, and a Summer Intern with the Laboratory for High Performance DSP and Network Computing Research, New Jersey Institute of Technology, Newark, NJ, USA, in 2014. His research is concerned with standard compliant waveform design and processing. He is a member of Tau Beta Pi and National Academy of Inventors.